UNIVERSITY OF CALIFORNIA
SANTA CRUZ

EXHUMATION OF THE PERUVIAN ANDES; INSIGHTS FROM MINERAL CHRONOMETERS

A dissertation submitted in partial satisfaction
of the requirements for the degree of

DOCTOR OF PHILOSOPHY

in

EARTH SCIENCES

by

Melanie J. Michalak

September 2013

The Dissertation of Melanie Michalak is approved:

_____
Professor Robert Coe, chair

_____
Daniel Farber, Ph.D.

_____
Professor Jeremy Hourigan

_____
Professor Noah Finnegan

_____
Tyrus Miller
Vice Provost and Dean of Graduate Studies

TABLE OF CONTENTS

LIST OF FIGURES

LIST OF APPENDICES

Acknowledgments

This PhD dissertation would not have been possible without the help of my advisor, Daniel Farber, and colleagues Sarah Hall, Jeremy Hourigan and Laurence Audin. Committee members Robert Coe and Noah Finnegan contributed greatly to my experience and approach as a graduate student at UC-Santa Cruz. Thanks to the various field assistants, labmates and student workers who helped and taught me; Sam Johnstone, Guangsheng Zhuang, Keith Hodson, Jon Perkins, Kerri Johnson, Jordan Murphy, and Carlos Benavente. This thesis relied heavily on labs at UC-Santa Cruz; thank you Jeremy Hourigan, Rob Franks and Dan Sampson for your patience and kindness.

Finally, thanks to the dynamic group of graduate and undergraduate students I have taught, worked with, and learned from during my seven years at UC-Santa Cruz.

An Abstract

for the dissertation

EXHUMATION OF THE PERUVIAN ANDES; INSIGHTS FROM MINERAL CHRONOMETERS

by

Melanie J. Michalak

The Andes of South America display the classic plate tectonic setting of oceanic-continental convergence. Subduction since the Mesozoic of the Nazca plate beneath the South American plate has produced the Andes, which are characterized by the second-largest plateau in the world, major deflections, flat-slab sections of subduction, and varying widths of high topography along-strike. While the general tectonic setting of the Andes is known, significant questions remain with respect to the timing and magnitude of the uplift of the Andes, the mechanisms responsible for uplift and exhumation, and how the tectonically segmented nature of the orogen affects its formation. Here, we use bedrock apatite and zircon (U-Th)/He thermochronology and bedrock and U-Pb zircon geochonology to determine rates and timings of crustal cooling due to exhumation, plutonic emplacement ages, and provenance of detritus, in order to investigate the evolution of topography and regional exhumation in the Peruvian Andes from 5 and 12°S. Six sample sites lie within different tectonomorphic and geologic regions of Peru, from the Mesozoic

Coastal Batholith of the Western Cordillera, to the Cordillera Blanca Batholith region to the Marañon corridor of the Eastern Cordillera.

In the Marañon Corridor of the Eastern Cordillera, we use both apatite and zircon (U-Th)He thermochronology to show that rock exhumation rates increased by roughly an order of magnitude from the Mesozoic by Late Miocene time, from ~0.04mm/yr to ~0.25mm/yr. U-Pb detrital zircon provenance from the Cretaceous aged-sandstones and quartzite samples from the Marañon sample sites shows that the ZHe cooling ages are not reflecting unreset cooling ages, rather, partial retention of He near the closure depth of Zr. The detrital U-Pb zircon ages from the sedimentary units show that during deposition in the Cretaceous, provenance sources changed spatially and temporally, from a dominant Paleozoic basement source, to Proterozoic cratonic sources from the Amazon shelf.

In the Coastal Batholith of the Western Cordillera in Peru, a Miocene rock cooling signal from both zircon and apatite (U-Th)/He thermochronologic systems characterizes three along-valley sample sites at 5, 8 and 12°S, while U-Pb zircon geochonologic ages on the same samples vary from late-Cretaceous to Oligocene. In the site at 12°S, along the Rio Rimac, the age spectra displays younging orogen-ward, indicating a spatial gradient in exhumation, where faster rock exhumation occurred in the internal part of the orogen, compared to the coast.

In summary, the results presented here constrain general rock uplift and exhumation timings of the Peruvian Andes. By the late Cretaceous, the Coastal

Batholith was being emplaced, while a back-arc basin lie to the east, fed by Amazon cratonic units. Slow rock exhumation and possibly little relief growth affected the Western and Eastern Cordilleras until the early Miocene, where we show rock exhumation rates accelerated. Secondly, we find that the general timings of regional rock exhumation in the north-central Peruvian Andes are similar to the timings of uplift and generation of modern topography documented in the Central Andean segment. Despite the tectonomorphic differences between the two regions, perhaps a unifying mechanism might exert a control on formation of the Andes. We suggest orogenesis and along-strike relief growth may be accomplished by a strong coupling of tectonic and climatic forces since Miocene time.

Chapter 1. Introduction

Mountain belts record the dynamic forces of lithospheric and surface processes. Their development and evolution are influenced by both continental-scale and localized lithospheric processes including plate motion magnitudes, volcanism, magmatism, and seismicity. At Earth's lithosphere-atmosphere boundary, mountains are further shaped by surface processes, such as rivers, glaciers, mass-wasting, weathering and wind. While mountainous topography is observed at all types of plate boundaries as well as by intra-plate deformation, convergent plate boundaries on Earth have produced some of the longest, highest and complex mountain belts, that have the ability to greatly influence atmospheric patterns and regional climates. For example, the presence of the Himalaya-Tibetan Plateau has played a significant role in developing the Asian Monsoon, which in turn contributes to the geomorphic dynamics of the range. The South American Andes induce a large orographic effect; they separate the Amazon rainforest from the Atacama desert, the wettest and driest places in the world. Indeed, the presence of vast, mountainous topography influences weather phenomenon, regional climate, and rates of erosion, weathering and soil development. Lithospheric processes that occur on geologic timescales are connected to surface processes occurring on shorter timescales in a way that is described as coupled. However, at present, it has proved difficult using quantitative and qualitative

methods in the Earth Sciences to unequivocally document lithosphere-atmosphere coupling and feedbacks in the tectonics-climate system.

In order to explore and quantify linkages in the tectonics-climate system, knowledge of the spatial and temporal uplift development of the orogen must be well-constrained, as well as the paleoclimate. Using techniques that quantify and characterize paleotopography, chronology of structural development, and paleoerosion rates are common approaches to establishing models of orogenic development. While it is challenging to separate correlation and causality as well as use techniques that are able to deconvolve the relative contributions of tectonics and surfaces processes to orogenesis, these kinds of studies are an important, active and evolving area of research in the Earth Sciences.

The major objective of this dissertation is to address models of uplift of the Andean orogen by using quantitative methods in the north-central Peruvian Andes. The Peruvian Andes are a region of the orogen that was well-studied by geologists in the 1920s through 1980s, but where there is currently a dearth of quantitative data that can complement and improve interpretations for orogensis. The geochronologic techniques used in this dissertation include (U-Th)/He low temperature thermochronology of apatite and zircon minerals, and U-Pb zircon geochronology by *in situ* laser-ablation inductively-coupled mass spectrometry. In Chapter 2, I give an overview of Andean tectonics, models for Andean uplift, and summarize the literature about the geology and tectonic chronology of the north-central Peruvian Andes.

Chapter 3 is a manuscript in preparation for the *Journal of South American Sciences*, where I use detrital U-Pb zircon geochronology to extract the provenance history, paleotopography and tectonic controls on the Cretaceous back-arc basin during the early formation of the Andean orogenesis in north-central Peru. Chapter 4 is a manuscript submitted to the journal *Lithosphere*, which explores the exhumation history of the Eastern Cordillera of north-central Peru, with the first quantitative controls on uplift in this part of the Andes, showing an accelerated signal of rock exhumation during the Late Miocene through present. Chapter 5 is a manuscript in preparation for submission to *Tectonics*, where I use both U-Pb zircon geochronology and (U-Th)/He thermochronology of the Coastal Batholith of the Western Cordillera of Peru to quantify exhumation and uplift, and place these results in context of other regions studied, to address along-strike variability in uplift and the applicability of currently proposed models elsewhere in the Andes for the north-central Peruvian Andes. Finally, in Chapter 6 I make concluding remarks about the contributions of my dissertation research.

Chapter 2. Andean Tectonics and Geology

2.1. Tectonic Plate Setting

The South American Andes are the classic example of orogenesis from oceanic-continental lithospheric plate convergence. The Nazca plate, which converges with the majority of the Andean margin, from 7°N to 40°S, has been subducting beneath the South American plate since Jurassic time (Fig. 2.1). South of 40°S, the South American plate comes into contact with the Antarctic plate. However, for this discussion, I focus on the Andean margin that is characterized by Nazca-South American convergence only. Present rates of convergence are ~6.7cm/yr, with the Nazca plate moving east-northeast and the South American plate migrating west. Plate reconstructions indicate this rate represents a recent slowing of convergence; average convergence over the past 10my is calculated at 10.3 ± 0.2 cm/yr, slowing to its present rate of 6.7 cm/yr (Gordon and Jurdy, 1986). Longer term reconstructions since the Eocene also indicate slowing (Somoza, 1998). Some have suggested this slowing is due to the topographic load of the Andes mountains (Norabuena et al., 1999; Iaffaldano et al., 2006).

The Andean margin is, to first-order, an ideal orogen from oceanic-continental plate convergence, consisting of an ocean trench, volcanic arc, and fold-and-thrust belt (e.g. James, 1971). In the Andes, these features are, from west to east, i) the Western Cordillera, containing the Coastal batholith, overlain by Cenozoic sediments and volcanics, ii) the Eastern Cordillera composed of folded and faulted Precambrian

basement, and iii) the Sub-Andean zone, folded and faulted Mesozoic-Cenozoic marine and continental sediments. In fact, it was recognized that the Andean margin served as an important analogy to understanding the Mesozoic tectonics of the Western U.S. (Hamilton, 1969; Jordan et al., 1983) and remains today as the "textbook example" of the orogenic features formed in a subduction zone.

2.2 Tectonic, morphologic and climate orogen segmentation

Although the Andes represent the archetypal orogen formed from oceanic-continental lithospheric convergence (Dewey and Bird, 1970; James, 1971), anomalies and variations along-strike arise along the margin, and the overall orogen morphology is often described as segmented. Variations along-strike occur i) tectonically, in age of the oceanic lithosphere, existence of buoyant ridges, and sections of flat slab tectonics, ii) structurally, as major deflections in the orientation of the range, iii) morphologically, as the width of the high topography is ~700km in the central Andes, but tapers to more narrow zones of ~200km to the north and south, and iv) climatically, as an extremely strong modern east-west climatic gradient in the north lessens toward the central Andes, and reverses in the south.

2.2.1 Tectonic variation

Tectonically, anomalies occur in the form of buoyant oceanic ridges that are presently being subducted along the margin; the Carnegie Ridge at ~0°, the Nazca

Ridge at ~15°S and the Juan Fernandez Ridge at ~31°S (Fig. 2.1). Other buoyant features such as an oceanic plateau termed the "Lost Inca Plateau," is suggested to have subducted in the Late Miocene and described to presently exist a few hundred kilometers inland between 0 and 5°S (Gutscher et al. 1999). The age of the oceanic crust also varies along the Andean margin, with older crust near the central Andes and younger crust to the north and south (Muller et al., 1997). This variability in age results in different thicknesses, where older crust is more negatively buoyant and thicker. This is thought to influence the traction of the downgoing plate on the upper plate, where older, thicker crust creates higher shear stresses and slower rollback, which Capitanio et al. (2011) use to explain the segmented morphology of the Andes; the higher, wider topography of the Central Andes and the existence of the Bolivian Orocline.

The other major tectonic change along strike of the Andes is the existence of two flat-slab zones (Sykes and Hayes, 1971; Barazangi and Isacks, 1976). Between 5°N and 2°S the subducting slab dips at 35° and represents a sector of "normal" subduction with active volcanism. At latitudes 5°S - 13.5°S seismic activity indicate that the Nazca Plate initially descends to a depth of 100 km at an angle of 30° before extending horizontally for several hundred km. Between 13.5°S and 28°S, normal angle subduction resumes. Another flat-slab zone exists between 28 and 33°, and south of this section, normal angle subduction continues. In both of these flat slab zones, the Nazca plate initially descends at an angle of ~30° to an depth of 100km,

but then flattens for hundreds of kilometers. While the change from normal angle to flat slab subduction is more gradual in the Chilean segment at ~28-33°S, the change in along-strike slab angle at ~13.5°S is abrupt, and was originally thought to represent a tear in the oceanic slab (Barazangi and Isacks, 1976) but with more seismic data available, later described as continuous flexures (Hasegawa and Sacks, 1981; Bevis and Isacks, 1984). With the discovery of these flat slab zones came the realization that they were associated with a distinct lack of active volcanic centers (Barazangi and Isacks, 1976). The cessation of volcanism as a result of a flattening slab is attributed to the suppression of corner flow in the asthenospheric wedge (Leeman, 1983).

It has been proposed that the spatial similarities of the subducting oceanic ridges and the flat-slab zones are not merely coincidental, but that buoyant ridges gravitationally support the flat-slab region in Peru (Sacks, 1983; Gutscher et al., 2002). Other explanations have used the peculiar convex geometry of the Arica Bend/ Bolivian Orocline to possibly induce flat slab subduction on its flanks (Bevis, 1986; Isacks, 1988; Cahill and Isacks, 1992; Gephart, 1994). However, at present there is no singular satisfying explanation for flat-slab subduction that is applicable to all flab-slab zones worldwide. Further, while the general slab structure between the two Andean flat-slab segments are similar, in their depths, lateral extent and seismic structure, differences exist; the Chilean flat-slab segment is associated with basement-involved “thick-skinned” style of uplift in the Sub-Andes fold-and-thrust belt, where

the Peruvian flat slab segment corresponds to thin-skinned deformation in the Sub-Andes.

2.2.2 Structural deflections

Structurally, deflections occur where the trend of the main spine changes in orientation, and very basically define segments of the Andes; called here, the Northern segment, the Peruvian segment and the Southern segment (Fig. 2.2). The Northern segment trends NE-SW and is bound to the north by the Caribbean Sea and the Huancabamba Deflection (6°S) in the south. Next is the Peruvian segment, trending NW-SE and is truncated to the south by the prominent Arica Deflection, (also called the Bolivian Orocline; 18°S), but within the segment contains the more subtle Abancay Deflection (13.5°S). The southernmost segment is the Chilean Segment which trends ~NNE-SSW and is continuous more or less for nearly 4000km, from 18°S to 52°S.

The Northern segment is the only segment where accretionary terranes are observed, which are of oceanic crust covered by flysch deposits, ranging in age from early Cretacous to early Tertiary (McCourt, 1984; DeSouza et al., 1984). The accreted terranes are separated from the Western Cordilleran rocks by suture zones. Otherwise, the geology of the Northern segment is basically continuous with the Peruvian Segment to the south. The Huancabamba Deflection at 6°S is expressed in the change of the strike of major fold axes of the Tertiary Marañon fold-and-thrust belt, and marks the location of the Cajamarca Fault zone (Cobbing et al., 1981).

The Peruvian segment is bounded by the Huancabamba deflection and the Arica Bend, and contains the Abancay deflection (~13.5ºS). The Abancay deflection marks a compositional boundary where the Precambrian basement (~2.0Ga) of the Arequipa massif, outcrops south of the Abancay deflection and may continue eastward at depth, but is not present north of the Abancay deflection (Cobbing et al., 1977; Cobbing et al., 1981). It also coincides with the location of the Nazca ridge as well as the sharp transition from flat slab to normal slab subduction discussed above. The strike of the Andean range changes orientation at the deflection, as well as the morphological change from the narrow zone of high topography to the wider central Andes, which contain the broad Altiplano-Puna Plateau.

Along the Southern, or Chilean segment, the strike of the range is structurally straight with no deflections, and is host to the other flat-slab zone, between 28 and 31ºS. This segment contains many of the same geologically continuous features as the Northern and Peruvian segments, a Western Cordillera which includes outcrops of the Coastal Batholith, the Paleozoic rocks of the Eastern Cordillera and an active fold-and-thrust belt of the Sub-Andes. However, in the Sub-Andean zone south of ~23°S, notably more Precambrian basement rocks have been brought to the surface by a thick-skinned style fold-and-thrust belt in the Santa Barbara System and the Sierra Pampeanas (Allmendinger and Gubbels, 1996; Kley et al., 1999), whereas the Sub-Andes in the Northern and Peruvian Segments display thin-skinned styles of fold-and-thrusting.

2.2.3 Morphological variations

One of the most striking features of the Andes is the Altiplano-Puna Plateau. Remarkably, the plateau averages over 4km of elevation, stretching for 1800km in length, up to 400km in width and is the largest continental plateau in a non-collisional orogen. Here, the Western and Eastern Cordilleras diverge, and flank either side of the Plateau. The central Andean region is also characterized by the prominent Arica Bend/Bolivian Orocline, which marks a concave bend in the oceanic trench as well as the shape of the orogen. To the north and south, the topography narrows considerably, the Eastern and Western Cordilleras converge, and they are characterized by a lower average elevation.

Explaining the unique morphology of the Andes has been the focus of much work over the last 30 years, where a variety of models have been suggested, and some include explanations for the existence of the tectonic segmentation as well, such as the flat slab segments. The first holistic model for the shape and growth of the Andes was that of Isacks et al. (1988), who postulated that increased crustal shortening due to normal angle subduction in the central Andes explained the high, thick, and broad crust of the Altiplano-Puna Plateau, as well as the existence of the Bolivian Orocline. In the model, the two segments of flat-slab subduction flanking the central Andes precluded plateau formation due to a lesser degree of crustal shortening and thinning. More recently, Capitanio et al. (2011) showed the difference in crustal thickness of the subducting oceanic lithosphere, which is age-dependent, is sufficient to produce

the topography and morphology observed in the Andes. The older subducting material of the central Andes drives traction toward the trench at the base of the upper plate, causing thickening as well as migration of the trench in that region.

Others have used climate to explain the morphology of the Andes. Montgomery et al. (2001) observed the elevation, width, and hypsometry of the Andes closely reflected the local degree of fluvial, glacial and tectonic processes, suggesting that climate is a first-order control on Andean morphology. Lamb and Davis (2003) postulated that the sediment-starved trench of the central Andes, due to more arid climate conditions, resulted in higher shear stresses between the subducting and overriding plate, causing crustal thickening that produced the Altiplano-Puna Plateau. Relatively more sediment in the northern and southern Andean trench allowed lower shear stresses, and thus less crustal thickening. I revisit these ideas, as well as others, in the context of the models for uplift of the Andean margin in the next section.

2.2.4 Climatic variations

As mentioned above, the modern climate in the Andes is highly variable; modern satellite imagery from the Tropical Rainfall Measuring Mission (TRMM) shows strong precipitation gradients from east-to-west, as well as a more subtle, but significant gradient north-to-south along the eastern flank of the Andes (Bookhagen and Strecker, 2008; Fig. 2.3). Precipitation amounts along the eastern flank of the

Andes are on the order of 400cm/yr, and drastically reduce to less than 50 cm/yr on the western flank, where some regions, notably the Atacama desert in southern Peru and northern Chile receives on average 0.3 - 1.5 cm of precipitation per year. In the Patagonian Andes, the precipitation gradient reverses, where the majority of precipitation comes from the Pacific Ocean to the west. The subpolar low pressure belt at approximately 60°S is more intense during the winter as ocean temperatures are on average higher than the continental temperatures, inducing air masses to move west and precipitate on the western flank of the Andes (Barros et al., 1979). Here, I describe in detail the modern climate patterns for the north-central Andes and do not include the Patagonian Andes in this discussion.

The main moisture source in South America is from the Atlantic Ocean to the east, along with recycled moisture from the Amazon Basin, as part of the South American Monsoon System (Eltahir and Bras, 1994; Vera et al., 2006). While the trade winds that bring moisture from the Atlantic Ocean are strong year-round, the warm season circulation over South American in the austral summer produces a monsoon that is responsible for the majority of precipitation received in the Andes. During the summer months, a warm-core anticyclone, the Bolivian High, develops over the Andes (Garreaud et al., 2003). To the east is an upper-level atmospheric trough that extends to the South Atlantic where the moisture sources are drawn. As a low pressure system develops inland, heating the continent and overlying airmass, (Zhou and Lau 1998; Nogués-Paegle et al. 2002), it controls moisture flux into the

eastern flank of the Central Andes by the low-level Andean jet (Salio et al., 2002). When the moisture-laden low-level flow travels from north to south, intense convective rainfall occurs along the eastern slopes of the Andes (Garreaud et al., 2003). The topography of the Andes produces the classic "orographic effect," where the heaviest precipitation occurs in a narrow band along the eastern flank of the Andes, and where the largest amount of rainfall is observed around 2km elevation (Bookhagen and Strecker, 2008).

As discussed earlier, many workers appreciated the asymmetry of the modern climate patterns, and noted the morphology of the Andes may be strongly controlled by these precipitation patterns (Masek et al., 1994; Montgomery et al., 2001; Lamb and Davis, 2003). Exactly when the modern moisture patterns developed is not well constrained, however, there is evidence from sedimentological records (Fig.ueiredo et al., 2009; Uba et al., 2009) and regional climate models (Ehlers and Poulsen, 2009; Poulsen et al., 2010) that the modern-day moisture patterns were established by the mid-to-late Miocene. Some studies suggest an increase in late Miocene-Pliocene sedimentation rates and precipitation amounts (Fig.ueiredo et al., 2009; Mulch et al., 2010). Without good constraints on the timing of development of the modern South American Monsoon system, as well as the paleoclimate on geologically relevant timescales, it is difficult to characterize the long-term effects climate has had on the evolution of the Andes. Further, it is exceptionally challenging to quantify paleoclimate and paleotopography independently; as topography and climate engage

in positive feedbacks (e.g. England and Molnar, 1990; Roe, 2005). Understanding the uplift of the Andes, with special attention to the uplift of the Altiplano-Puna plateau has been a major focus of the Earth Science community over the past 40 years, as it is crucial for our understanding of both the tectonic and climatic evolution of the orogen over geologic time.

2.3 Models of Andean Uplift

Despite long-lived subduction since the Jurassic, it is recognized that the modern topography of the Andes was generated in the Cenozoic (Isacks, 1988; Sempere, 1990; Allmendinger et al., 1997; Gregory-Wodzicki, 2000). Isacks' (1988) model of orogen formation suggests that the differing cross-sections of high topography along-strike are formed from differential shortening around the Arica Bend facilitated by localization of advective heat transfer in direct response to the geometry of the subducting plate. However, once crustal shortening estimates were better constrained, it was clear that shortening alone could not account for the thick crust of the Central Andes and the crustal volume of the Alitplano-Puna Plateau, and other mechanisms such as lower-crustal flow, delamination of the lower lithosphere, and addition of material through sedimentation and/or magmatism were proposed (Kay and Kay, 1993; Lamb and Hoke, 1997; Beck and Zandt, 2002; Husson and Sempere, 2003).

Some recent data suggests rapid uplift of the central Andes during the last 10Ma (e.g. Gregory-Wodzicki, 2000; Ghosh et al., 2006; Hoke et al., 2007; Quade et al., 2007; Schildgen et al. 2009, Garzione et al., 2008), calling for mechanisms that can support a rapid rise in elevation. For example, uplift simply by crustal thickening may likely happen gradually, over tens of millions of years. Thus, the "rapid rise" model (e.g. Garzione et al. 2008) for the Central Andes suggests removal of the gravitationally unstable lower lithosphere by delamination, and subsequent uplift by isostatic rebound. Schildgen et al. (2009), who also show a rapid signal of uplift by quantifying canyon incision along the Western Cordilleran flank of the Plateau, however, postulate delamination is unlikely in their field area, as the crust is thin and cold so close to the trench. They suggest that lower crustal flow outward from the Plateau is a more likely mechanism for the uplift they document.

Support for the lithospheric delamination model for uplift of the Altiplano comes from several paleoaltimetry techniques that are climate-sensitive, and thus have been met with some skepticism (Ehlers and Poulsen, 2009). These techniques include paleobotany physiognomy (Gregory-Wodzicki, 2000), soil carbonate $\delta^{18}O$ values (Garzione et al., 2006), clumped-isotope paleothermometry (Ghosh et al., 2006), and stable isotopes of mammalian teeth (Bershaw et al., 2010). These methods rely on the assumption that climate did not change during deposition of the paleoaltimetry proxies. If regional climate changed during the late Cenozoic, it would deplete the oxygen isotope concentration of paleoprecipitation throughout this time,

thus without taking these changes into account, paleoaltimetry reconstructions using stable isotopes may overestimate the uplift estimates significantly, by 1-2km (Ehlers and Poulsen, 2009). Certainly, as surface uplift occurs, it may drive climate change, but without independent knowledge of paleoclimate, or uplift, it cannot be ruled out that the signal of these studies could be due to climate change alone. Ehlers and Poulsen (2009) modeled regional climate change to test how the paleoclimate data would be affected, and determined that the error of the paleoaltimetry measurement due to paleoclimate uncertainty is too large to reasonably support the rapid rise model. Instead, they advocate a model for slower, more gradual uplift since Eocene time. Barnes and Ehlers (2009) review all known geologic and geophysical observations as well as quantitative data in order examine these two models in more detail, concluding that slower and more steady uplift since ~40Ma is more probable given the available literature.

In investigating these models for uplift of the Andes, two important caveats must be mentioned. First, as stated previously, it is difficult to deconvolve the relative contributions of climate and tectonics, as many quantitative techniques may capture ambiguous signals. The strong coupling of tectonics and climate in the Andes is a compelling idea, one that has been put forth by simple observations of orogen morphology, climate gradients and river steepness (Masek et al., 1994; Montgomery et al., 2001), spatial correlation of faster long-term exhumation rates with wetter modern climates (Barnes and Pelletier, 2006) and the correlation of eclogite

production of overthickened crust with erosion rates, where the higher erosion rates in the northern Andes inhibit eclogitization of the lower crust and thus delamination (Pelletier et al., 2010). While these studies only begin to address the tectonic-climate coupled models that control the morphology of the range, they are nonetheless provocative. Secondly, nearly all of the quantitative data that address models of uplift are taken from the central Andes, especially from the Bolivian Altiplano and the Argentine Puna Plateau. Any mechanism proposed as an explanation for the formation of the Andes must account for the along-strike morphologic, tectonic and climatic segmentation. Thus, one of the outstanding questions this dissertation work addresses is whether or not the dynamical mechanisms proposed to accommodate uplift and deformation of the central Andes apply more generally to the Andes as a whole. The general field area that is investigated in this dissertation work, are the north-central Peruvian Andes, defined here, between 5 and 12°S (Fig. 2.4).

2.4 Geology and Tectonics of the north-central Peruvian Andes

The geological setting of the Andes in Peru, from the oceanic trench to the Brazilian Shield, define three parallel major regions, the Western Cordillera, the Eastern Cordillera, and the Sub-Andes. In the north-central Peruvian segment of the Andes, from west to east these are i) the Coastal Batholith associated with Mesozoic volcanism which has intruded into Precambrian metamorphic rocks and is overlain by Cenozoic continental sediments and volcanics, ii) folded and faulted Precambrian-

Paleozoic low-grade metamorphic basement and minor intrusive rocks and iii) folded and faulted Mesozoic-Cenozoic marine and continental sedimentary deposits of the Sub-Andean fold-and-thrust belt (Fig. 2.5; James, 1971; Cobbing and Pitcher, 1972; Megard, 1984; Sebrier et al., 1988; Lamb and Hoke, 1997).

In the early-to-mid 20th century, exploration of the geology of Peru began; early workers studied the morphology and geology of the range, and its geography relevant to human activity, transportation and resource potential (Bowman, 1906; McLaughlin, 1924; Steinmann, 1929; Weeks, 1948; Carey, 1955). By examining stratigraphic relationships in the rock record and geomorphic surfaces, it was recognized that Peru had experienced periods of intense deformation and surface uplift. An enigmatic feature described by McLaughlin (1924), was a nearly flat surface at 4200-4400m.a.s.l in south-central Peru, which he called the Puna surface. Other regionally extensive, planar topographic surfaces were mapped and eventually led workers to conclude that the Peruvian Andes had undergone three pulses of deformation in the Late Mesozoic and Cenozoic time; the first in the Late Cretaceous, the second in the early-to-mid Tertiary and the third in the late Tertiary (Bowman, 1916; McLaughlin, 1924; Steinmann 1929). Assigning ages, even approximate, to the stratigraphy of the Western and Eastern Cordilleras was a difficult task, due to the paucity of fossils. As geochronologic methods including the K-Ar and U-Pb systems became increasingly reliable in the 1970's, as well as the developing understanding of the Andean orogen in a plate tectonic context (i.e. James, 1971), the chronology and

ages of igneous rock units, geomorphic surfaces, deformation and uplift events were better constrained and characterized throughout the following two decades (e.g. Stewart et al., 1974; Farrar and Noble, 1976; McKee et al., 1975; Noble et al., 1975; Wilson, 1975; Noble et al., 1978; Tosdal et al., 1981; Tosdal et al., 1984; Megard et al., 1984; 1985; Mukasa, 1986; Sebrier et al., 1988; Noble et al., 1990).

2.4.1 General Geology of the Peruvian Andes

Here I describe the basic geology from the coast of Peru in the west to the Brazilian craton to the east, which consists of parallel morphotectonic elements including the forearc, batholithic rocks and volcanics of the Western Cordilera, the Paleozoic-Mesozoic rocks of the Eastern Cordillera and the Sub-Andean basins and fold-and-thrust belt (Fig. 2.5). The forearc includes the submerged Andean slope and the emergent coast. They are bordered to the east by the Coastal Batholith and to the west by the Peru-Chile trench. The forearc basins are filled with Jurassic-early Tertiary marine and continental sedimentary deposits; these include the Talara, Sechura, Trujillo, Yauquina, Salaverry, Lima, East Pisco, West Pisco, Caballas, Mollendo, and Moquegua Basins (Dunbar, 1990). South of the Abancay Deflection (~13.5°S) the forearc basins are mainly filled with Oligocene through Holocene shallow marine and continental alluvium interspersed with ignimbrites of the same age range. This southern region of Western Peru is also host to abundant Quaternary

volcanic rocks, mainly andesite and rhyolite, but these units are not present north of the Abancay Deflection, due the absence of active volcanism.

The steep westward slope of the Western Cordillera from the forearc marks the transition to the Coastal Batholith, which crops out, about 50km wide, along the entire western margin of Peru, and is overlain by Cenozoic volcanics and sedimentary deposits. The Coastal Batholith is composed of 1000+ plutons of mainly granodiorite and tonalite, ranging in age from 100-34Ma, although the bulk of emplacement occurred in the mid-late Cretaceous (Giletti and Day 1968; Pitcher, 1978; Cobbing et al., 1981). Bussell and Pitcher (1985) described the different lithologies in detail and also suggested that the magmas rose everywhere to a similarly shallow crustal level independent of the time of emplacement. Haederle and Atherton (2002) suggested that the melts ascended to within 2 to 3 km of the surface up dyke-like conduits, then spread laterally to form thin tabular plutons. Younger plutons are observed east of the Coastal Batholith, representing eastward migration of the locus of magmatism. The youngest magmatism in Peru is the late Miocene-Pliocene Cordillera Blanca Batholith (CBB). Unlike the Coastal Batholith, which is continuous for 1600km, the CBB outcrops only between 9 and 10°S, about 50km east of the Coastal Batholith. Rock types of the CBB are of trondhjemite-tonalite-dacite suites, and geochemical evidence suggest a different source of melting than the Coastal Batholith, from recently underplated basaltic crust (Atherton and Petford, 1993). The CBB is topographically the highest chain in Peru, characterized by very fast uplift

accommodated by the Cordillera Blanca Detachment System (McNulty et al., 1998; McNulty and Farber, 2002).

East of the Western Cordillera lies the deformed Precambrian-Paleozoic rocks of the Eastern Cordillera. These are primarily shales, sandstones, and carbonates with thicknesses of 10-15km, where low-grade metamorphism of greenschist facies is common (Megard, 1987). Late Paleozoic plutonic bodies and volcanic rocks are widespread in the Eastern Cordillera, but volumetrically minor, compared to the Cretaceous Coastal Batholith. The volcanic signature is of alkaline, peralkaline and shoshonitic lavas, characteristic of a continental rift setting (Noble et al., 1978). The boundary between the Western and Eastern Cordilleras in the Peruvian Andes changes along-strike, specifically at ~12ºS. North of this, the Marañon fold-and-thrust belt roughly denotes the boundary between the Mesozoic-Cenozoic rocks of the Western Cordillera, and the Precambrian-Paleozoic basement of the Eastern Cordillera (Megard, 1987). South of ~12ºS, the Eastern and Western Cordilleras are separated by the northern tip of the Altiplano Plateau. The Plateau is an internally drained basin, consisting of Mesozoic and Cenozoic clastic sedimentary rocks, up to 15km thick, derived from the surrounding Western and Eastern Cordilleras (Newell, 1949). Cenozoic calc-alkaline and andesitic rocks occur on the Altiplano and western flank of the Eastern Cordillera (Megard, 1987).

Finally, to the east of the Eastern Cordillera is the Sub-Andean fold-and-thrust belt. In most places along Peru, the boundary between these two zones is marked by

Mesozoic shallow marine sedimentary rocks which flank the Paleozoic basement of the Eastern Cordillera. The SubAndes include the Late Miocene-Pliocene fold-and-thrust belt, which is characterized by thin-skinned tectonics, varying in width between 100 to 150km between 3 and 8ºS, and is only 50km wide at 11ºS (Megard, 1984). Seismic profiling around 5 - 7ºS indicates it consists of a major sole-thrust that is horizontal and located around 9-10km depth at the top of the Paleozoic basement, to which all faults are connected (Megard, 1987; Hermoza et al., 2005).

2.4.2 Tectonic Chronology of the Peruvian Andes

From this great effort of geologic mapping, stratigraphy, and dating of volcanic and magmatic rocks over the 20th century, emerged a tectonic model for the Peruvian Andes that divided the orogenic evolution into three time periods, i) the pre-Andean period of the Precambrian-Paleozoic, ii) the pre-orogenic Andean period, occurring during most of the Mesozoic, and iii) the Andean orogenic period, from the late Cretaceous through the present (Megard, 1987). The pre-orogenic Andean period today is preserved in Proterozoic cratons of the South American shelf, Precambrian-Paleozoic metamorphic basement rocks of the Western and Eastern Cordillera, and a small Paleozoic terrane of the very northern tip of Peru at ~4.5ºS, which is thought to be an exotic terrane accretion (Mourier et al., 1986). The Arequipa massif of Southern Peru is the oldest Precambrian rocks of the Andes, and are 2Ga granulites that outcrop only in the Western Cordillera (~16-18ºS). The major Paleozoic tectonic events

include the Hercynian orogeny in the Carboniferous, which created a 200m wide fold-and-thrust belt, then switched to a tensional regime by the late Permian, where it is believed a continental rift formed (Noble et al., 1978; Kontak et al., 1985). During the Mesozoic, "pre-orogenic Andean period," the Peruvian Andes were dominated by shallow marine and terrestrial sequences in basin development. Between 7 and 13.5ºS, two basins developed on either side of the Marañon anticline in what is today the Eastern Cordillera, the Western Peruvian Trough and the Eastern Peruvian Trough. By the Upper Cretacous, the magmas of the Coastal Cordillera were being emplaced west of the Marañon anticline, in an oceanic basin, floored by thin, ensialic crust (Atherton et al., 1983;1985).

Importantly, it became clear from stratigraphic and geologic evidence, the modern Andes formed during the Cenozoic, despite subduction since the Jurassic. Starting with Steinmann's (1929) early observations and modified later (i.e. McKee and Noble, 1982; Megard et al., 1984), a view emerged that the Peruvian Andes experienced short-lived phases (on the order of 100ky-1my) of intense tectonism, separated by periods of quiescence during the Cenozoic "Andean orogenic" period. The first major phase of deformation recognized within the Peruvian Andes, the 'Peruvian phase' began ~85-70Ma, affecting the Precambrian-Paleozoic rocks of the Eastern Cordillera and was coincident with intense volcanism along the entire Andean arc as well as emplacement of the Coastal Batholith (Megard, 1978). The deformation front propagated eastward in the Paleocene-Eocene 'Incaic phases' (I and II) which

affected the Eastern Cordillera and produced the Marañon fold-and-thrust belt in north-central Peru, and is commonly considered the main phase of shortening in the Peruvian Andes (Steinmann, 1929; McKee and Noble, 1982; Megard et al., 1984). Erosional surfaces believed to have formed contemporaneously with Incaic-aged uplift are reported (McLaughlin, 1929; Noble et al., 1974; Tosdal et al., 1984; Noble et al., 1990). Based on radiometric ages of volcanic rocks unconformably overlying these erosional surfaces, the Incaic phase was divided into the Incaic I and II phases by Bussell (1983), McKee (1990) and Noble et al. (1985).

The Incaic I event is poorly constrained but Bussell (1983) and Noble et al. (1985) assign an early Tertiary age. It was most likely caused by a change in the convergence direction of the South American and the Farallon plates from north and/or north-northeast to northeast (Pardocasas and Molnar, 1987). The Incaic II phase was the result of intensified compressional deformation (Farrar et al., 1988; Horton et al., 2001; McQuarrie and DeCelles, 2001), and assigned a Paleocene or early Eocene age (Bussell, 1983). It is suggested that the Incaic II event is somehow linked to a major reorganization of the motion of the Pacific plate which is recorded by the Hawaiian-Emperor Elbow (Gordon and Jurdy, 1986). This phase produced isoclinal and locally recumbent folds and imbricate thrust faults in central and northern Peru (Megard, 1984), as well as the unroofing of Late Cretaceous and early Paleogene aged plutons (Noble et al., 1978). Stratigraphic details and radiometric ages of volcanic rocks that overlie this Incaic II unconformity demonstrate that the

deformation was essentially completed prior to 41 Ma (Noble et al., 1979). Small volumes of volcanics are present above the dated horizons; and only few intrusive bodies with ages between ~35 and ~25 Ma are known from northern or central Peru (Cobbing et al., 1981; Noble et al., 1990; Soler and Bonhomme, 1987, 1990) indicating that the interval between the late Eocene and the late Oligocene was a period of tectonic and magmatic quiescence (Baker and Francis, 1978; McKee et al., 1990; Petersen, 1958).

Following the Paleocene-Eocene Incaic phases are the Miocene-Pliocene 'Quechua phases' (I, II, and III), resulting in crustal thickening and uplift (Megard, 1984; Sebrier et al., 1988; Noble et al., 1990). The extent of the "Quechua I" is loosely bracketed between 21.5 and 12.5Ma; in some localities between 21.5 and 17Ma by McKee and Noble (1982). Structures related to this tectonic pulse, monoclinal folds and reverse faults, appear to have reactivated some of the Incaic structures of the Western Cordillera and affect part of the Eastern Cordillera (Megard, 1987). This reactivation led to uplift of 400m (Sebrier et al., 1988) and triggered large scale incision (Sebrier et al., 1988; Sebrier et al., 1979; Tosdal et al., 1984; Tosdal et al., 1981). Valleys were cut to approximately their present depth in central Peru (Noble et al., 1990) as well as in southern Peru (Tosdal et al., 1981). The "Quechua II" event lasted from ~10 to ~8 Ma (Megard et al., 1984; Sebrier and Soler, 1991) and marked the transfer of active deformation eastward (Jaillard et al., 2000). In basins in the Eastern Cordillera, the Quechua II phase is recorded as dextral slip along

northwest-southeast trending faults. Prior and contemporaneously to the Quechua II phase paleo-valleys were filled and mantled by sheets of ignimbrites. Their radiometric ages (K/Ar) range from 14.2 Ma to 8.9 Ma in the south (Noble et al., 1990; Thouret et al., 2005; Tosdal et al., 1981) and from 10.2 to 8 Ma in the north (Farrar and Noble, 1976; McKee et al., 1986; Noble et al., 1984). Finally, the contractional "Quechua III" phase took place 7-4 Ma and is the result of east-west shortening, documented along the whole Andean chain, giving rise to the SubAndean fold-and-thrust belt.

In summary, the 20th century view of the tectonics of the modern Peruvian Andes is that they formed in the latest Mesozoic through Cenozoic, consisting of emplacement of the Coastal Batholith in the Late Cretaceous Peruvian phase, intense compressive deformation, including the formation of the Marañon fold-and-thrust belt of the Eocene Incaic phase, and the Quechua phases that uplifted much of the Eastern Corilldera, and formed the Sub-Andean fold-and-thrust belt, . While this view provides the backbone of our understanding of Andean tectonics, recent work has modified these findings, providing better constraints of timing, and illuminated more complexities in the range. For example, emerging evidence from geochronologic techniques, paleomagnetism and modern-day GPS data indicate the Western Cordilleran forearc has been subjected to active deformation accommodated along faults, and recent landscape modification, notably with high rates of canyon incision, perhaps as a response to late Miocene through recent uplift (Armijo and Thiele, 1990;

Audin et al., 2003; Gonzalez et al., 2003; Allmendinger et al., 2005a, 2005b; Gonzalez et al., 2006; Schildgen et al., 2007; Hall et al., 2012). Other quantitative techniques, low temperature thermochronology of the (U-Th)/He system and fission tracks, are used by several to quantify rates of exhumation in the Western and Eastern Cordilleras of Peru (Laubacher and Naeser, 1994; Garver et al., 2005; Wipf, 2006; Schildgen et al., 2007; Giovanni, 2007), which this thesis contributes to. Taken together, the studies in the past decade show that the Late Miocene through present is an important time period to the tectonic development and uplift of the Andes.

Despite the major structural, geophysical, morphological and climatic variation and segmentation occurs drastically along-strike, an emerging view of Andean tectonics suggests that the orogen has experienced major uplift and continuous deformation since the late Miocene. However, outstanding problems remain. How do prior inherited crustal homogeneities or features from the pre-Andean orogenic period play a role in the segmentation observed today? How does range segmentation play a role in the timing and mechanisms that accommodate deformation and uplift? How do the coupling of tectonics and climate influence the formation of the topography? How do the north-central Peruvian Andes compare to models proposed for Altiplano uplift, and how does this influence our view of Andean orogensis?

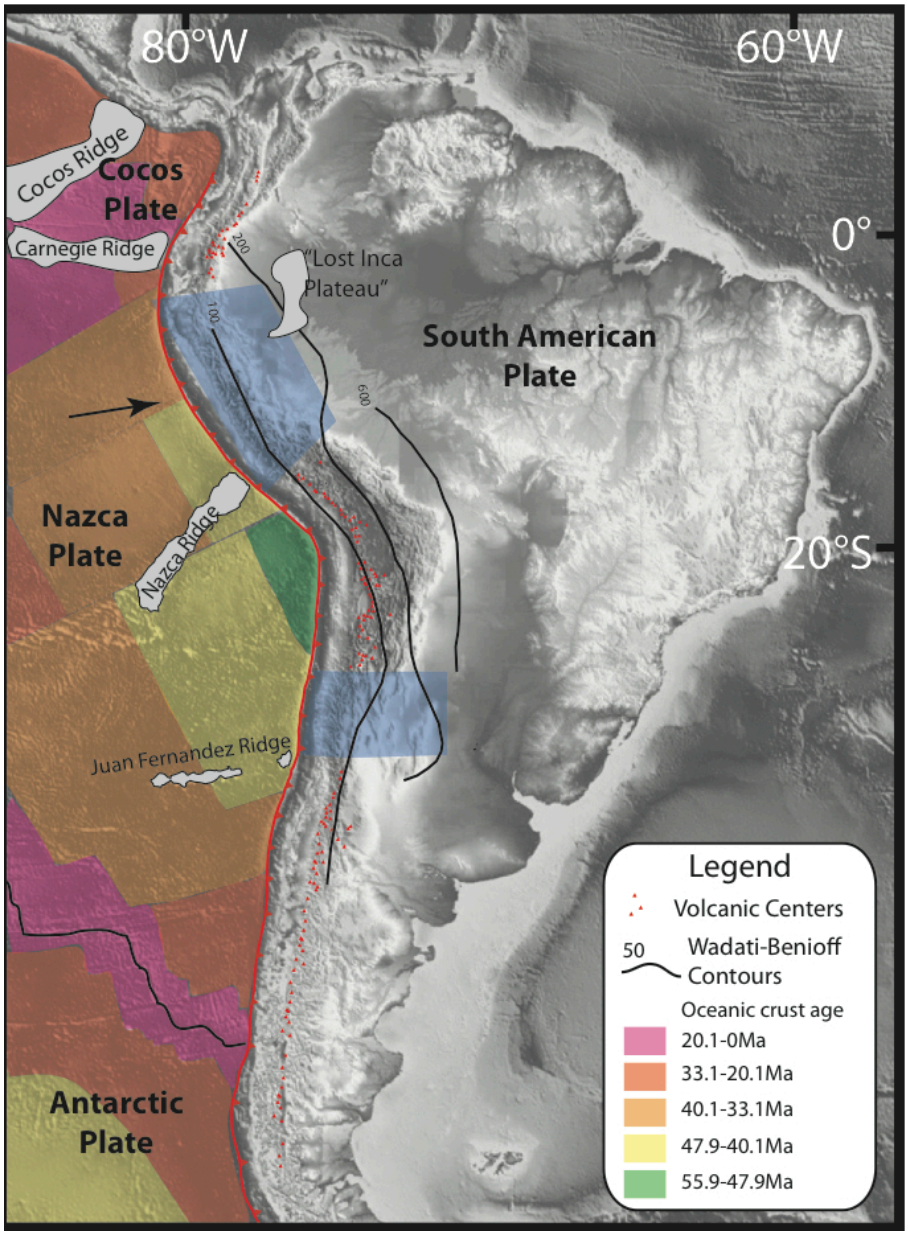

Figure 2.1 shows the tectonic features and segmentation along the margin of South America. Adapted from Allmendinger, 1997; Gutscher et al., 1999; Wipf, 2006.

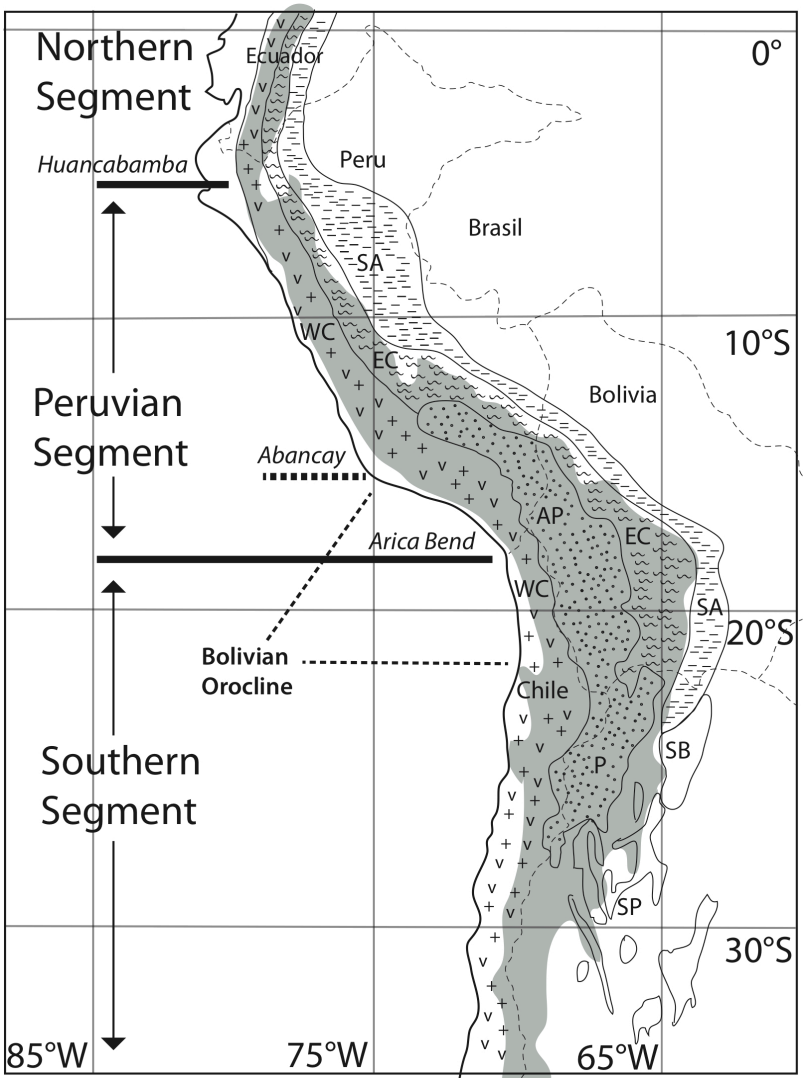

Figure 2.2 is a morphostructural map of South America. Deflections are labeled by horizontal lines. WC=Western Cordillera; EC=Eastern Cordillera; AP=Altiplano; P=Puna Plateau; SA= SubAndes; SB=Santa Barbara Thrust System; SP=Sierra Pampenas Thrust System. Modified from Gregory-Wodziki, 2000; Garver et al., 2005.

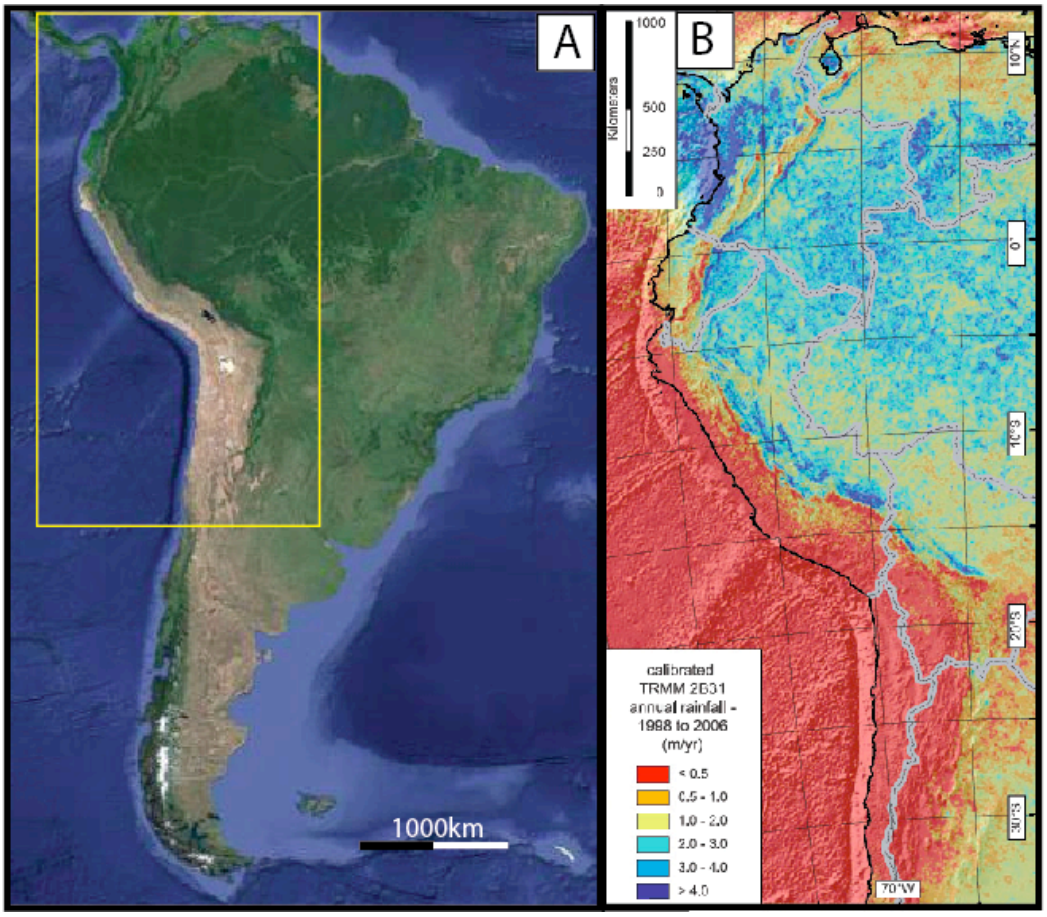

Figure 2.3.A shows satellite imagery from Google Earth depicting the modern patterns of vegetation, which are correlated with general climate. The yellow box describes the area presented in 2.3B, from Bookhagen et al., 2008, showing satellite-derived precipitation date from the Tropical Rainfall Measuring Mission.

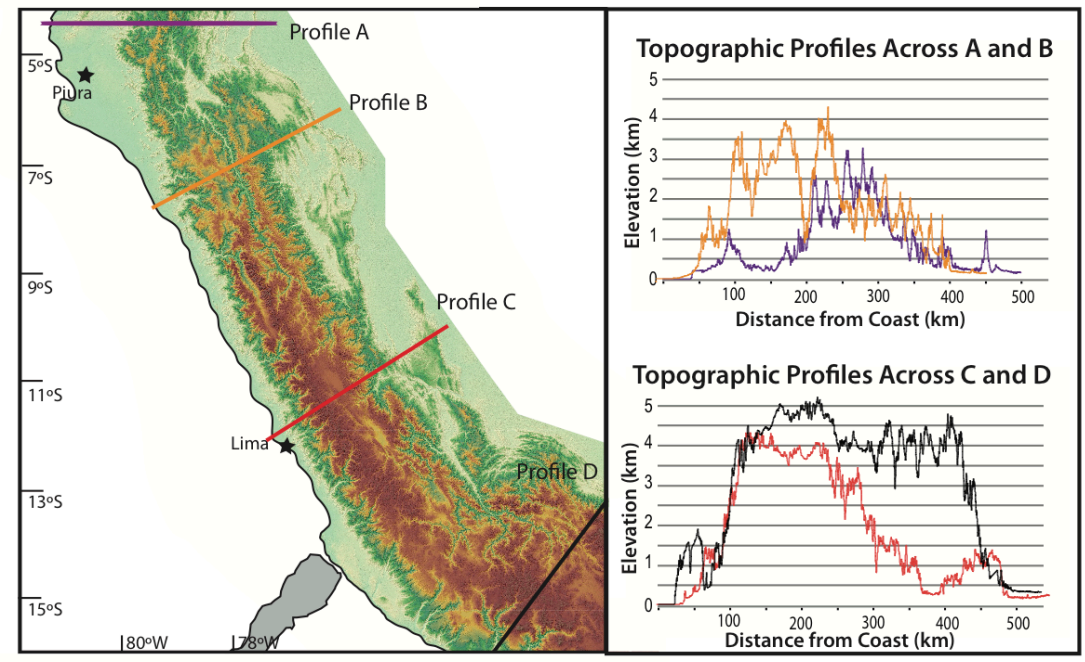

Figure 2.4 shows four general topographic profiles extracted across the Peruvian Segment of the Andes, perpendicular to strike, showing the general morphological changes along this segment.

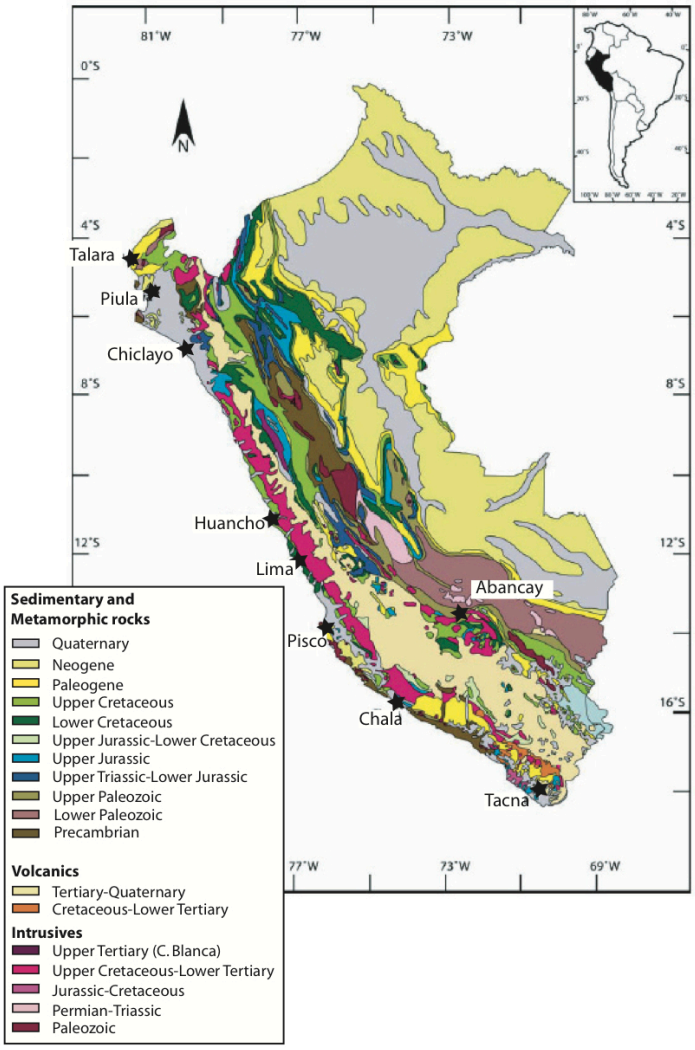

Figure 2.5 Geologic map of Peru. From Wipf, 2006.

2.5 References

Allmendinger, R.W., and Grubbels, T., 1996. Pure and simple shear plateau uplift, Altiplano-Puna, Argentina and Bolivia, Tectonophysics, 259, 1-13.

Allmendinger, R.W., Jordan, T.E., Kay, S.M. and Isacks, B.L., 1997. The evolution of the Altiplano-Puna plateau of the Central Andes. Annual Review Of Earth and Planetary Sciences, 25: 139-174.

Allmendinger, R.W., Smalley, R., Bevis, M., Caprio, H., and Brooks, B., 2005. Bending the Bolivian orocline in real time. Geology, 33(11), 905-908.

Atherton, M.P., and Petford, N., 1993. Generation of sodium-rich magmas from newly underplated basaltic crust. Nature, 362, 144-146.

Atherton, M.P., Warden, V., and Sanderson, L.M., 1985, The Mesozoic marginal basin of Central Peru: A geochemical study of within-plate-edge volcanism, in Pitcher, W.S., Cobbing, E.J., and Beckinsale, R.D., eds., Magmatism at a Plate Edge: The Peruvian Andes: London, Blackie Halsted Press, p. 47-58.

Barnes, J.B., and Pelletier, J.D., 2006. Latitudinal variation of denudation in the evolution of the Bolivian Andes, American Journal of Science, v. 306, 1-31.

Baker, M.C.W., and Francis, P.W., 1978, Upper Cenozoic Volcanism in Central Andes -Ages and Volumes: Earth and Planetary Science Letters, v. 41, p. 175-187.

Barazangi, M., and Isacks, B.L., 1976, Spatial-Distribution of Earthquakes and Subduction of Nazca Plate beneath South-America: Geology, v. 4, p. 686-692.

Bevis, M., 1986, The Curvature of Wadati-Benioff Zones and the Torsional Rigidity of Subducting Plates: Nature, v. 323, p. 52-53.

Beck, S.L. and Zandt, G., 2002. The nature of orogenic crust in the central Andes. Journal Of Geophysical Research-Solid Earth, 107(B10).

Bookhagen, B., and Strecker, M. R., 2008. Orographic barriers, high-resolution TRMM rainfall, and relief variations along the eastern Andes: Geophysical Research Letters, 35(6), doi: 10.1029/2007GL032011.

Bowman, I. 1906. The Andes of southern Peru´ , Geological reconnaissance along the 73 meridian. Am. Geogr. Soc. Spec. Publ. 1, 336 p.

Bowman, I., 1916. The Andes of Southern Peru, American Geographical Society, NY, 336p.

Bussell, M.A., 1983, Timing of tectonic and magmatic events in the Central Andes of Peru, v. 140, p. 279-286.

Bussell, M.A. and Pitcher, W.S., 1985. The structural control of batholith emplacement, *in* Atherton, M.P., Cobbing, E.J., and Beckinsale, R.D., eds., Magmatism at a Plate edge: The Peruvian Andes: Glasgow, 167-176.

Cahill, T.A. and Isacks, B.L., 1992. Seismicity and shape of the subducted Nazca Plate. Journal of Geophysical Research, 97(12), 17,503-17,529.

Carey, S.W., 1958. A tectonic approach to continental drift. In: Carey, S.W. (Ed.), Continental drift. A symposium. Hobart, Tasmania, pp. 177±355.

Cobbing, E.J., Ozard, J.M, and Snelling, N.I., 1977. Reconnaissance geochronology of the crystalline basement rocks of the Coastal Cordillera of southern Peru. Bulletin of the Geological Society of America (88), 241-246.

Cobbing, E.J., Pitcher, W.S., Wilson, J.J., Baldock, J.W., Taylor, W.P., McCourt, W.J., and Snelling, N.J., 1981. The geology of the western Cordillera of Northern Peru, Overseas Memoir of the Institute of Geological Sciences London, 5, 143 p.

De Souza, H.A., Espinosa, A., and Delaloye, M., 1984. K-Ar ages of basic rocks in the Patia valley southwest Colombia, Tectonophysics, 107, 135-145.

Dunbar, R.B., Marty, R.C., and Baker, P.A., 1990, Cenozoic Marine Sedimentation in the Sechura and Pisco Basins, Peru: Palaeogeography Palaeoclimatology Palaeoecology, v. 77, p. 235-261.

Farrar, E., Clark, A.H., Kontak, D.J., and Archibald, D.A., 1988, Zongo-San Gaban Zone Eocene Foreland Boundary of the Central Andean Orogen, Northwest Bolivia and Southeast Peru: Geology, v. 16, p. 55-58.

Farrar, E., and Noble, D.C., 1976, Timing of Late Tertiary Deformation in Andes of Peru: Geological Society of America Bulletin, v. 87, p. 1247-1250. 33

Fukao, Y., Yamamoto, A., and Kono, M., 1989. Gravity anomaly across the Pervian Andes, Journal of Geophysical Research, 943867-3890.

Garzione, C.N., Molnar, P., Libarkin, J.C. and MacFadden, B.J., 2006. Rapid late Miocene rise of the Bolivian Altiplano: Evidence for removal of mantle lithosphere. Earth And Planetary Science Letters, 241(3-4): 543-556.

Garzione, C.N., Hoke, G.D., Libarkin, J.C., Withers, S., MacFadden, B., Eiler,J., Ghosh, P., Mulch, A., 2008. Rise of the Andes, Science, 320, 1304-1307.

Gephart, J.W., 1994. Topography And Subduction Geometry In The Central Andes - Clues To The Mechanics of a noncollisional orogen. Journal Of Geophysical Research-Solid Earth, 99(B6): 12279-12288.

Giletti, B.J.and Day, H.W., 1968. Potassium-argon ages of igneous intrusive rocks of Peru, Nature, 220, 570-572.

Garver, J.I., Reiners, P.W., Walker, L.J., Ramage, J.M., and Perry, S.E., 2005, Implications for timing of Andean uplift from thermal resetting of radiation damaged zircon in the Cordillera Huayhuash, northern Peru: Journal of Geology, v. 113, p. 117-138.

Gordon, R.G., and Jurdy, D.M., 1986, Cenozoic global plate motions: Journal of Geophysical Research, v. 91, p. 12389-12406.

Gutscher, M.A., Olivet, J.L., Aslanian, D., Eissen, J.P., and Maury, R., 1999, The "Lost Inca Plateau": cause of flat subduction beneath Peru?: Earth and Planetary Science Letters, v. 171, p. 335-341.

Gregory-Wodzicki, K.M., 2000. Uplift history of the Central and Northern Andes: review. Geological Society of America Bulletin, 112(7): 1091-1105.

Gutscher, M.A., 2002. Andean subduction styles and their effect on thermal structure and interplate coupling. Journal of South American Earth Sciences, 15(1): 3-10.

Jaillard, E., Herail, G., Monfret, T., and Diaz Martinez, E., 2000, Tectonic evolution of the Andes of Equador, Peru, Bolivia and northernmost Chile In: Tectonic

evolution of South America, in Cordani Umberto, G., Milani Edison, J., and Thomaz Filho, A., eds., Tectonic Evolution of South America, In-Folo Producao Editorial Grafica e Programacao Visual. Rio de Janeiro Brazil. 2000., p. 481-559.

Hoke, G.D., Isacks, B.L., Jordan, T.E., Blanco, N, Tomlinson, A.J., and Ramezani, J., 2008. Geomorphic evidence for post-10 Ma of the western flank of the central Andes 18°30'-22°S

Hoke, G.D., and Garzione, C.N., 2008. Paleosurfaces, paleoelevation, and the mechanisms for the late Miocene topographic development of the Altiplano plateau, Earth and Planetary Science Letters, 271, 192-201.

Haederle, M., and Atherton, M.P., 2002, Shape and intrusion style of the Coastal Batholith, Peru: Tectonophysics, v. 345, p. 17-28.

Hasegawa, A., and Sacks, I.S., 1981, Subduction of the Nazca Plate beneath Peru as Determined from Seismic Observations: Journal of Geophysical Research, v. 86, p. 4971-4980.

Horton, B., Hampton, B., and Wanders, G., 2001. Paleogene synorogenic sedimentation in the Altiplano plateau and implications for the initial mountain building in the central Andes, Geological Society of America Bulletin, 113, 1387-1400.

Husson, L. and Sempere, T., 2003. Thickening the Altiplano crust by gravity-driven crustal channel flow. Geophysical Research Letters, 30(5).

Isacks, B.L., 1988. Uplift of the Central Andean plateau and bending of the Bolivian orocline. Journal Of Geophysical Research-Solid Earth And Planets, 93(B4): 3211-3231.

James, D.E., 1971a. Andean Crustal and Upper Mantle Structure, Journal of Geophysical Research, 76(4), 3246-3271.

James, D.E., 1971b. Plate-tectonic model for the evolution of the central Andes, Geological Society of America Bulletin (82): 3325-3346.

Jordan, T.E., Isacks, B.L., Ramos, V.A., and Allmendinger, R.W., 1983. Mountain Building in the Central Andes, Episodes, 20-26.

Kay, R., and Kay, S., 1993. Delamination and delamination magmatism, Tectonophysics, 219, 177-189.

Kley, J., 1999. Geologic and geometric constrains on a kinematic model of the Bolivian orocline, Journal of South American Earth Sciences, v. 12, 221-235.

Kley, J., Monaldi, C.R., and Salfiity, J.A., 1999. Along-strike segmentation of the Andean foreland: Causes and consequences, Tectonophysics, 310, 75-94.

Lamb, S., and Davis, P., 2003. Cenozoic climate change as a possible cause for the rise of the Andes, Nature, 425(23).

Lamb, S., and Hoke, L., 1997. Origin of the high plateau in the Central Andes, Bolivia, South America, Tectonics, 16(4), 623-649.

Laubacher, G. and Naese, C.W., 1994. Fission-track dating of granitic-rocks from the Eastern Cordillera of Peru – Evidence for late Jurassic and Cenozoic cooling, Journal of the Geological Society, 151, 473-483.

McCourt, W.J., Aspden, J.A., and Brook, M., 1984. New geological and geochronological data from the Colombian Andes – Continental growth by multiple accretion, Journal of the Geological Society, 141, 831-845.

McKee, E.H. and Nobel, D.C., 1982. Miocene volcanism and deformation in the Western Cordillera and High Plateaus of South-Central Peru, Geological Society of America Bulletin, 93, 657-662.

McLaughlin, D.H., 1924. Geology and physiography of the Peruvian cordillera, Departments of Junin and Lima. Geological Society of American Bulletin, 35: 591-632.

McNulty, B.A., Farber, D.L., Wallace, G.S., Lopez, R., and Palacios, O., 1998. Role of plate kinematics and plate-slip-vector partitioning in continental magmatic arcs: Evidence from the Cordillera Blanca, Peru, Geology 26(9), 827-830.

Noble, D.C., McKee, E.H., Eyzaguirre, V.R., and Marocco, R., 1984a, Age and Regional Tectonic and Metallogenetic Implications of Igneous Activity and Mineralization in the Andahuaylas-Yauri Belt of Southern Peru: Economic Geology, v. 79, p. 172-176.

Noble, D.C., McKee, E.H., Farrar, E., and Petersen, U., 1974, Episodic Cenozoic Volcanism and Tectonism in Andes of Peru: Earth and Planetary Science Letters, v. 21, p. 213- 220.

Noble, D.C., McKee, E.H., and Megard, F., 1978, Eocene Uplift and Unroofing of Coastal Batholith near Lima, Central Peru: Journal of Geology, v. 86, p. 403-405.

Noble, 1979b, Early Tertiary Incaic Tectonism, Uplift, and Volcanic Activity, Andes of Central Peru: Geological Society of America Bulletin, v. 90, p. 903-907.

Noble, D.C., McKee, E.H., Mourier, T., and Megard, F., 1990, Cenozoic Stratigraphy, Magmatic Activity, Compressive Deformation, and Uplift in Northern Peru: Geological Society of America Bulletin, v. 102, p. 1105-1113.

Noble, D.C., Sebrier, M., Megard, F., and Mckee, E.H., 1985, Demonstration of 2 Pulses of Paleogene Deformation in the Andes of Peru: Earth and Planetary Science Letters, v. 73, p. 345-349.

Megard, F., 1984. The Andean orogenic period and its major structure in central and northern Peru. Geological Society of London, 141, 893-900.

Montgomery D.R., Balco, G., and Willett, S.D., 2001. Climate, tectonics, and the morphology of the Andes, Geology, 29(7), 579-582.

Mckee, E.H., and Noble, D.C., 1982, Miocene Volcanism and Deformation in the Western Cordillera and High Plateaus of South-Central Peru: Geological Society of America Bulletin, v. 93, p. 657-662.

McKee, E.H., Noble, D.C., Ericksen, G.E., Pinochet, M.T., and Reinemund, J.A., 1990, Cenozoic tectonic events, magmatic pulses, and base- and precious-metal mineralization in the Central Andes In: Geology of the Andes and its relation to hydrocarbon and mineral resources, Circum-Pacific Council for Energy and Mineral Resources. Houston TX United States. 1990 35

McKee, E.H., Noble, D.C., and Vidal, C., 1986, Timing of Volcanic and Hydrothermal Activity, Huancavelica Mercury District, Peru: Economic Geology, v. 81, p. 489-492.

McLaughlin, D.H., 1924, Geology and physiography of the Peruvian cordillera, Departments of Junin and Lima: Geological Society of America Bulletin, v. 35, p. 591-632.

McLaughlin D.H., 1929, Review of Steinmann, G: Geologie von Peru-Heidelberg, Carl Winters Universitätsbuchhandlung, 448p.: Economic Geology, v. 24, p. 664-669.

McNulty, B., and Farber, D., 2002, Active detachment faulting above the Peruvian flat slab:Geology, v. 30, p. 567-570.

McQuarrie, N., and DeCelles, P., 2001, Geometry and structural evolution of the central Andean backthrust belt, Bolivia: Tectonics, v. 20, p. 669-692.

Megard, F., 1978, Etude géologique des Andes du Péroucentral: Mémoirs ORSTOM, v. 86, p. 310.

Megard, 1984, The Andean Orogenic Period and Its Major Structures in Central and Northern Peru: Journal of the Geological Society, v. 141, p. 893-900.

Mukasa, S.B., 1986, Zircon U-Pb Ages of Super-Units in the Coastal Batholith, Peru - Implications for Magmatic and Tectonic Processes: Geological Society of America Bulletin, v. 97, p. 241-254.

Muller, R.D., Roest, W.R., Royer, J.Y., Gahagan, L.M., and Sclater, J.G., 1997, Digital isochrons of the world's ocean floor: Journal of Geophysical Research-Solid Earth, v. 102, p. 3211-3214.

Newell, N.D., 1949. Geology of the Lake Titicaca region, Peru and Bolivia. Geological Society of America Memoir, 36, 111p.

Nobel, D.C., McKee, E.H., Mourier, T., and Megard, F., 1990. Cenozoic stratigraphy, magmatic activity, compressive deformation, and uplift in northern Peru, Geological Society of American Bulletin, 102, 1105-1113.

Norabuena, E., Leffler-Griffin, L., Mao, A., Dixon, T., Stein, S., Sacks, I.S., Ocola, L., and Ellis, M., 1998. Space geodetic observations of Nazca-South America convergence across the Central Andes. Science. 279(5349): 358-362.

Pitcher, W.S., 1978. The anatomy of a batholith. Journal of the Geological Society,

135, 157-182. Pardocasas, F., and Molnar, P., 1987, Relative Motion of the Nazca (Farallon) and South-American Plates since Late Cretaceous Time: Tectonics, v. 6, p. 233-248.

Petersen, U., 1958, Structure and uplift of the Andes of Peru, Bolivia, Chile and adjacent Argentina: Sociedad Geológica del Perú, v. 33, p. 57-129.

Sebrier, M., Lavenu, A., Fornari, M., and Soulas, J.P. 1988. Tectonics and uplift in Central Andes (Peru, Bolivia, and Northern Chile) from Eocene to present. Géodynamique. 3(1-2), 85-106.

Sempere, T., Hérail, G., Oller, J. and Bonhomme, M.G., 1990. Late Oligocene Early Miocene major tectonic crisis and related basins in Bolivia. Geology, 18(10): 946-949.

Sacks, I.S., 1983, The Subduction of Young Lithosphere: Journal of Geophysical Research, v. 88, p. 3355-3366.

Sebrier, M., Marocco, R., Gross, J.J., Macedo, S., and Montoya, R., 1979, Evolucióннéeogena del piedemonte Pacifico de los andes del surdel Péru, Segundo Congresso GeologicóChileno: Arica, p. 177-178.

Sebrier, M., and Soler, P., 1991, Tectonics and magmatism in the Peruvian Andes from late Oligocene time to the present In: Andean magmatism and its tectonic setting: Geological Society of America Bulletin Special Paper, v. 265, p. 259-278.

Soler, P., and Bonhomme, M.G., 1987, K-Ar Radiochronological Data on the Granitoids of the Eastern Cordillera of Central Peruvian Andes - Tectonic Implications: Comptes Rendus De L Academie Des Sciences Serie Ii, v. 304, p. 841-845.38

Soler, 1990, Relations of magmatic activity to Plate dynamics in Central Peru from Cretaceous to Present, in Kay, S.M., and C.W., R., eds., Plutonism from Antarctica to Alaska, Volume 241, Geological Society of America, p. 173-191.

Stewart, J.W., Evernden, J.F., and Snelling, N.J., 1974, Age-Determinations from Andean Peru - Reconnaissance Survey: Geological Society of America Bulletin, v. 85, p. 1107-1116.

Steinmann, G., 1929. Geologie von Peru, Carl Winters Universitatsbuchhandlung, 448p.

Thouret, J.-C., Wörner, G., Singer, B., and Finizola, A., 2005, The Central Andes in Peru: "Old" valleys in a "young" mountain range?, 6th. International Symposium on Andean Geodynamics (ISAG 2005), Volume Extended Abstracts: Barcelona, p. 726-729.

Tosdal, R.M., Farrar, E., and Clark, A.H., 1981, K-Ar Geochronology of the Late Cenozoic Volcanic-Rocks of the Cordillera Occidental, Southernmost Peru: Journal of
Volcanology and Geothermal Research, v. 10, p. 157-173.

Tosdal, R.M., Clark, A.H. and Farrar, E., 1984. Cenozoic polyphase landscape and tectonic evolution of the Cordillera Occidental, southernmost Peru. Geological Society of America Bulletin, 95(11): 1318-1332.

Weeks, L.G., 1948. Paleogeography of South America, Bulletin of the Geological Society of America, 59, 249-282.

Chapter 3.

Provenance and structure of the Cretaceous back-arc basin of the Northern Andes: insights from U-Pb detrital zircon geochronology

3.0 Abstract

While the Andean orogeny began with subduction in the Jurassic, the Eastern Cordillera in the north-eastern Andes of Peru appears to have remained largely unaffected by deformation and shortening until Eocene time, instead, it was characterized by a back-arc basin during the late Jurassic through Cretaceous, situated east of a magmatic arc. Reconstructions of the paleotopography of this basin are solely from stratigraphical relationships. Here, we use *in situ* LA-ICP-MS detrital zircon geochronology to investigate the provenance of the Early-to-mid Cretaceous basin of the West Peruvian Trough, by using the unique geochronologic characteristics of cratonic and basement rocks as tracers. We find that sources changed spatially and temporally, from a dominant Paleozoic basement source, to Proterozoic cratonic sources. We believe this shift in provenance occurred due to subsidence and burial of the Marañon High, as well as possible fluvial reorganization, delivering sediment predominantly from the north-western part of the Amazon craton.

3.1 Introduction

The South American continental plate represents a complex record of orogeny, rifting and passive margins since the Proterozoic. While the modern Andean orogen makes a strong overprint on the western margin of South American, Precambrian through Proterozoic cratons are preserved in the South American shelf (e.g. Ramos et

al., 1986; Hoffman, 1991; Sadowski and Bettencourt, 1996; Tosdal, 1996). Isolated blocks of Paleozoic basement and accreted terranes also crop out within the modern Andes (e.g. Bard et al., 1974; Mourier et al., 1988; Spikings et al., 2005; Miskovic et al., 2009). This fragmented pre-Mesozoic geology has been used to reconstruct the Neoproterozoic and Paleozoic tectonic and paleographic history of the South American plate, prior to the modern Andean orogenic cycle (e.g. Megard, 1971; Bond et al., 1984; Kontak et al., 1985; Forsythe et al. 1993; Rapela et al., 1998; Cawood et al., 2001; Sempere et al., 2002; Cawood and Buchan, 2007; Ramos, 2008.) The geographical distribution and geochronologic signature of the pre-Mesozoic basement is fairly unique, affording the opportunity to use these units as provence tracers, to infer paleotopographical and tectonic constraints of Andean evolution (Fig. 3.1).

We use in situ laser ablation-inductively coupled plasma-mass spectrometry (LA-ICP-MS) U-Pb detrital zircon geochronology from meta-sedimentary and sedimentary sequences deposited during Cretaceous development of the Andean back-arc basin in north-central Peru, situated east of the magmatic arc and west of Amazonia. By the Cretaceous, subduction had initiated the modern Andean orogeny, forming a magmatic arc that is now exposed in the Western Cordillera, and a back-arc basin, known as the West Peruvian Trough (WPT) that persisted as a low-lying, undeformed basin throughout the Cretaceous, then was inverted, forming the Tertiary Marañon fold-and-thrust belt within the Eastern Cordillera of the Andes of Peru (Wilson, 1963; Mégard, 1987). Stratigraphical and structural details of basin

development were studied by early workers in Peru (McLaughlin, 1924; Steinmann, 1929; Benavides-Caceres, 1956; Wilson, 1963; Mégard, 1987) and revisited more recently (Carlotto et al., 2009; Scherrenberg et al., 2012). However, details of basin structural development, paleotopography and provenance of the WPT prior to Tertiary deformation are not well constrained. We use the unique age signatures of the cratons of Amazonia and Paleozoic basement rocks as tracers to investigate the provenance and paleotopography of the Eastern Peruvian margin in the early-to-mid Cretaceous phase of Andean orogeny. Our results show a continuous, but minor source of Amazon cratonic units older than 1.5Ga, a persistent ~1.5Ga source, and a dramatic change from dominant to nonexistent early Paleozoic sources. This change is observed spatially, from south to north along the WPT, and temporally, from the earliest to early-to-mid Cretaceous.

3.2 Tectonic setting

The South American plate is a composite of multiple orogeny cycles over the past several billion years (Fig. 1). The oldest crust is the Amazon craton, which formed parts of the Sunsas orogeny between the Laurentia and Amazonia continents c.a. 1.2 - 0.95Ga (Ramos et al., 1986; Tosdal, 1996; Jaillard et al., 2000). The Arequipa block of Southern Peru and Northern Chile is also thought to be related to Laurentian orogeny, but its exact relationship is unclear (Shackleton et al., 1979; Dalziel et al., 1994; Loewy et al., 2004). In the mid-to-late Neoproterozoic, westward drift of Laurentia with the break-up of Rodinia created a rifting zone between the

Arequipa-Antofalla craton and Amazonia (Rapela et al., 2007). In the Early Cambrian, convergent tectonics resumed, accreting the Arequipa-Antofalla craton with Amazonia in the Pampean orogeny (Ramos, 2008). The suture zone between the Arequipa and Amazonia cratons is a long-lived feature of crustal weakness that today is occupied by the Rio Marañon, called the Marañon lineament (Mišković et al., 2009).

In the early Paleozoic, subduction continued, emplacing the San Nicolas Batholith of Southern Peru (Sempere, 1995), followed by a period of magmatic quiescence in the mid-Paleozoic, which is interpreted as existence of a passive margin along the western edge of the continent (Mégard, 1973). Arc activity resumed in the Late Paleozoic by the Early Mississippian Eohercynian orogeny, documented by intrusives emplaced parallel to the Marañon lineament, within the Ordivician-aged metamorphic rocks of the Marañon Complex (Mégard et a., 1971; Dalmayrac, 1980; Schreiber, 1989; Mišković et al., 2005). Continental thinning ensued in the Late Permian through Early Jurassic, giving rise to volcanics of the Mitu Group (Sempere et al., 2002). With the onset of renewed easterly subduction of the proto-Pacific plate in the Early Jurassic, the Andean orogeny began, focusing arc magmatism along what is today the coastal margin, thus putting the Eastern Cordillera, including the Marañon lineament, in a back-arc position (Mégard, 1987; Mišković et al., 2009). Through the Cretaceous, terrestrial and marine sediments accumulated in two basins that flanked the Marañon high; the Western Peruvian Trough (WPT) and the Eastern

Peruvian Trough (EPT) (Fig. 2A; Mégard, 1987). In the early Cenozoic, a major tectonic compressional event, the Incaic phase of Andean orogeny, inverted the basin, forming the Marañon fold-and-thrust belt (Wilson et al., 1967; Mégard, 1987; Noble et al., 1990).

3.3 Cretaceous basin sequences of the West Peruvian Trough

The Cretaceous stratigraphy of the Marañon fold-and-thrust (MTFB) belt is laterally discontinuous, changing facies and significantly thinning from west to east (Fig. 2B; Benavides-Caceres, 1956; Wilson, 1963; Janjou et al., 1981). Basement rocks include the Neoproterozoic through Cambrian Marañon complex, consisting of folded phyllitic schists, and only crop out in the east (Bard et al., 1974; Zeil, 1983). Stratigraphically above the Marañon complex are late Paleozoic through Jurassic sedimentary rocks and volcanics, cropping out along some sections of the MFTB. The Cretaceous sequences significantly thin from west to east, from an estimated 3000m thickness in the west, to 1000m thickness in the east (Scherrenberg et al., 2012). Thickness and facies variations laterally are interpreted as a deepening shelf to deep basin from east-to-west (Scherrenberg et al., 2012).

The base of the Cretaceous stratigraphy are thin-bedded, sub-greywacke sandstone and carbonaceous shale of the Oyon Formation, which only exist in the western part of the WPT, and do not appear in the east (Wilson, 1963). Overlying the Oyon in the west and the basement rocks in the east, is the Lower Cretaceous

Goyllarisquizga Group, a dominantly sandstone sequence that shows distinct lateral facies changes from west to east. In the west, the Goyllarisquizga is divided into the Chimu, Santa, Carhuaz and Farrat Formations (Benavides-Caceres, 1956; Wilson, 1963). The formations of the Goyllarisquizga in the east record transitions from a desert environment to fluvial-deltaic system, to brackish, oolitic tidal facies to a shallow marine transgression. In the east the Goyllarisquizga is largely undifferentiated sandstone. The westernmost detrital sample in this study is sampled from the Oyon Fm. in the western part of the central WPT (~8.5degS), and the other two detrital samples are taken from the Goyllarisquizga group, one from the northern WPT (~7degS), and one from the central WPT (~8.5degS).

Above the Goyllarisquizga concordantly lies the Pariahuanca Formation, a fine-grained sandstone with a calcareous matrix. Conformably above the Pariahuanca are the Chulec and Paritambo Formations, marking a transition from shallower to deeper marine (Wilson, 1963). Thick, Late Cretaceous limestone sequences cap the Chulec and Paritambo, indicating an epicontinental carbonate platform, and demonstrate eustatic sea-level variations ranging up to maximum transgressive sea-level stands (Benavides-Caceres, 1956; Jaillard and Sempere, 1989). In summary, the Cretaceous formations show variation in the upper and lower levels from the west-to-east in both northern and central Peru; this has led to suggestions that the WPT may have been divided into smaller basins by active structural boundaries, but the extent and timing of these structures are poorly constrained by the stratigraphy. Further, the

large overprint of Tertiary deformation may have obscured evidence for structures that were present in the Cretaceous (Mégard, 1987). Here, we use detrital U-Pb zircon geochronology to characterize the provenance of two formations of the Lower Cretaceous, from three sample sites in the north-central Peruvian Andes to investigate the paleotopography of the WPT during the Late Mesozoic stage of Andean orogeny.

3.4 Method and Results

The three bedrock samples of the Oyon and Goyllarisquizga Cretaceous Formations were crushed, sieved, and typical mineral separation techniques were applied. Individual grains were picked onto sticky tape with R-33, SL-2 and Plescovice zircon standards, mounted with epoxy and sanded and polished. 100-150 individual zircon grains were randomly selected from each sample for in-situ spot analysis.

In situ laser ablation-inductively coupled plasma-mass spectrometry (LA-ICP-MS) was conducted on 332 individual zircon grains at the UCSC LA-ICP-MS laboratory, which couples a Thermo Element XR single-collector ICP-MS to a Photon Machines Analyte 193H ArF excimer laser ablation system. Analyses included 26um spot-sizes, 30 seconds of baseline data collection followed by 30 seconds of on-peak data collection. The ablated zircon material is carried from the ablation cell by helium gas, mixed with argon sample gas and injected into an inductively coupled plasma stream where it is measured using the XR single-collector ICP-MS. Data reduction was conducted using Iolite, a free software available on the Igor Pro platform (Paton

et al., 2011) where downhole fractionation and common-Pb corrections were made. (See Appendix 3.1 for a data table of individual analyses).

U-Pb zircon ages are shown as probability density functions with histograms, each bin represents 100my (Fig. 3A-C). Locations of the three samples are shown on regional geologic maps (Fig. 3D). Sample RP07-1 is a fine-grained quartzite of the lower Cretaceous Oyon Formation, sample RM07-P6 is a course-grained quartzite with 20cm thick cross-bedding, of the lower Goyllarisquizga Chimu Formation and sample RM07-5 is a coarse-grained sandstone of the Goyllarisquizga Group. RP07-1 (n=94) contains zircons from 240.6 ± 2.5Ma (youngest) to 3036 ± 17Ma (oldest), and shows a distinct peak at 500-600-Ma and smaller peaks at 0.8-1.2Ga and 1.3-1.6Ma. A lack of ages exists between 2.1 and 2.6Ga. RM07-P6 (n=140) shows a similar peak of 500-600Ma compared to RP07-1, but its highest peak lies between1.0-1.2Ga. The youngest age is 196.4 ± 1.2Ma and the oldest 2757 ± 14Ma. where only small gaps of ~100Ma exist, showing a more or less continuous age spectra from 200Ma to 2.8Ga. Finally, RM07-5, the most northern sample, shows two sharp peaks, aged 1.1-1.2Ga and 1.5Ga. Only four grains exhibit ages less than 0.8Ga, two older than 1.8Ga, and none older than 2Ga. The majority of ages lie between 0.9 and 1.7Ga.

3.5 Discussion

The variation in thickness of the Early-to-mid Cretaceous sequences of the WPT led to suggestions that numerous smaller basins comprised the WPT. This could be due to structures that separated the smaller basins during basin formation, or

inherited topography from the Paleozoic through Jurassic basement rocks. As basement rocks are rarely exposed in the MTFB, their regional significance and paleodistribution are not well understood. It is clear however, from stratigraphic relationships, that the WPT was separated from the EPT by the Marañon High, or as it was first termed, the "Marañon geanticline" (Wilson, 1963; Soto, 1979; Mégard, 1987). The topography and extent of the Marañon High during basin deposition and subsidence is unknown. Mégard (1987) hypothesized that during the earliest Cretaceous, the quartzose sand of the Amazon platform to the east was so abundant that it filled the EPT and overflowed the Marañon High, spilling into the WPT. Paleocurrent indicators in some of the lower Cretaceous units, such as the Chimu Fm, contain wave ripples that show currents in a W, SW and S direction; which Scherrenberg et al. (2012) interpreted as evidence for a fluvial-deltaic system that had an eastern source area, probably from the Amazon craton.

There are several major suites of provenance to consider for the detrital signal we show in the Cretaceous basin; i) the cratonic units of the Amazon platform (Fig. 1), ii) the late Paleozoic through Triassic magmatic rocks that intruded along the Marañon crustal lineament (Fig. 3D) iii) the metamorphic basement of the Marañon complex, which was likely outcropping in the Marañon High during parts of the Cretaceous (Fig. 3D), and iv) Jurassic-Cretaceous volcanics that were erupting prior to and coevally with basin development. While the geochronologic signatures of the Amazon craton, the late Paleozoic-Triassic magmatic rocks, and the Jurassic-

Cretaceous volcanic rocks provinces are unique, providing a fairly clear fingerprint for detrital sources, the metamorphic basement rocks of the Marañon complex are problematic for two reasons. First, the shales, sandstones and carbonates of the Marañon complex were derived from the Amazon cratonic units themselves, and then metamorphosed in the Paleozoic; Fig. 3E shows a compilation of all U-Pb data from the metamorphic rocks of the Marañon complex (Cardona et al., 2010). Thus, the detrital signature from the Marañon complex is somewhat ambiguous with the Amazon cratonic units, as both could be probable sources for the Cretaceous detritus. However, the Marañon complex has a very unique detrital peak (Fig. 3D) at ~500Ma. The source of the 450-550Ma peak is puzzling, as no magmatic, volcanic or cratonic units have been found in the vicinity of the north-central Peruvian Andes in this age range. This has led Chew et al. (2008) to suggest that a magmatic arc persisted during the Neoproterozoic through earliest Paleozoic, in northern Peru/Ecuador, which is currently covered by Sub-Andean rocks and sediments. If this magmatic arc existed in the Neoproterozoic, and it outcropped during the Cretaceous, the source of the ~500Ma peak of detrital zircons we see in the Cretaceous basin units is ambiguous; it could be from the Marañon complex, or from this arc.

Both samples RP07-1 and RM07-P6 contain a strong ~500Ma peak, but RM07-5 is practically devoid of all zircons younger than 900Ma. We can say with certainty that neither the Marañon Complex or the proposed Neoproterozoic magmatic arc rocks were primary sources for RM07-5, a sandstone from the north-

easterly WPT. On the other hand, the most frequent zircon ages in RP07-1 of a 500-600Ma peak, as well as the more minor peaks of 800-1200Ma and ~1500Ma, match the composite distribution (n=911) of U-Pb ages in the Marañon Complex from Chew et al. (2008; Fig. 3D). We infer the dominant provenance source for the lower Cretaceous Oyon Fm sample (RP07-1) was the Marañon Complex, demonstrating that in early Cretaceous time, the Marañon High was a significant topographical feature, enough to isolate the WPT from the Amazon shelf, and eolian-fluvial sands were eroding from the Marañon High into the WPT. Mégard's (1987) hypothesis that during the earliest Cretaceous, the quartzose sand of the Amazon platform to the east was so abundant that it filled the EPT and overflowed the Marañon High, spilling into the WPT is not likely correct, at least during this depositional timeframe. In RM07-P6 however, from the Chimu Fm. of the lower Goyllarisquizga, shows a strong peak of 1.0-1.2Ga, and a diminishing 500-600Ma peak, relative to RP07-1. It also shows a higher proportion of ages older than 1.5Ma, which must come from the Amazon craton. The smaller, but still significant 500-600Ma peak requires erosion from the Marañon Complex, but the relatively higher contribution of 1.0-1.2Ga and >1.5Ga ages points to a cratonic source, likely the Sunsas craton for the 1.0-1.2Ga signal, and a combination of sources from the cratons of the Amazon Craton suite for the >1.5Ga signal. Alternatively, the 500-600Ma peak could come from the Neoproterozoic magmatic arc, however, the presence of ages from 200-400Ma likely means the Permo-Triassic magmatic rocks

of the Marañon crustal lineament were also exposed, along the Marañon High, leading us to believe the Marañon High must have been outcropping, and is a more likely source than the supposed Neoproterozoic arc for the ~500-600Ma signal. Thus the notion that sand from the Amazon shelf spilled into the WPT from the EPT is a possibility, at least during the formation of the lower Goyllarisquizga, but not during formation of the Oyon. Perhaps rivers reorganized to flow through or around the Marañon High. Base level drop due to subsidence is one possibility, as subsidence rates are inferred to have been high during the early Cretaceous (Jaillard and Soler, 1996).

The RM07-5 sample is the most northern sample location, taken from the easterly section of the WPT, where sequences thin out. The sample is believed to be part of the Goyllarisquizga Group, but it is not known if this sample reflects a time period before, contemporaneous or after the sample RM07-P6, from the Chimu Fm. of the Goyllarisquizga Grp. The detrital zircon age signal from RM07-5 is drastically different than RM07-P6, where two prominent peaks at 1.1-1.2Ga and 1.5Ga are clear, and lack zircons younger than 900Ma and older than 1.8Ga. We explore two possibilities. One, that the provenance sources shifted temporally, and RM07-5 represents a depositional time after RM07-P6, where the Marañon High was shut off as a source to the entire basin at this time, perhaps due to subsidence and burial. Or, this scenario could be explained by a spatial shift in paleocurrents, that precluded the Marañon High from delivering sediment to this part of the WPT, from major fluvial

reorganization, either due to eustatic changes, or tectonic activity that isolated the northern WPT from the central WPT, or some combination of both. However, the probable sources of the 1.1-1.2Ga and 1.5Ga peaks are from the Sunsas and Rondonia-San Ignacio cratons, requiring westward movement of material from the cratons into the WPT. As the Marañon Complex was not a major contributor, or any of the Permo-Triassic magmatic rocks, the simplest explanation points to the burial of the Marañon High during this time of deposition.

3.6 Conclusions

While the modern Andean orogen has formed during the Cenozoic, the South American plate has a complex history of multiple cycles of orogeny. Inherited structures and crustal homogeneities likely play a role in influencing the Cenozoic tectonics of the Andes, but the pre-Andean tectonics are not well understood. During the Cretaceous, subduction of the Nazca plate underneath the South American caused a magmatic arc, creating a back-arc basin to the east. In this back-arc basin, the Marañon complex, which lies along a long-lived crustal lineament was inferred to be at a topographic high, due to block faulting that uplifted it, and basins on either side, the West and East Peruvian Troughs, accumulating large volumes of sediment and carbonates during the Cretaceous, until deformation propagated eastward, created the Tertiary Marañon fold-and-thrust belt. Here, we show the detrital sources of the Cretaceous back-arc basin changed temporally and spatially. In the earliest

Cretaceous, it appears the Marañon High was the only significant source for detritus in the Oyon Fm of the WPT; it's topography, due to graben-style normal faulting that uplifted it, not allowing delivery of detritus from the Amazon shelf. Shortly after, during deposition of the lower Goyllarisquizga group, sources included both the Marañon Complex and Permo-Triassic magmatic rocks of the Marañon High, but also included a significant cratonic sources from the Amazon shelf. This could support Mégard's (1987) hypothesis of massive sedimentation that spilled over the Marañon High, or it could be explained by large rivers flowing around and/or through the Marañon High. In the northern WPT, it appears the Marañon High was buried during deposition of the Goyllarisquizga Group, and delivery of cratonic sources was limited to the Sunsas and Rondonia-San Ignacio cratons of the Amazon shelf. Overall, the paleotopography of the Andean back-arc basin during the Early-to-mid Cretaceous seems to be characterized by graben-style block normal faulting in the earliest Cretaceous, where the Marañon High was the dominant source of detritus, regional basin subsidence may have accelerated, and fluvial-deltaic systems reorganized, resulting in a shift of provenance to the Amazon cratons. This scenario does not preclude active faulting from occurring within the WPT, but the back-arc basin appears to be tectonically quiescent during the Early-to-mid Cretaceous, and major uplift and deformation did not occur until the Cenozoic.

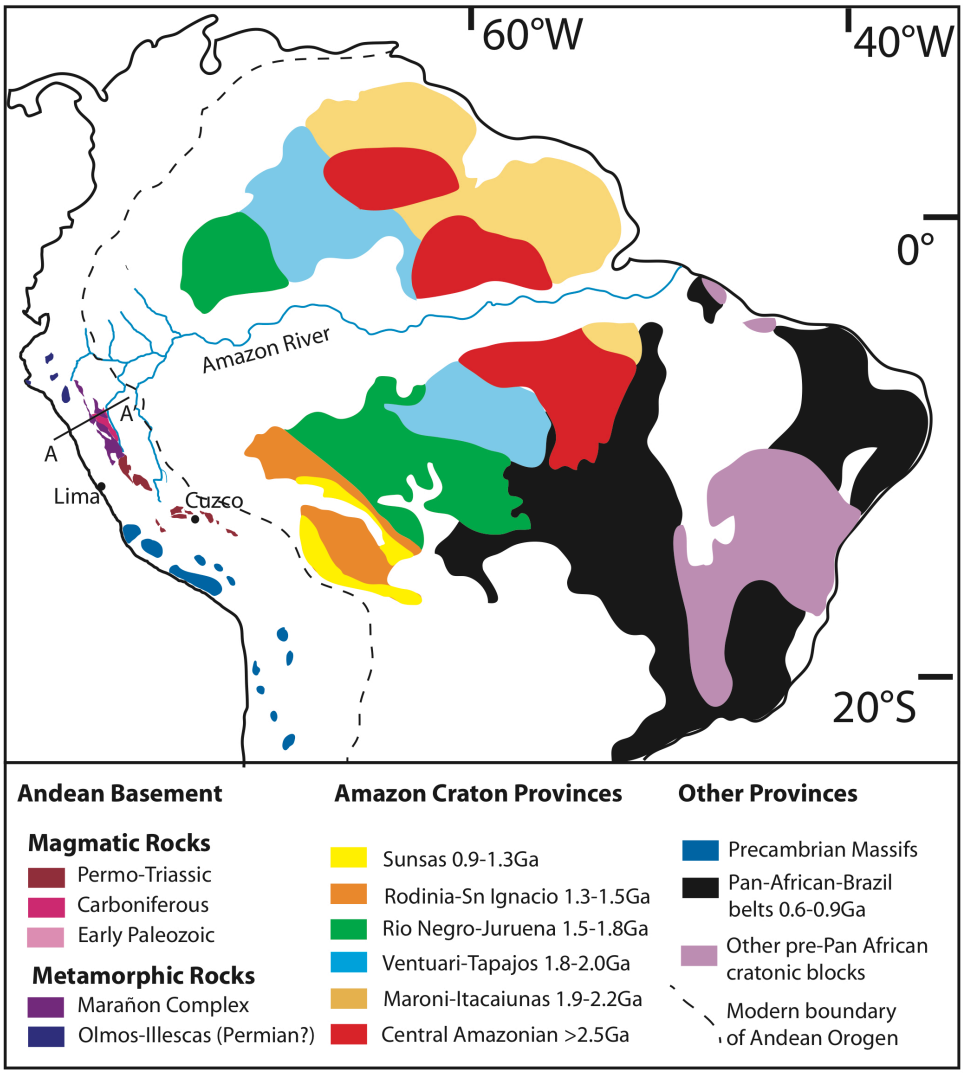

Figure 3.1. Basement and cratonic units of the Andean orogen and Amazon shield. Modified from Cardona et al., 2010 and Chew et al., 2008. A-A' cross section line refers to Fig. 3.2.

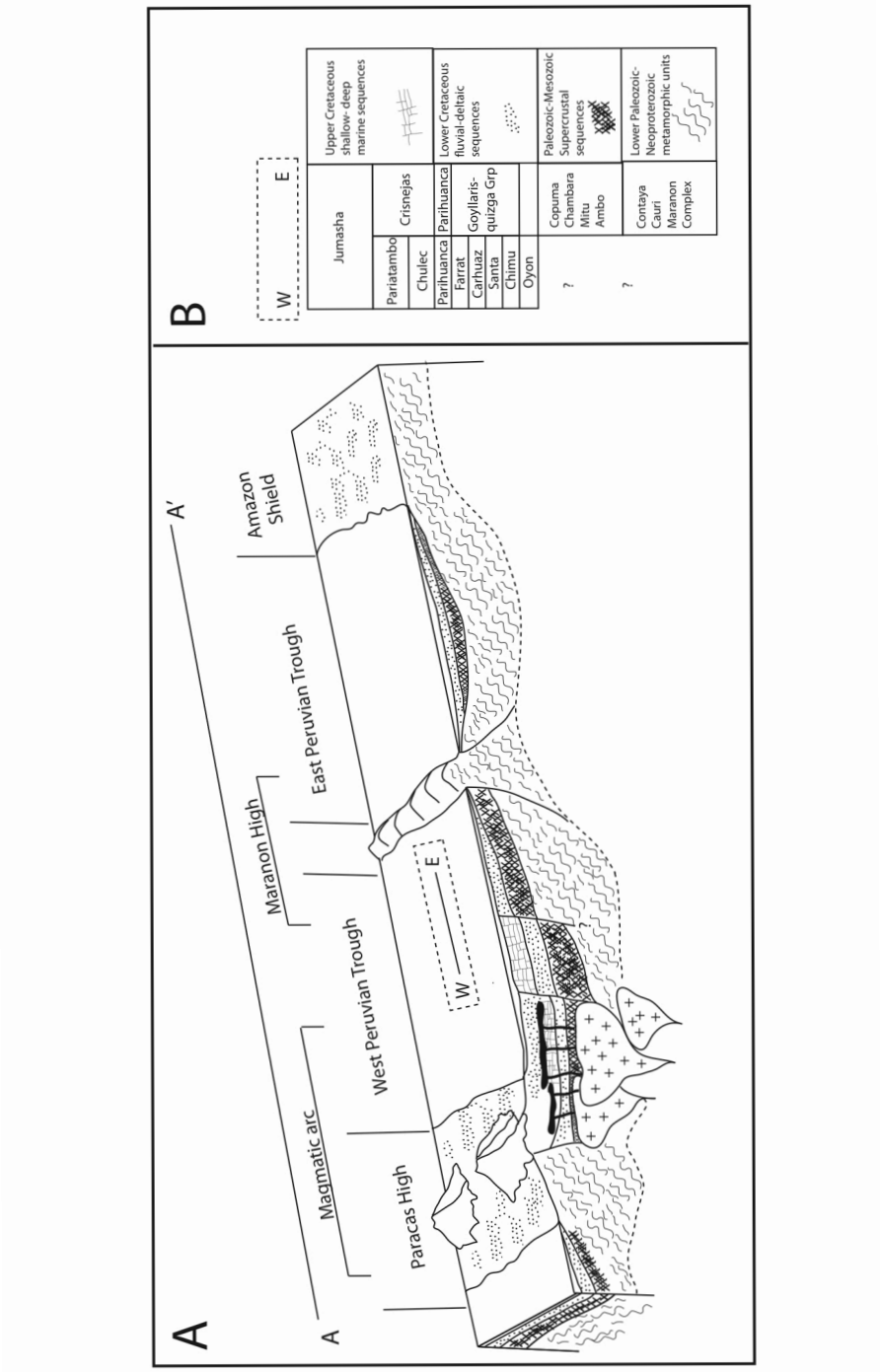

Figure 3.2. A.Interpretation of a cross section across ~10 degrees south in Late Cretaceous time. After Megard, 1987. B. Generalized stratigraphy of the West Peruvian trough in the western and eastern sections, after Scherrenberg et al., 2012.

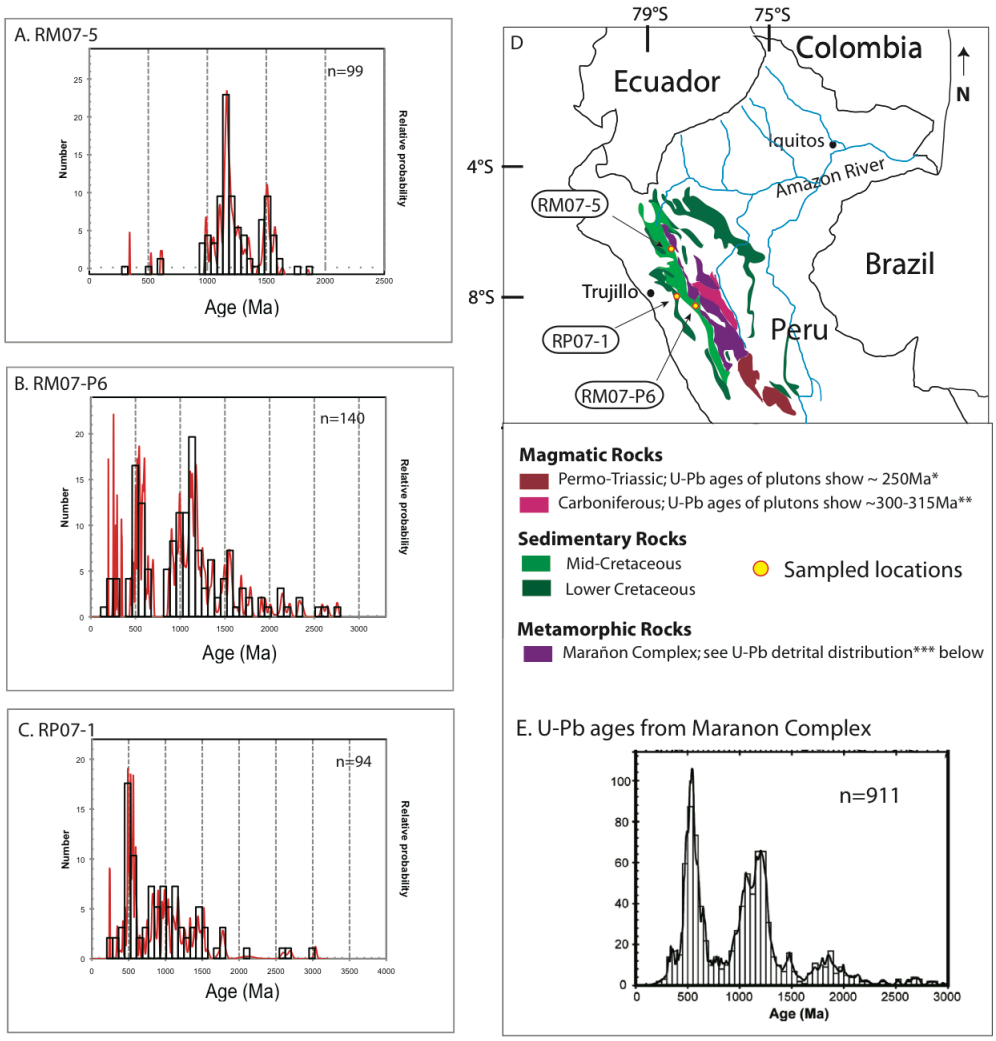

Figure 3.3. U-Pb zircon results shown in A-C as histograms, each age bin is 100Ma, and a probability distribution function, which includes individual grain internal and external errors. D. shows Paleozoic through Cretaceous geology of the north-central Peruvian Andes. Sample locations are indicated with yellow dots. *Miskovic et al., 2009; **Miskovic et al., 2009; ***Cardona et al., 2009

Appendix 3.1: Data table for U-Pb analyses

Sample Name	U (ppm)	U (ppm) 2-sigma error	Th (ppm)	Th (ppm) 2-sigma error	U/Th	U/Th 2-sigma error	Age (Ma)	Age (Ma) 2-sigma error
RM07_P6_1	205.50	2.80	68.69	0.73	2.97	0.03	2589.00	16.00
RM07_P6_2	76.30	2.90	72.70	3.30	1.09	0.01	517.80	5.80
RM07_P6_3	97.20	3.60	23.50	1.40	4.13	0.09	1172.10	9.20
RM07_P6_4	203.20	3.30	114.00	2.30	1.77	0.02	1785.00	11.00
RM07_P6_5	90.60	1.00	33.60	1.10	2.71	0.09	1628.00	21.00
RM07_P6_6	311.50	5.50	160.80	4.00	1.91	0.02	293.80	2.10
RM07_P6_7	176.10	6.00	53.30	2.50	3.36	0.05	502.50	3.90
RM07_P6_8	109.40	1.50	19.51	0.62	5.58	0.13	691.70	8.10
RM07_P6_9	36.94	0.84	17.08	0.36	2.12	0.02	1085.40	9.80
RM07_P6_11	111.30	1.70	28.47	0.67	3.82	0.05	1135.40	8.30
RM07_P6_12	180.20	6.30	77.50	3.40	2.31	0.03	553.50	4.40
RM07_P6_13	254.00	5.90	50.63	0.89	4.83	0.05	1214.50	8.00
RM07_P6_14	253.40	4.70	151.20	4.70	1.62	0.02	254.20	2.20
RM07_P6_16	13.33	0.19	2.46	0.05	5.24	0.13	1058.00	16.00
RM07_P6_17	85.70	2.70	19.20	0.66	4.34	0.10	1332.00	31.00
RM07_P6_18	74.60	4.30	14.47	0.66	4.82	0.08	1266.00	14.00
RM07_P6_19	427.00	12.00	10.94	0.12	37.80	1.10	2757.00	14.00
RM07_P6_20	220.30	4.40	32.48	0.76	6.50	0.06	1029.40	6.90
RM07_P6_21	157.90	3.30	28.70	0.64	5.26	0.05	1174.00	8.00
RM07_P6_22	82.10	1.20	13.36	0.20	5.87	0.07	1056.00	11.00
RM07_P6_23	242.60	4.70	77.40	2.20	3.05	0.04	1193.90	8.60
RM07_P6_24	121.30	1.00	55.32	0.50	2.10	0.02	1791.00	17.00
RM07_P6_25	48.10	1.00	11.25	0.36	4.09	0.06	1133.30	9.70
RM07_P6_26	700.00	24.00	244.00	11.00	2.75	0.06	1336.00	19.00
RM07_P6_27	250.90	3.70	120.40	1.20	2.00	0.02	1362.20	8.50
RM07_P6_28	121.77	0.84	66.55	0.45	1.74	0.02	532.00	4.10
RM07_P6_29	371.40	9.40	3.92	0.09	90.60	1.30	640.40	4.30
RM07_P6_30	189.90	4.10	47.33	0.87	3.80	0.03	1952.00	11.00
RM07_P6_31	222.60	4.00	48.25	0.97	4.38	0.04	1113.80	7.50
RM07_P6_32	277.00	11.00	184.40	9.90	1.44	0.02	296.20	6.80
RM07_P6_33	102.10	2.40	26.55	0.69	3.63	0.03	1189.90	8.30
RM07_P6_34	87.10	1.70	15.54	0.19	5.33	0.09	1135.20	8.50

Appendix 3.1: Data table for U-Pb analyses

Sample Name	U (ppm)	U (ppm) 2-sigma error	Th (ppm)	Th (ppm) 2-sigma error	U/Th	U/Th 2-sigma error	Age (Ma)	Age (Ma) 2-sigma error
RM07_P6_35	80.20	2.20	27.08	0.97	2.80	0.04	1122.00	10.00
RM07_P6_36	63.00	1.90	23.12	0.72	2.50	0.03	540.90	5.00
RM07_P6_37	63.50	2.00	23.04	0.31	2.69	0.12	2366.00	18.00
RM07_P6_38	207.60	4.50	62.40	1.00	3.12	0.04	1375.00	11.00
RM07_P6_39	99.00	1.70	25.35	0.47	3.69	0.04	1567.30	9.60
RM07_P6_40	42.90	0.45	6.95	0.09	5.81	0.08	1184.00	11.00
RM07_P6_41	89.30	1.70	27.09	0.41	3.10	0.03	579.00	4.70
RM07_P6_42	143.60	8.90	76.00	21.00	3.12	0.18	1442.00	34.00
RM07_P6_43	71.41	0.93	38.56	0.59	1.76	0.02	996.90	8.00
RM07_P6_44	97.90	1.50	24.75	0.44	3.73	0.04	1162.60	8.10
RM07_P6_45	386.10	9.50	172.80	5.00	2.08	0.02	277.80	2.10
RM07_P6_46	538.60	5.70	120.36	0.69	4.22	0.05	504.50	3.50
RM07_P6_47	52.70	1.30	20.90	0.32	2.36	0.04	1180.00	13.00
RM07_P6_48	80.59	0.81	22.27	0.25	3.41	0.03	1226.70	9.80
RM07_P6_49	48.69	0.98	20.02	0.44	2.29	0.02	905.40	7.50
RM07_P6_50	292.00	3.50	113.70	1.30	2.40	0.02	254.60	2.30
RM07_P6_51	52.86	0.80	30.40	0.78	1.61	0.03	599.70	6.10
RM07_P6_52	49.30	1.80	10.17	0.43	4.56	0.06	1121.00	10.00
RM07_P6_53	167.00	3.30	58.10	1.30	2.71	0.03	498.50	4.00
RM07_P6_54	474.10	6.80	93.30	1.30	4.77	0.04	1541.90	8.70
RM07_P6_55	8.82	0.18	0.23	0.03	80.00	15.00	1259.00	22.00
RM07_P6_56	35.17	0.54	19.60	0.32	1.70	0.02	994.60	8.50
RM07_P6_57	59.11	0.41	11.80	0.10	4.70	0.05	1171.90	9.20
RM07_P6_58	41.90	1.10	9.77	0.27	4.06	0.05	985.30	8.90
RM07_P6_59	735.00	17.00	149.00	15.00	7.32	0.66	2118.00	73.00
RM07_P6_60	325.00	35.00	19.10	1.30	25.80	3.60	1182.00	65.00
RM07_P6_61	179.90	3.00	154.40	4.10	1.11	0.03	1010.00	21.00
RM07_P6_64	39.00	0.54	10.71	0.20	3.45	0.04	1499.00	11.00
RM07_P6_65	56.84	0.72	27.70	0.33	1.94	0.02	910.20	8.40
RM07_P6_66	35.42	0.57	14.14	0.24	2.36	0.03	541.90	5.60
RM07_P6_67	46.27	0.88	20.12	0.44	2.18	0.02	1585.00	12.00
RM07_P6_68	195.10	5.40	45.20	1.10	4.21	0.11	2007.00	17.00
RM07_P6_69	74.79	0.65	123.10	1.30	0.57	0.01	2137.00	15.00

Appendix 3.1: Data table for U-Pb analyses

Sample Name	U (ppm)	U (ppm) 2-sigma error	Th (ppm)	Th (ppm) 2-sigma error	U/Th	U/Th 2-sigma error	Age (Ma)	Age (Ma) 2-sigma error
RM07_P6_70	83.20	1.30	17.75	0.33	4.45	0.04	1244.00	10.00
RM07_P6_71	121.40	2.30	22.90	0.43	5.10	0.05	1033.80	7.40
RM07_P6_72	140.40	2.40	46.58	0.79	2.87	0.02	347.70	2.60
RM07_P6_73	243.90	3.90	53.40	0.94	4.35	0.04	1285.20	8.40
RM07_P6_74	182.40	6.90	47.20	1.90	3.96	0.32	1019.00	11.00
RM07_P6_75	98.30	4.70	67.80	1.10	1.34	0.04	649.80	8.60
RM07_P6_76	10.78	0.36	3.21	0.11	3.19	0.06	1202.00	17.00
RM07_P6_77	76.00	3.80	12.00	0.41	5.85	0.13	1171.00	13.00
RM07_P6_78	137.10	7.60	71.80	5.40	2.01	0.06	1745.00	17.00
RM07_P6_79	231.30	6.00	46.40	1.10	4.75	0.05	1267.00	10.00
RM07_P6_80	76.30	1.60	16.49	0.35	4.39	0.07	1152.00	14.00
RM07_P6_81	352.50	6.30	70.10	1.40	4.85	0.04	947.60	6.20
RM07_P6_82	115.20	1.40	93.43	0.96	1.19	0.01	602.70	4.50
RM07_P6_83	277.10	2.70	90.60	1.10	2.94	0.03	590.90	4.10
RM07_P6_84	149.50	6.60	90.10	2.50	1.59	0.04	1002.20	8.40
RM07_P6_85	79.70	0.65	26.31	0.23	2.94	0.03	1135.00	8.20
RM07_P6_86	614.00	17.00	81.40	2.50	7.38	0.09	1554.00	10.00
RM07_P6_87	1954.00	13.00	816.10	9.10	2.33	0.02	251.10	5.50
RM07_P6_88	824.00	26.00	268.00	14.00	3.15	0.07	444.90	5.10
RM07_P6_89	164.00	3.90	36.70	1.00	4.37	0.05	1180.60	8.10
RM07_P6_90	86.50	1.50	36.14	0.80	2.36	0.03	698.50	5.80
RM07_P6_91	35.27	0.43	18.82	0.17	1.85	0.02	1073.60	9.60
RM07_P6_92	224.20	1.90	74.01	0.84	2.97	0.03	1137.70	8.40
RM07_P6_93	40.02	0.96	15.06	0.53	2.69	0.04	2646.00	18.00
RM07_P6_94	58.20	1.30	11.63	0.25	5.19	0.25	1107.80	9.20
RM07_P6_96	51.45	0.44	28.56	0.25	1.80	0.02	892.60	7.80
RM07_P6_97	44.10	1.70	29.00	1.20	1.53	0.02	1541.00	11.00
RM07_P6_98	361.50	5.30	151.90	2.30	2.40	0.02	1509.70	9.40
RM07_P6_100	253.60	2.90	84.23	0.61	3.03	0.03	603.70	4.20
RM07_P6_2-1	291.00	3.60	266.40	2.30	1.13	0.01	1563.00	14.00
RM07_P6_2-2	115.90	2.70	104.20	3.30	1.19	0.02	1088.00	12.00
RM07_P6_2-3	546.50	7.00	259.40	4.20	2.25	0.03	960.60	5.70
RM07_P6_2-4	80.86	0.60	27.41	0.31	3.07	0.03	971.40	8.00

Appendix 3.1: Data table for U-Pb analyses

Sample Name	U (ppm)	U (ppm) 2-sigma error	Th (ppm)	Th (ppm) 2-sigma error	U/Th	U/Th 2-sigma error	Age (Ma)	Age (Ma) 2-sigma error
RM07_P6_2-39	74.50	1.80	25.37	0.54	3.01	0.04	873.60	8.20
RM07_P6_2-40	121.63	0.82	81.02	0.59	1.51	0.02	1685.00	10.00
RM07_P6_2-41	136.50	1.20	60.51	0.64	2.25	0.02	1103.00	8.10
RM07_P6_2-42	583.00	21.00	329.00	12.00	1.75	0.01	342.10	2.20
RM07_P6_2-43	557.40	7.30	390.40	3.70	1.42	0.03	2156.00	17.00
RM07_P6_2-44	56.10	1.00	253.70	6.40	0.23	0.00	592.90	7.10
RM07_P6_2-45	130.70	2.50	72.76	0.59	1.92	0.04	1095.30	8.60
RM07_P6_2-46	6299.00	96.00	6080.00	35.00	1.26	0.02	196.40	1.20
RM07_P6_2-47	359.00	17.00	252.00	11.00	1.80	0.02	923.40	7.30
RM07_5_1	129.50	1.60	46.92	0.64	2.86	0.02	1144.40	7.30
RM07_5_2	96.40	2.00	50.60	1.20	2.01	0.02	1854.00	13.00
RM07_5_3	109.40	1.80	45.21	0.66	2.52	0.03	1192.10	8.80
RM07_5_4	161.90	1.50	26.30	1.20	6.68	0.24	1119.10	8.90
RM07_5_5	88.59	0.83	35.36	0.32	2.65	0.03	1171.20	8.90
RM07_5_6	41.90	1.50	12.99	0.52	3.38	0.10	1243.00	13.00
RM07_5_7	42.11	0.73	15.35	0.28	2.90	0.03	1103.50	8.50
RM07_5_8	121.80	1.60	31.09	0.34	4.13	0.04	1154.10	7.40
RM07_5_9	382.00	4.70	94.18	0.79	4.27	0.05	1354.00	11.00
RM07_5_10	115.40	1.80	16.93	0.41	7.26	0.09	1307.00	8.10
RM07_5_11	140.60	6.40	64.20	2.40	2.69	0.19	1107.50	8.40
RM07_5_12	141.30	2.90	51.40	1.20	2.97	0.03	1167.60	7.90
RM07_5_13	63.20	2.50	18.66	0.88	3.55	0.06	1106.00	15.00
RM07_5_14	150.70	2.00	30.64	0.65	5.28	0.06	1322.80	8.20
RM07_5_15	132.30	3.10	36.10	1.50	4.02	0.08	1157.70	9.00
RM07_5_16	178.60	3.30	40.05	0.54	4.81	0.05	1095.60	6.70
RM07_5_17	152.30	1.10	37.69	0.36	4.36	0.04	1225.50	7.50
RM07_5_18	25.53	0.43	17.86	0.22	1.55	0.02	1037.00	10.00
RM07_5_19	54.90	0.55	19.81	0.21	2.99	0.04	1286.60	9.40
RM07_5_20	126.10	3.50	39.00	1.10	3.50	0.03	1151.90	8.60
RM07_5_21	261.40	6.80	79.80	2.10	3.54	0.03	1485.10	8.40
RM07_5_22	106.20	2.10	31.03	0.48	3.80	0.04	1170.20	8.40
RM07_5_23	54.30	2.20	15.11	0.71	3.97	0.05	1215.00	10.00
RM07_5_24	161.50	2.80	28.00	0.64	6.39	0.07	1054.80	7.40

Appendix 3.1: Data table for U-Pb analyses

Sample Name	U (ppm)	U (ppm) 2-sigma error	Th (ppm)	Th (ppm) 2-sigma error	U/Th	U/Th 2-sigma error	Age (Ma)	Age (Ma) 2-sigma error
RM07_P6_2-5	179.80	2.90	89.60	1.30	2.09	0.02	1249.50	6.90
RM07_P6_2-6	454.10	5.60	201.00	2.40	2.34	0.02	623.70	7.30
RM07_P6_2-7	476.60	4.70	116.60	1.60	4.19	0.05	902.20	6.00
RM07_P6_2-8	370.00	9.10	102.60	1.90	3.64	0.08	531.80	4.00
RM07_P6_2-9	226.20	2.70	150.20	5.80	1.58	0.04	519.90	3.80
RM07_P6_2-10	35.79	0.62	1.78	0.12	24.10	1.60	923.40	9.60
RM07_P6_2-12	218.00	10.00	263.00	16.00	0.86	0.02	1153.40	8.60
RM07_P6_2-13	292.00	11.00	270.00	12.00	1.08	0.01	545.00	4.20
RM07_P6_2-14	177.10	2.30	106.00	1.40	1.67	0.01	1680.60	8.90
RM07_P6_2-15	400.30	3.20	552.30	7.50	0.73	0.01	596.80	4.40
RM07_P6_2-16	286.90	3.80	230.60	3.50	1.23	0.01	539.40	4.20
RM07_P6_2-17	81.00	2.00	45.00	0.83	1.81	0.05	947.00	11.00
RM07_P6_2-18	236.10	4.30	125.20	2.00	1.86	0.02	1109.70	8.50
RM07_P6_2-19	130.50	3.50	182.60	1.50	0.70	0.02	681.40	8.00
RM07_P6_2-20	575.00	19.00	767.00	26.00	0.76	0.01	571.90	3.80
RM07_P6_2-21	146.80	9.10	218.00	14.00	0.69	0.01	472.80	6.10
RM07_P6_2-22	544.00	26.00	787.00	37.00	0.69	0.01	1910.00	10.00
RM07_P6_2-23	287.00	11.00	395.00	15.00	0.72	0.02	462.50	3.50
RM07_P6_2-24	938.00	10.00	721.80	4.60	1.31	0.01	478.90	7.10
RM07_P6_2-25	562.00	22.00	324.60	9.00	1.67	0.03	1493.60	8.10
RM07_P6_2-26	285.80	4.40	264.30	5.90	1.11	0.01	1476.40	7.90
RM07_P6_2-27	170.80	3.90	159.00	3.00	1.09	0.01	553.10	5.00
RM07_P6_2-28	481.70	7.30	412.00	6.60	1.20	0.01	1336.00	16.00
RM07_P6_2-29	143.50	1.10	124.10	1.20	1.17	0.01	582.90	6.10
RM07_P6_2-30	234.70	4.20	225.50	3.20	1.05	0.01	582.30	5.30
RM07_P6_2-31	409.00	25.00	356.00	14.00	1.08	0.02	1554.00	27.00
RM07_P6_2-32	235.10	2.90	138.10	1.20	1.69	0.02	2225.00	16.00
RM07_P6_2-33	75.79	0.55	125.40	1.90	0.59	0.01	526.20	6.10
RM07_P6_2-34	130.00	2.30	61.54	0.61	2.10	0.03	1454.00	11.00
RM07_P6_2-35	174.90	3.30	166.60	2.90	1.04	0.01	991.90	6.50
RM07_P6_2-36	460.50	5.60	290.50	4.30	1.60	0.01	517.30	3.20
RM07_P6_2-37	115.40	1.40	43.09	0.57	2.71	0.03	1111.80	7.30
RM07_P6_2-38	352.90	8.70	224.70	6.10	1.62	0.01	2332.00	14.00

Appendix 3.1: Data table for U-Pb analyses

Sample Name	U (ppm)	U (ppm) 2-sigma error	Th (ppm)	Th (ppm) 2-sigma error	U/Th	U/Th 2-sigma error	Age (Ma)	Age (Ma) 2-sigma error
RM07_5_25	76.70	1.30	19.97	0.30	4.21	0.04	1142.60	8.30
RM07_5_26	207.30	6.00	27.22	0.79	8.42	0.10	616.10	4.70
RM07_5_27	70.50	1.20	14.14	0.25	5.44	0.06	1208.00	30.00
RM07_5_28	128.90	2.10	45.72	0.91	3.19	0.04	1510.90	9.80
RM07_5_29	82.80	1.50	26.89	0.49	3.44	0.03	1157.40	8.10
RM07_5_30	84.60	1.30	63.40	1.40	1.48	0.02	1498.00	11.00
RM07_5_31	161.10	2.70	19.65	0.42	9.06	0.10	1568.00	10.00
RM07_5_32	629.90	7.80	148.60	1.60	4.70	0.04	1578.00	9.60
RM07_5_33	206.90	3.80	80.90	2.00	2.88	0.04	1563.00	11.00
RM07_5_34	91.60	2.20	21.30	0.52	4.78	0.05	1429.00	11.00
RM07_5_35	74.10	1.30	27.64	0.78	3.03	0.04	1166.50	8.60
RM07_5_36	58.30	1.90	28.90	2.10	2.52	0.08	1000.80	9.00
RM07_5_37	93.80	2.30	21.90	0.72	4.80	0.06	1175.90	9.60
RM07_5_38	61.28	0.99	25.31	0.50	2.72	0.03	1172.70	8.50
RM07_5_39	283.20	4.90	77.60	1.70	4.10	0.04	1473.30	9.10
RM07_5_40	169.70	5.30	36.91	0.49	5.06	0.14	1073.20	7.70
RM07_5_41	129.80	2.40	27.32	0.59	5.30	0.05	1510.60	9.50
RM07_5_42	65.10	1.20	38.93	0.87	1.89	0.02	1503.00	12.00
RM07_5_43	42.80	1.20	21.96	0.61	2.18	0.02	985.00	10.00
RM07_5_44	144.30	4.80	38.20	1.70	4.28	0.07	1166.10	7.20
RM07_5_45	96.20	2.00	19.62	0.30	5.48	0.07	1260.60	8.40
RM07_5_46	17.62	0.28	7.56	0.24	2.69	0.08	1020.00	12.00
RM07_5_47	74.50	2.10	16.49	0.54	5.22	0.08	1191.20	9.40
RM07_5_48	178.80	1.50	24.45	0.22	8.13	0.08	1535.00	10.00
RM07_5_49	214.00	13.00	75.30	4.80	3.20	0.05	1755.00	35.00
RM07_5_50	101.10	3.20	24.42	0.76	4.59	0.05	1451.00	12.00
RM07_5_51	64.90	1.30	16.63	0.33	4.39	0.05	1321.00	12.00
RM07_5_52	81.10	1.30	28.94	0.66	3.12	0.04	1206.50	8.60
RM07_5_53	81.30	4.80	30.50	1.10	2.80	0.07	1258.00	12.00
RM07_5_54	156.60	3.20	22.40	0.50	7.82	0.08	1581.00	10.00
RM07_5_55	178.00	1.70	73.80	1.10	2.68	0.03	1348.50	8.40
RM07_5_56	93.00	2.00	23.00	1.00	4.94	0.20	1220.00	13.00
RM07_5_57	118.90	2.20	37.59	0.77	3.55	0.03	1192.20	7.90

Appendix 3.1: Data table for U-Pb analyses

Sample Name	U (ppm)	U (ppm) 2-sigma error	Th (ppm)	Th (ppm) 2-sigma error	U/Th	U/Th 2-sigma error	Age (Ma)	Age (Ma) 2-sigma error
RM07_5_58	229.10	5.00	32.67	0.30	7.83	0.16	1509.00	10.00
RM07_5_59	21.21	0.54	3.84	0.09	6.12	0.11	1249.00	14.00
RM07_5_60	55.20	1.10	22.35	0.51	2.87	0.08	522.50	4.80
RM07_5_61	267.80	6.00	72.50	1.90	4.11	0.04	1501.10	9.20
RM07_5_62	124.70	3.10	91.70	2.60	1.52	0.01	341.90	2.70
RM07_5_63	256.60	3.90	18.92	0.27	14.73	0.33	604.70	4.70
RM07_5_64	170.00	13.00	19.24	0.31	10.03	0.83	1573.00	11.00
RM07_5_65	179.40	4.80	55.80	1.60	3.67	0.04	1473.00	12.00
RM07_5_66	61.00	1.60	17.04	0.38	3.91	0.04	1165.40	8.00
RM07_5_67	157.60	3.00	32.25	0.73	5.36	0.05	1184.30	7.30
RM07_5_68	81.60	1.10	19.48	0.43	4.61	0.06	1155.80	7.70
RM07_5_69	82.60	4.00	22.73	0.61	3.73	0.10	1363.50	8.80
RM07_5_70	128.20	1.70	46.93	0.85	3.05	0.04	1056.00	10.00
RM07_5_71	86.10	0.66	20.24	0.28	4.62	0.06	985.90	7.30
RM07_5_72	119.10	2.60	40.60	1.00	3.14	0.04	1109.00	10.00
RM07_5_73	28.94	0.94	9.08	0.36	3.77	0.15	1635.00	16.00
RM07_5_74	133.80	1.50	63.57	0.66	2.26	0.02	1028.70	6.30
RM07_5_75	57.46	0.46	14.00	0.33	4.48	0.12	1106.00	11.00
RM07_5_76	117.53	0.82	31.52	0.27	4.00	0.04	1167.50	8.70
RM07_5_77	126.60	1.80	31.55	0.38	4.26	0.04	1289.30	8.20
RM07_5_78	145.90	3.60	49.10	1.50	3.18	0.03	1045.00	11.00
RM07_5_79	119.50	1.90	22.15	0.39	5.72	0.06	1517.00	11.00
RM07_5_80	23.20	1.00	16.53	0.75	1.53	0.04	1639.00	33.00
RM07_5_81	53.24	0.92	21.68	0.24	2.58	0.04	1202.00	11.00
RM07_5_82	70.80	1.80	20.64	0.69	3.66	0.05	1143.70	7.90
RM07_5_83	271.60	2.20	75.74	0.70	3.78	0.04	1175.00	13.00
RM07_5_84	85.17	0.77	27.28	0.29	3.26	0.04	1512.00	10.00
RM07_5_85	337.90	6.50	93.90	2.50	3.82	0.04	1343.20	8.70
RM07_5_86	76.20	1.60	18.18	0.42	4.34	0.05	1541.00	11.00
RM07_5_87	54.60	2.30	17.90	0.56	3.28	0.08	1213.80	9.60
RM07_5_88	28.68	0.71	12.85	0.30	2.29	0.02	992.50	9.30
RM07_5_89	26.89	0.87	7.52	0.28	3.71	0.05	1162.00	12.00
RM07_5_90	62.13	0.55	11.59	0.15	5.52	0.06	1185.90	9.00

Appendix 3.1: Data table for U-Pb analyses

Sample Name	U (ppm)	U (ppm) 2-sigma error	Th (ppm)	Th (ppm) 2-sigma error	U/Th	U/Th 2-sigma error	Age (Ma)	Age (Ma) 2-sigma error
RM07_5_91	57.28	0.97	17.33	0.32	3.42	0.05	1241.60	9.60
RM07_5_92	111.60	5.50	38.60	1.60	2.84	0.04	1273.00	11.00
RM07_5_93	54.40	1.60	21.50	0.65	2.49	0.03	1535.00	15.00
RM07_5_94	72.30	1.50	27.14	0.61	2.75	0.03	1270.00	11.00
RM07_5_95	155.60	4.10	35.70	1.20	4.41	0.07	1488.00	11.00
RM07_5_96	105.20	3.70	44.80	2.20	2.42	0.05	1127.00	12.00
RM07_5_97	91.30	6.00	14.96	0.96	6.10	0.07	1188.00	12.00
RM07_5_98	16.98	0.27	5.36	0.10	3.15	0.05	1152.00	13.00
RM07_5_99	163.60	3.70	38.76	0.61	4.16	0.04	1490.00	11.00
RM07_5_100	67.70	2.70	31.40	2.30	2.58	0.16	988.40	8.40
RP07_1_1	89.50	2.00	20.29	0.51	4.40	0.05	1113.10	9.00
RP07_1_2	60.50	0.86	35.75	0.69	1.70	0.02	1487.00	31.00
RP07_1_3	58.00	1.20	23.95	0.55	2.45	0.03	562.30	5.30
RP07_1_4	95.73	0.85	15.91	0.18	6.13	0.07	561.60	4.60
RP07_1_5	102.80	3.00	59.20	2.10	1.80	0.02	491.80	4.30
RP07_1_6	39.04	0.72	9.87	0.18	4.12	0.06	1101.90	9.40
RP07_1_7	168.00	9.00	83.10	4.80	2.14	0.05	1442.00	19.00
RP07_1_8	29.07	0.53	16.43	0.32	1.79	0.02	531.10	5.70
RP07_1_9	310.00	30.00	91.00	3.20	3.26	0.19	1767.00	24.00
RP07_1_10	213.50	3.50	132.80	1.50	1.63	0.02	582.20	4.80
RP07_1_11	135.00	11.00	58.60	3.30	2.32	0.06	1366.00	20.00
RP07_1_12	282.60	6.30	131.60	4.00	2.29	0.05	494.60	4.30
RP07_1_13	182.30	3.10	41.23	0.48	4.48	0.08	896.40	6.30
RP07_1_14	225.80	3.80	54.60	1.40	4.27	0.05	1035.30	6.10
RP07_1_15	336.00	17.00	22.38	0.31	15.63	0.73	1013.20	9.90
RP07_1_16	437.80	8.80	190.80	4.50	2.37	0.02	488.60	3.00
RP07_1_17	747.00	21.00	297.80	7.80	2.60	0.03	1523.60	8.50
RP07_1_18	412.60	6.80	255.80	3.70	1.67	0.01	3036.00	17.00
RP07_1_19	142.30	2.80	40.74	0.40	3.64	0.05	524.10	3.90
RP07_1_20	294.50	4.70	126.50	1.90	2.45	0.07	1172.00	11.00
RP07_1_21	1159.80	9.90	452.00	12.00	2.71	0.09	1147.80	9.60
RP07_1_22	206.90	5.10	54.90	2.60	4.60	0.28	478.80	8.80
RP07_1_23	139.40	3.30	40.70	1.10	3.60	0.04	1128.00	8.40

Appendix 3.1: Data table for U-Pb analyses

Sample Name	U (ppm)	U (ppm) 2-sigma error	Th (ppm)	Th (ppm) 2-sigma error	U/Th	U/Th 2-sigma error	Age (Ma)	Age (Ma) 2-sigma error
RP07_1_24	91.50	2.40	59.20	1.10	1.63	0.02	529.10	6.00
RP07_1_25	77.00	1.60	22.37	0.47	3.68	0.04	754.00	13.00
RP07_1_26	338.30	4.10	143.80	2.40	2.48	0.04	246.30	2.50
RP07_1_27	113.10	2.30	22.21	0.35	5.42	0.08	2695.00	26.00
RP07_1_28	139.50	5.30	66.10	2.60	2.24	0.02	528.40	7.90
RP07_1_29	200.60	9.20	39.20	2.90	5.24	0.19	827.00	25.00
RP07_1_30	59.10	3.60	31.70	1.90	1.96	0.03	507.50	7.20
RP07_1_31	62.55	0.72	6.22	0.16	10.81	0.21	1263.00	14.00
RP07_1_32	51.70	2.00	11.37	0.92	4.78	0.34	2114.00	86.00
RP07_1_33	198.60	4.50	48.05	0.95	4.40	0.04	452.80	4.20
RP07_1_34	110.60	6.50	79.40	6.30	1.48	0.08	649.00	8.80
RP07_1_35	85.40	4.30	34.80	3.00	3.22	0.15	1049.00	11.00
RP07_1_36	37.63	0.97	31.35	0.86	1.33	0.03	484.00	16.00
RP07_1_37	145.30	2.60	53.07	0.96	2.92	0.03	991.00	10.00
RP07_1_38	95.50	1.50	28.34	0.57	3.65	0.04	1335.70	8.60
RP07_1_39	354.20	3.90	232.10	2.60	1.63	0.01	597.30	4.30
RP07_1_40	270.50	2.30	109.30	1.70	2.64	0.04	554.70	5.30
RP07_1_41	170.40	2.60	58.80	0.80	3.11	0.05	1488.00	13.00
RP07_1_42	50.10	1.40	14.83	0.58	3.35	0.08	982.00	16.00
RP07_1_43	81.40	2.40	35.40	1.50	2.37	0.04	1739.00	39.00
RP07_1_44	176.10	2.30	33.40	3.80	7.05	0.56	1520.20	9.20
RP07_1_45	85.70	6.20	42.80	3.30	2.11	0.03	1570.00	22.00
RP07_1_46	448.00	10.00	11.47	0.42	44.51	0.83	564.10	3.60
RP07_1_47	434.40	5.80	58.80	1.40	8.20	0.23	604.00	7.10
RP07_1_48	98.60	1.30	12.97	0.17	8.20	0.10	844.20	7.80
RP07_1_49	46.46	0.92	29.71	0.98	1.69	0.05	855.00	27.00
RP07_1_50	249.20	8.30	93.70	2.20	2.91	0.05	505.20	5.30
RP07_1_51	28.89	0.69	12.79	0.39	2.45	0.03	973.00	11.00
RP07_1_52	107.10	1.50	24.02	0.57	4.81	0.07	951.50	6.80
RP07_1_53	422.00	4.40	9.17	0.70	62.50	3.90	567.40	3.80
RP07_1_54	397.10	9.70	50.98	0.58	8.31	0.21	1461.00	19.00
RP07_1_55	201.10	2.80	10.68	0.16	20.18	0.21	594.40	4.10
RP07_1_56	82.00	1.60	27.04	0.61	3.27	0.04	1013.00	12.00

Appendix 3.1: Data table for U-Pb analyses

Sample Name	U (ppm)	U (ppm) 2-sigma error	Th (ppm)	Th (ppm) 2-sigma error	U/Th	U/Th 2-sigma error	Age (Ma)	Age (Ma) 2-sigma error
RP07_1_57	108.90	1.70	32.96	0.54	3.46	0.05	1167.00	12.00
RP07_1_58	385.30	6.20	36.85	0.73	11.37	0.11	528.40	3.50
RP07_1_59	179.30	5.40	88.50	3.80	2.22	0.03	1781.00	16.00
RP07_1_60	521.00	11.00	60.30	5.60	13.80	1.00	753.50	9.90
RP07_1_61	59.70	1.30	44.20	1.20	1.45	0.03	1805.00	25.00
RP07_1_62	177.40	3.50	38.72	0.93	5.17	0.09	1178.00	13.00
RP07_1_63	402.00	15.00	100.70	5.40	4.42	0.07	989.80	7.60
RP07_1_64	266.20	4.30	92.60	1.50	3.05	0.06	1252.00	27.00
RP07_1_65	285.00	14.00	24.10	1.10	12.90	0.20	1260.00	28.00
RP07_1_66	278.00	16.00	56.10	3.40	5.16	0.09	706.00	10.00
RP07_1_67	182.70	5.10	42.16	0.49	4.64	0.14	1090.70	8.30
RP07_1_68	208.00	12.00	61.80	4.10	4.46	0.32	850.00	41.00
RP07_1_69	106.20	1.20	62.93	0.93	1.79	0.02	511.30	4.80
RP07_1_70	93.50	6.80	41.90	1.00	2.54	0.24	387.00	25.00
RP07_1_71	340.00	11.00	61.10	1.10	5.91	0.13	788.00	17.00
RP07_1_72	332.20	2.30	97.30	1.80	3.60	0.07	1394.00	9.90
RP07_1_73	283.00	10.00	39.07	0.74	7.51	0.23	829.10	7.50
RP07_1_74	86.60	3.40	23.78	0.91	3.87	0.08	819.60	8.00
RP07_1_75	165.80	5.00	88.80	2.70	1.96	0.03	423.80	5.90
RP07_1_76	112.23	0.97	20.06	0.23	5.91	0.08	546.40	4.50
RP07_1_77	644.00	15.00	68.10	2.70	10.03	0.22	1199.00	25.00
RP07_1_79	145.80	3.40	69.50	1.90	2.17	0.02	869.00	21.00
RP07_1_80	206.40	5.90	102.00	2.30	2.09	0.04	240.60	2.50
RP07_1_81	301.00	11.00	64.40	2.20	4.77	0.08	957.30	9.00
RP07_1_82	73.10	1.20	27.94	0.42	2.70	0.04	2604.00	33.00
RP07_1_83	119.20	4.50	42.00	2.10	3.06	0.07	1180.00	25.00
RP07_1_84	222.20	4.30	162.30	2.50	1.37	0.03	346.90	6.80
RP07_1_85	265.40	6.60	24.90	1.50	12.17	0.97	489.10	6.20
RP07_1_86	100.20	1.50	48.93	0.65	2.12	0.03	582.00	5.60
RP07_1_87	358.70	7.50	75.90	1.50	4.86	0.05	1046.00	12.00
RP07_1_88	75.10	3.10	28.90	1.90	2.78	0.09	545.00	5.80
RP07_1_89	99.00	2.60	17.51	0.54	5.86	0.08	906.50	7.20
RP07_1_90	80.50	1.60	47.28	0.89	1.77	0.04	549.10	8.40

Appendix 3.1: Data table for U-Pb analyses

Sample Name	U (ppm)	U (ppm) 2-sigma error	Th (ppm)	Th (ppm) 2-sigma error	U/Th	U/Th 2-sigma error	Age (Ma)	Age (Ma) 2-sigma error
RP07_1_91	443.00	22.00	34.70	2.60	21.20	2.50	1440.00	11.00
RP07_1_92	130.80	4.80	77.00	3.20	1.72	0.02	909.00	11.00
RP07_1_93	141.80	2.00	57.80	3.10	2.72	0.14	1414.00	22.00
RP07_1_94	16.86	0.17	7.16	0.15	2.41	0.05	1329.00	14.00
RP07_1_95	107.30	2.00	21.40	1.20	5.30	0.21	612.10	6.80

3.7 References

Bard, J.-P., Botello, R., Martinez, C., Subieta, T., 1974. Relations entre tectonique, me´tamorphisme et mise en place d'un granite e´ohercynien a` deux micas dans la Cordille`re Real de Bolivie (massif de Zongo-Yani). Cahiers ORSTOM, Se´rie Ge´ologie 6, 3– 18.

Benavides-Cáceres, V.E., 1956. Cretaceous system in northern Peru. Bulletin of the American Museum of Natural History 108, 353e494.

Bond, G.C., Nickeson, P.A., and Kominz, M.A., 1984. Breakup of a supercontinent between 625 Ma and 555 Ma: new evidence and implications for continental histories. Earth and Planetary Science Letters, v.70, p. 325-345

Cardona, A., Cordani, U.G., Ruiz, J., Valencia, V.A., Armstrong, R., Chew, D.,Nutman, A., Sánchez, A.W., 2009. U-Pb zircon geochronology and Nd isotopic signatures of the pre-Mesozoic metamorphic basement of the eastern Peruvian Andes: growth and provenance of a Late Neoproterozoic to Carboniferous accretionary orogen on the northwest margin of Gondwana. The Journal of Geology 117, 285e305.

Cardona, A., Chew, D., Valencia, V.A., Bayona, G., Miskovic, A., Ibanez-Mejia, M., 2010. Grenvillian remnants in the Northern Andes: Rodinian and Phanerozoic paleogeographic perspectives. Journal of South American Earth Sciences, v29, p.92-104

Carlotto, V., Quispe, J., Acosta, H., Rodríguez, R., Romero, D., Cerpa, L., Mamani, M., Díaz-Martínez, E., Navarro, P., Jaimes, F., Velarde, T., Lu, S., Cueva, E., 2009. Dominios Geotéctonicos y Metalogenésis del Perú. Boletín Sociedad Geológica del Perú 103, 1e89.

Cawood, P.A., and Buchan, C., 2007, Linking accretionary orogenesis with supercontinent assembly: Earth- Science Reviews, v. 82, p. 217–256, doi: 10.1016/j.earscirev.2007.03.003.

Cawood, P.A., Mccausland, P.J.A., Dunning, G.R., 2001. Opening Iapetus: constraints from the Laurentian margin in Newfoundland. Geological Society of America Bulletin 113, 443–453.

Chew, D.M., Schaltegger, U., Košler, J., Whitehouse, M., Gutjahr, M., Spikings, R.A., and Mišković, A., 2007, U-Pb geochronologic evidence for the evolution of the Gondwanan margin of the north-central Andes: Geological Society of America Bulletin, v. 119, p. 697– 711, doi: 10.1130/B26080.1.

Chew, D.M., Magna, T., Kirkland, C.L., Miškovic, A., Cardona, A., Spikings, A., Schaltegger, U., 2008. Detrital zircon fingerprint of the Proto-Andes: evidence for a Neoproterozoic active margin? Precambrian Research 167, 186–200.

Dalmayrac, B., Laubacher, G., Marocco, R., 1980. Caractères généraux de l'évolution géologique des Andes péruviennes. In: Travaux et Documents de l'ORSTOM, vol. 122, Paris, 501 pp.

Dalziel, I.W.D., Dalla Salda, L., and Gahagan, L.M., 1994, Paleozoic Laurentia-Gondwana interaction and the origin of the Appalachian-Andean mountain system: Geological Society of America Bulletin, v. 106, p. 243–252, doi: 10.1130/0016-7606(1994)106<0243:PLGIAT> 2.3.CO;2.

Forsythe, R.D., Davidson, J., Mpodozis, C., and Jesinkey, C., 1993, Lower Paleozoic relative motion of the Arequipa block and Gondwana: Paleomagnetic evidence from Sierra de Almeida of Northern Chile: Tectonics, v. 12, p. 219–236, doi: 10.1029/92TC00619.

Hoffman, P.F., 1991, Did the breakout of Laurentia turn Gondwanaland inside-out?: Science, v. 252, p. 1409– 1412, doi: 10.1126/science.252.5011.1409.

Jaillard, E. and Soler P., 1996. Cretaceous to Early Paleogene tectonic evolution of the northern Central Andes (0-18S) and its relations to geodynamics, Tectonophysics 259, p41-53.

Jaillard, E., and Sempere, T., 1989, Cretaceous sequence stratigraphy of Peru and Bolivia: Simposios Sobre Cretácico de América Latina, Proceedings, p. A1–A27.

Jaillard, E., Hérail, G., Monfret, T., Díaz-Martínez, E., Baby, P., Lavenu, A., and Dumont, J.F., 2000, Tectonic evolution of the Andes of Ecuador, Peru, Bolivia and northernmost Chile, in Cordani, U., Milani, E.J., Thomaz Filho, A., and Campos Neto, M.C., eds., Tectonic evolution of South America: Rio de Janeiro, 31st International Geological Congress, p. 481–559.

Janjou, D., Bourgois, J., Mégard, F., Sornay, J., 1981. Rapports paléogéographiques et structuraux entre Cordillères occidentale et orientale des Andes nordpéruviennes: les écailles du Marañon (7S, Départements de Cajamarca et de Amazonas, Pérou). Bulletin de la Société Géologique de France 23 (6), 693e705 (7).

Kontak, D.J., Clark, A.H., Farrar, E., Archibald, D.A., and Baadsgaard, H., 1990, Late Paleozoic-early Mesozoic magmatism in the Cordillera de Carabaya, Puno, southeastern Peru: Geochronology and petrochemistry: Journal of South American Earth Sciences, v. 3, p. 213–230, doi: 10.1016/0895-9811(90) 90004-K.

Loewy, S.L., Connelly, J.N., and Dalziel, I.W.D., 2004, An orphaned basement block: The Arequipa-Antofalla basement of the central Andean margin of South America: Geological Society of America Bulletin, v. 116, p. 171–187, doi: 10.1130/B25226.1.

Mišković, A., Schaltegger, U., and Chew, D., 2005, Carboniferous plutonism along the Eastern Peruvian Cordillera: Implications for the Late Paleozoic to early Mesozoic Gondwanan tectonics: Barcelona, 6th International Symposium on Andean Geodynamics, IRD Editions (Institut de Recherche pour le Développement , Paris), p. 508–511.

Mišković, A., Spikings, R.A., Chew, D.M., Kosler, J., Ulianov, A., and Schaltegger, Urs., 2009. Tectonomagmatic evolution of Western Amazonia: Geochemical characterization and zircon U-Pb geochronologic constraints from the Peruvian Eastern Cordilleran granitoids. Geological Society of America Bulletin, v.121, no 9-10; 1298-1324

Mégard, F., 1973, Étude géologique d'une transversale des Andes au niveau du Pérou Central [Ph.D. thesis]: Université de Montpellier, 264 p.

Mégard, F., Dalmayrac, B., Laubacher, G., Marocco, R., Martinez, C., Paredes, J., and Tomasi, P., 1971, La chaîne hercynienne au Pérou et en Bolivie: Premiers résultats: Cahiers de l'ORSTOM, série géologie 3, 5 p.

Mégard, F., 1987. Cordilleran Andes and Marginal Andes: A Review of Andean Geology North of the Arica Elbow (18 S). ????

McLaughlin, D.H., 1924. Geology and physiography of the Peruvian Cordillera, Departments of Junin and Lima. Geological Society of America Bulletin 35, 591e632.

Mourier, T., Bengtson, P., Bonhomme, M., Buge, E., Cappetta , H., Crochet, J.-Y., Feist, M., Hirsch, K., Jaillard , E., Laubacher, G., Lefranc, J.-P., Moullade, M., Noblet, C., Pons, D., Rey, J., Sigt, B., Tambareau, Y., and Taquet, P., 1988, The Upper Cretaceous–Lower Tertiary marine to continental transition in the Bagua basin, Northern Peru: Newsletters on Stratigraphy, v. 19, p. 143–177.

Noble, D.C., McKee, E.H., Mourier, T., and Megard, F., 1990. Cenozoic stratigraphy, magmatic activity, compressive deformation, and uplift in northern Peru, Geological Society of American Bulletin, 102, 1105-1113.

Paton, C., Hellstrom, J., Paul, B., Woodhead, J., and Hergt, J., 2011. Iolite:Freeware for the visualization and processing of mass spectrometric data. J. Anal. At. Spectrom, DOI: 10.1039/c1ja10172b

Ramos, V.A., 2008, The basement of the Central Andes: The Arequipa and related terranes: Annual Review of Earth and Planetary Sciences, v. 36, doi: 10.1146/ annurev.earth.36.031207.124304.

Ramos, V.A., Jordan, T.E., Allmendinger, R.W., Mpodozis, C., Kay, S.M., Cortés, J.M., and Palma, M., 1986, Paleozoic terranes of the Central Argentine-Chilean Andes: Tectonics, v. 5, p. 855–880, doi: 10.1029/ TC005i006p00855.

Rapela, C.W., Pankhurst, R.J., Casquet, C., Baldo, E., Saavedra, J., Galindo, C., 1998. Early evolution of the Proto-Andean margin of South America. Geology 26 (8), 707–710.

Rapela, C.W., Pankhurst, R.J., Casquet, C., Fanning, C.M., Baldo, E.G., Gonz.lez-Casado, J.M., Galindo, C., Dahlquist, J., 2007. The R.o de la Plata craton and the assembly of SW Gondwana. Earth Science Reviews 83, 49–82.

Sadowski, G.R., and Bettencourt, J.S., 1996, Mesoproterozoic tectonic correlations between eastern Laurentia and the western border of the Amazon Craton: Precambrian Research, v. 76, p. 213–227, doi: 10.1016/ 0301-9268(95) 00026-7.

Shackleton, R.M., Ries, A.C., Coward, M.P., and Cobbold, P.R., 1979, Structure, metamorphism and geochronology of the Arequipa Massif of coastal Peru: Journal of the Geological Society, v. 136, p. 195–214, doi: 10.1144/gsjgs. 136.2.0195.

Scherrenberg, A.F., Jacay, J., Holcombe, R.J., Rosenbaum, G., 2012. Stratigraphic variations across the Marañon Fold-Thrust Belt, Peru: Implications for the basin architecture of the West Peruvian Trough. Journal of South American Earth Sciences, v. 38, p. 147-158

Schreiber, D.W., Fontboté, L., and Lochmann, D., 1990, Geologic setting, paragenesis, and physicochemistry of gold quartz veins hosted by plutonic rocks in the Pataz region: Economic Geology and the Bulletin of the Society of Economic Geologists, v. 85, p. 1328–1347.

Soto, V. 1979. Facies y ambientes deposicionalescretácicos ,área Centro-Sur de la Cuenca Marañón. Bol.' Soc: Geol. PerÚ, 60, 233-250. Lima.

Sempere, T., 1995, Phanerozoic evolution of Bolivia and adjacent regions, in T ankard, A.J., Suarez, R., and Welsink , H.J., eds., Petroleum basins of South America: American Association of Petroleum Geologists Memoir, v. 62, p. 207–230.

Sempere, T., Carlier, G., Soler, P., Fornari, M., Carlotto, V., Jacay, J., Arispe, O., Néraudeau, D., Cárdenas, J., Rosas, S., and Jiménez, N., 2002, Late Permian–Middle Jurassic lithospheric thinning in Peru and Bolivia, and its bearing on Andean tectonics: Tectonophysics, v. 345, p. 153–181, doi: 10.1016/ S0040-1951 (01)00211-6.

Spikings, R.A., Winkler, W., Hughes, R.A., and Handler, R., 2005, Thermochronology of allochthonous terranes in Ecuador: Unravelling the accretionary and post-accretionary history of the Northern Andes: Tectonophysics, v. 399, p. 195–220, doi: 10.1016/j.tecto. 2004.12.023.

Steinmann, G., 1929. Geologie von Peru. Karl Winter Universitat, Heidelberg, 248 p.

Tosdal, R.M., 1996, The Amazon-Laurentian connection as viewed from the Middle Proterozoic rocks in the central Andes, western Bolivia and northern Chile: Tectonics, v. 15, p. 827–842, doi: 10.1029/95TC03248.

Wilson, J.J., 1963. Cretaceous stratigraphy of central Andes of Peru. American Association of Petroleum Geologists Bulletin 47 (1), 1e34.

Wilson, J.J., Reyes, L., Garayar, J., 1967. Geología de los cuadrángulos de Mollebamba, Tayabamba, Pomabamba y Huarí, Lima, Peru. Servicio de Geología y Minería del Perú, Boletín 16, 95.

Zeil, W., 1983, Das präkambrische Basement der Anden: Ein Überblick, in Miller, H., and Rosenfeld, U., eds., Geowissenschaftliches Lateinamerika-Kolloquium: Teil I, Zentralblatt für Geologie und Paläontologie, p. 246–254.

Chapter 4.

Miocene-Pliocene accelerated exhumation in the north-central Peruvian Andes

4.0 Abstract

Using low-temperature (U-Th)/He thermochronology from apatite and zircon at three locations spanning 200 km of latitude in the north-central Peruvian Andes, we document a previously unrecognized, but important Miocene-Pliocene acceleration in rock exhumation rates. At two sites within the Rio Marañon river system we show an increase in exhumation rate of roughly an order of magnitude by the end of the Miocene, while a third site shows a rapid signal of accelerated exhumation from the Pliocene to present. We interpret these data to represent two spatial signals of exhumation; the former an along-strike, regional signal, likely a result of uplift of the Eastern Peruvian Andes and the latter, related to batholithic cooling and fault-driven exhumation along the Cordillera Blanca Detachment System. However, taken together, these two signals support a model of late Cenozoic uplift in the north-central Andes of Peru (5-8°S).

4.1 Introduction

While the South American Andes represent the classic orogenic setting of oceanic-continental collision, even the most fundamental processes controlling the

generation and maintenance of the high topography remain controversial. The majority of studies investigating paleoelevation and uplift in the Andes have focused on the Altiplano-Puna, recognizing that despite long-lived subduction since the Jurassic, uplift of the Altiplano has occurred since 40 Ma (Isacks, 1988; Sempere, 1990; Allmendinger et al., 1997; Capitanio et al., 2011). Some work supports a period of very rapid uplift between 10 and 4 Ma (Gregory-Wodzicki, 2000; Ghosh et al., 2006; Hoke et al., 2007; Garzione et al., 2008; Lamb, 2011) whereas other suggests more protracted uplift since Eocene time (McQuarrie et al., 2005; Barnes and Ehlers, 2009). The proposed mechanisms to accommodate Altiplano uplift include crustal shortening (Isacks et al., 1988), lithospheric delamination (Kay and Kay, 1993; Garzione et al., 2006), lower-crustal ductile flow (Beck and Zandt, 2002; Husson and Sempere, 2003), mass addition through sedimentation and magmatism (Lamb and Hoke, 1997), and dynamic effects of the subducting oceanic lithosphere (Capitanio et al., 2011). However, any mechanism proposed as an explanation for the formation of the Andes must account for the along-strike morphologic, tectonic and climatic segmentation. At present, it is not known whether or not these dynamical mechanisms apply more generally to the Andes as a whole or are restricted to the Altiplano region.

The Altiplano region is characterized by a wider zone of high topography, arc-like crustal heat flow and a "normal" angle of subduction. In contrast, the region of focus in this study, the north-central Peruvian Andes (Fig. 4.1), are characterized by flat-slab subduction (Barazangi and Isacks, 1976), relatively low heat flow (Henry

and Pollack, 1988), and a narrow zone of high topography. Further, the north and central Andes have highly asymmetric east-to-west modern precipitation, with the eastern flank receiving the majority of the precipitation, and a subtle north-south precipitation gradient (Bookhagen and Strecker, 2008). Exactly when the modern moisture patterns developed is not well constrained, however, there is evidence from sedimentological records (Fig.ueiredo et al., 2009; Uba et al., 2009) and regional climate models (Ehlers and Poulsen, 2009; Poulsen et al., 2010) for an increase in precipitation along the eastern Andean flank during the mid-to-late Miocene.

Both far-field tectonic forces (i.e. subduction angle) and climate (i.e. strong precipitation gradients) are reflected in the segmented morphology of the Andes, suggesting potential couplings (Isacks, 1988; Masek, 1994; Montgomery et al., 2001, Pelletier et al., 2010). While it remains challenging to isolate potential feedbacks between far-field and near-field forces driving the Andean orogenic system, understanding the locus and chronology of uplift is critical for deconvolving the relative contributions of tectonic and climatic processes (e.g. Strecker et al., 2007; Barnes et al., 2008; McQuarrie et al., 2008; Whipple et al., 2009).

Low-temperature thermochronometer systems, such as (U-Th)/He in apatite and zircon, are able to constrain exhumational histories of the shallow (<10 km depth) crust and are thus extremely powerful for the study of growth and decay of orogens (e.g. Stockli et al., 2000; Ehlers and Farley, 2003; Reiners and Brandon, 2006). Here, we use (U-Th)/He thermochronology to quantify crustal exhumation in order to

develop a regional model of crustal exhumation and uplift using both apatite and zircon (U-Th)/He from transects at three locations spanning ~200 km along-strike.

4.2 Deformation and Uplift in the north-central Peruvian Andes

Long-lived subduction of the Nazca plate under the South America plate (e.g. James, 1971) has produced the classic, "Andean-style" margin, consisting of a subduction trench, forearc basin, magmatic arc and foreland fold and thrust belt (e.g. Dewey and Bird, 1970). In the Peruvian Andes between ~5°S-15°S, the structural zones from west to east (Fig. 4.2) are i) the Western Cordillera, including the Coastal Batholith associated with Mesozoic magmatism which has intruded into Precambrian metamorphic rocks and is overlain by Cenozoic continental sediments and volcanics, ii) the Eastern Cordillera, folded and faulted Precambrian-Paleozoic low-grade metamorphic basement and minor intrusive rocks, and iii) the Sub-Andean fold and thrust belt, involving Mesozoic through Cenozoic marine and continental sedimentary deposits (James, 1971; Cobbing and Pitcher, 1972; Megard, 1984; Sebrier et al., 1988; Lamb and Hoke, 1997; Hermoza et al., 2005; McQuarrie et al., 2005). In addition, the north-central Peruvian Andes are host to the Cordillera Blanca (Fig. 4.2), which consists mainly of a late Miocene granodioritic batholith (Atherton and Petford, 1993; McNulty et al. 1998). The Cordillera Blanca batholith is thought to represent the last episode of magmatism prior to initiation of flat slab subduction of

the Nazca plate along the north-central Peruvian Andean margin (McNulty and Farber, 2002). Soon after intrusion, the Cordillera Blanca Batholith was uplifted along the west-dipping Cordillera Blanca detachment system, which extends for ~200 km along the range (McNulty and Farber, 2002; Garver et al., 2005; Giovanni et al., 2010). Rapid rock uplift and exhumation of the Cordillera Blanca has occurred since 6 Ma (Garver et al., 2005, Giovanni et al., 2010).

The first major phase of deformation recognized within the Peruvian Andes, the 'Peruvian phase' began ~85-70 Ma, affecting the Paleozoic rocks of the eastern side of the Western Cordillera and was coincident with intense volcanism along the entire Andean arc (Megard, 1978). The deformation front propagated eastward in the Paleocene-Eocene 'Incaic phases' (I and II) producing the Marañon fold and thrust belt, followed by the Miocene-Pliocene 'Quechua phases' (I, II, and III) that primarily affected the Eastern Cordillera and Sub-Andean zones (Megard, 1984; Noble et al., 1990; Sebrier et al., 1988). At present the major crustal deformation is focused along the Sub-Andean fold and thrust belt (Horton and DeCelles, 1997; Hermoza et al., 2005).

In the Peruvian Andes, the tectonic chronology has been described in terms of five or temporally restricted pulses of compressive tectonism, separated by longer periods of quiescence or extensional stress (McKee and Noble, 1982; Megard et al., 1984; Noble et al., 1990). Several studies suggest that the major uplift event was the Eocene Incaic phase of tectonic shortening (e.g. Megard, 1984; Sebrier et al., 1988;

Noble et al., 1990). However, these estimates of the timing of uplift are based on structural studies and not on data that can directly constrain rock or surface uplift. In Peru, workers have identified three regional scale erosional surfaces; from oldest to youngest these are the Puna, Vallé and Cañon surfaces. The Puna surface is thought to have been cut at sea level, is now at 4200-4400 m.a.s.l. and has developed in volcanics as young as 15 Ma of the Calipuy Group (Bowman 1906, McLaughlin, 1924, Tosdal et al., 1984). The Vallé stage is characterized by incision of river valleys in response to initial surface uplift which occurred in the mid-to-late Miocene. The 2 km thickness of the Forteleza Ignimbrite suggests that at least this much relief formed by 5-7 Ma. The Cañon stage, which cuts both the Puna and Valle surfaces, is the most recent uplift episode, thought to account for 2-3 km of uplift since the Pliocene (Myers, 1980; Cobbing et al. 1981, 1997; Garver et al., 2005).

4.3 Previous thermochronologic studies

Through much of the Andes, workers have undertaken thermochronologic studies investigating the timing, amount and style of deformation, and rock uplift and exhumation. The areas best studied include the Bolivian Andes (e.g. Benjamin et al., 1987; Gillis et al., 2006; Safran et al., 2006; Ege et al. 2007; Barnes et al., 2008), the Western Cordillera of Southern Peru (Schildgen et al., 2007; 2009; Gunnell et al., 2010) and the Puna Plateau in NW Argentina (e.g. Sobel et al., 2003; Carrapa et al.,

2005; Coutand et al., 2006). Many of these studies have related the timing of deformation, uplift and exhumation of the central Andes to the uplift of the Altiplano-Puna Plateau.

However, in the Andes of north-central Peru, outside of the Altiplano-Puna Plateau region, studies are fewer and more spatially confined. From fission track work, Laubacher and Naeser (1994) interpret post 30 Ma cooling from the Eastern Cordillera of Central Peru near Huachon (~10.5°S) to represent 4-6 km of erosion. Garver et al. (2005) suggest late Miocene zircon fission track (ZFT) and zircon (U-Th)/He (ZHe) ages from the Cordillera Huayhuash record an adjustment of the geothermal gradient due to post-intrusive cooling from the adjacent Cordillera Blanca batholith, canyon incision and associated isostatic rebound. Pliocene apatite (U-Th)/He cooling ages from the Cordillera Blanca batholith have been interpreted as a signal of rapid exhumation of the batholith achieved by a combination of batholitic cooling and uplift along the Cordillera Blanca detachment fault (Giovanni, 2007). In the Western Cordillera of Peru, Wipf (2006) used apatite and zircon fission track and (U-Th)/He apatite ages from mostly lower elevations (<500m) along the western flank of the Coastal Batholith to investigate rates of exhumation along-strike from 5°S to 15°S. They show that ZFT ages range between 130 and 45 Ma, AFT ages lie between 124 and 24 Ma, and suggest that there is little correlation between cooling age and latitudinal position in along-strike age spectra.

4.4 Apatite and zircon (U-Th)/He thermochronology

Thermochronology measures the time at which a rock, due to rock exhumation, cools through a closure isotherm. In the (U-Th)/He isotopic system, radiogenic helium produced by alpha decay diffuses out of the mineral at high temperatures, but below its closure temperature (Dodson, 1973), ^{4}He is retained, thus starting the radioactive "clock." The time since the sample cooled through the closure isotherm is referred to as a cooling age. Cooling ages are calculated from the measured ratios of $^{4}He/^{3}He$, and parent nuclides $^{238}U/^{233}U$, $^{236}U/^{233}U$ and $^{232}Th/^{229}Th$ (Farley, 2000; Reiners et al., 2004), and we apply an alpha ejection correction based on mineral volume and shape (Hourigan et al., 2005).

In this study, we use both apatite and zircon (U-Th)/He thermochronology, closure temperatures of 60ºC, (Farley, 2002) and 180ºC (Reiners at al., 2005), respectively, because the combination of these systems allows us to obtain a more robust time-averaged exhumation rates across a thicker section of crust. If the different mineral thermochronometers from a single surface sample yield substantially different cooling ages, it is possible to calculate acceleration or deceleration of the rock exhumation rate over time (Reiners and Brandon, 2006).

In order to determine exhumation rates we implement a first-order approach of sampling bedrock transects of both apatite and zircon for (U-Th)/He analysis (i.e. Braun, 2002a). From north to south these locations are: 1) the Balsas region within

the Eastern Cordillera (~6°S), 2) the Sihuas region east of the Cordillera Blanca (~8°S), and 3) along the Rio Pampas River just north of the Cordillera Blanca (~7°S; Fig. 4.2). These three locations display different source rocks, elevations and relief within different tectonomorphic provinces in the north-central Peruvian Andes. The first two locations are within river valleys that are part of the Rio Marañon drainage system, ultimately flowing east to the Amazon basin. The Rio Pampas section is a west-draining system connected to the Pacific Ocean lying north of the Cordillera Blanca Batholith (Fig. 4.2).

4.5 Results

Each of the three sites contain one sub-vertical transect; each transect contains four to five samples, where apatite (AHe) and/or zircon (ZHe) (U-Th)/He cooling ages have been measured. All ages reported here are mean ages, which are calculated from a weighted mean of four to six individual grain-ages (Appendix 4.1).

The Balsas transect spans 900 vertical meters and contains four samples yielding both good quality zircon and apatite grains (Fig. 4.3A). All four samples are taken within granitic units mapped as late Paleozoic (INGEMMET, 1998). AHe ages are mid-late Miocene (8.1 ± 1.2 to 10.7 ± 1.8 Ma), while the ZHe ages are scattered from Paleozoic to Mesozoic. Several of the ZHe samples exhibit poor reproducibility across the measured grain-ages, which is reflected in large errors. However, the AHe

ages are much younger, and more reproducible.

The Sihuas transect is ~200 km south of Balsas, spans ~1800 m of elevation and contains four high-quality apatite samples with mid-to-late Miocene AHe ages (6.4± 3.8 to 9.5 ± 2.3 Ma) and five samples with scattered Paleozoic to Mesozoic ZHe ages (Fig. 4.3B). All the apatite samples were taken from the Precambrian Marañon complex gneiss, or Paleozoic granitic units, and the five zircon samples were sampled from both igneous and sedimentary lithologies, mapped as Precambrian to Cretaceous in age (INGEMMET, 1995a).

The Rio Pampas transect (~600 m vertical), contains four samples where we were able to measure ZHe ages and a single sample that yielded an AHe age (Fig. 4.4). The upper three sample locations are within Jurassic-Cretaceous metasedimentary rocks and yielded ZHe ages from early-to-mid-Miocene, but the samples yield no apatite grains. The sampled transect extends across the Rio Pampas; the lowest elevation sample from a mapped Neogene granitic bedrock unit (INGEMMET, 1995b) yielded a very young age from both ZHe and AHe, 2.7 ± 0.39 Ma and 2.0 ± 0.24 Ma, respectively.

4.6 Regional rock exhumation rates

A vertical transect sampling-strategy is a powerful tool for first-order approaches to calculating exhumation rates by examining the age vs. elevation

relationship (Braun, 2002a). While not exact, this method combined with knowledge of the regional tectonics, thermal structure and/or paleotopography can provide accurate estimations of exhumation rates from calculations incorporating (U-Th)/He ages. In order to interpret our data, we investigate two end-member model cases of crustal thermal structure: 1) a flat closure isotherm and 2) a closure isotherm that mimics topography (Fig. 4.5). Higher temperature thermochronometers, due to their significant closure depths, will not closely mimic topography, and are thus less thermally perturbed by surficial modification (Fig. 4.5A). Lower temperature thermochronometers on the other hand, will closely mimic topography, as their shallow closure depths are significantly perturbed by surface topography (Fig. 4.5B). However, the wavelength of surface topography also influences the shape of closure isotherms of both high and low thermochronometers. Short-wavelength topography, i.e. a valley to peak distance that is less than ~12 km, (Braun, 2002b) does not significantly perturb the isotherms hotter than 100°C. In cases where the wavelength of topography is large enough that the geothermal gradient is the same everywhere, closure isotherms of all low-temperature thermochronometers will mimic topography. Based on the horizontal distances of 5-18 km in our transects, the end-member case where the isotherms are flat relative to the topography (Fig. 4.5A) is more suitable for our ZHe ages, whereas the thermal structure for the AHe ages likely behaves similarly to Fig. 4.5B. Unless local relief is changing faster than the isotherms can adjust, or a large thermal perturbation occurs during the time frame sampled, a flat closure

isotherm will remain stationary with respect to topography throughout the duration of a particle's passage of the isotherm to Earth's surface and a vertically sampled transect will record the exhumation rate of the time frame measured, without requiring independent knowledge of the thermal structure (Braun, 2002a). However, if the closure isotherm mimics topography, surface samples along a vertical transect will give an overestimation of exhumation rate, in extreme cases, an apparently infinitely fast exhumation rate (Fig. 4.5B; Braun, 2002b).

The exhumation signal recorded by the zircons at the Balsas site is largely Mesozoic, sampled from plutonic units mapped as Carboniferous-Permian (INGEMMET, 1998). While the precise age(s) of the plutonic units we sampled are unknown, other plutons within the Balsas section have been dated by U-Pb zircon geochronology, ranging from 309-320 Ma (Mišković et al., 2009). The ZHe age spectrum we show, 280 ± 60 Ma and 213 ± 20 Ma vs. 137 ± 80 Ma and 101 ± 34 Ma, within these plutons do not reflect crystallization ages. We attribute the age scatter and poor reproducibility to partial retention of He near the zircon closure isotherm. The Sihuas transect, which is 200 km south of the Balsas site, also yields zircon ages showing considerable scatter across the transect. As the Sihuas zircon were sampled from mostly meta-sedimentary rocks, it is not clear whether the range and apparent scatter within each sample is due to detrital zircons within the meta-sedimentary units that were not reset, or to partial retention of He. The major outlier to the age spectra pattern in the ZHe ages from Balsas and Sihuas is the lone Oligocene age, 28.0 ± 4.5

Ma and the only ZHe age that exhibits good reproducibility. Although the sample is from a plutonic rock mapped as Carboniferous, we have a preliminary U-Pb zircon age on this sample that indicates crystallization in the Eocene. As there are few known plutons in this age range in this region, we note this anomalous plutonic and cooling age, but do not use it in our exhumation calculations, as we believe it records localized cooling and our focus is on estimated regional rock exhumation rates.

Although the age range and scatter in ZHe ages from both the Balsas and Sihuas sections makes extracting precise exhumation rates difficult, these data show that this section of crust has remained above or near the ZHe closure isotherm (~6 km depth) but below the AHe closure isotherm (~2 km depth) since Mesozoic time. However, the structural and sedimentological interpretations of the Eocene Incaic orogeny in this region (Megard et al., 1984) suggest a significant period of uplift in the mid-to-late Eocene. Our ZHe results indicate that the Eocene Incaic orogeny was characterized by slow rock exhumation, and possibly little relief growth. By averaging ZHe ages from both Sihuas and Balsas and assigning a 25°C/km geothermal gradient and 180°C closure isotherm we estimate approximate regionally-averaged exhumation rates that are 0.03-0.07 mm/yr for Balsas and 0.04-0.21 mm/yr for Sihuas, where the larger range at Sihuas is due to the larger spread in ZHe ages. Using a mean-weighted average approach for these ranges, 0.05 mm/yr is the spatially and temporally averaged exhumation rate for the Balsas and Sihuas sections during the Mesozoic and early Cenozoic.

The AHe ages from both Balsas and Sihuas are significantly younger than the ZHe ages, adding an important piece to the time-temperature history of this region. The eight AHe ages (4 from each site) lie within a remarkably small time-span of 4 myr, between 6.5 and 10.5 Ma. In both transects, the AHe data display steeply dipping age-elevation relationships (AER), which we believe is most likely an overestimation of exhumation rate due to the sensitivity of the AHe system to topography (see Fig. 4.5B). Within error, however, a positive AER relationship is possible, and one interpretation of the steeply dipping AERs is that a brief period of rapid exhumation (>1 mm/yr) records a pulse of incision of the Rio Marañon. The mean AHe age obtained from the Sihuas transect is younger than the age at Balsas, to the north, which is consistent with a wave of incision propagating south. However, this scenario is unlikely, as we would expect to see older cooling ages in the higher elevations, as exhumation would have been locally focused within the river channel. In both transects, the AHe age from the highest elevations are younger than those from the lowest elevations, in disagreement this notion. Another possibility is to interpret the AERs as having a slightly negative slope indicative of steady relief lowering (Braun 2002b), however, given recent relief generation observed elsewhere in the north-central Peruvian Andes (McNulty and Farber, 2002; Giovanni et al., 2010) and preservation of the long recognized (McLaughlin, 1924) high-elevation, low-relief surfaces that are thought to have been uplifted from near sea level to up to 4.4 km above sea level mostly since the Miocene (Garver et al., 2005) this is unlikely.

Instead, we explore the idea that the increase in exhumation rate is recording an increase in regional erosion rates, perhaps coupled with rock uplift. If we assume that the AHe closure isotherm is adjusted to topography fully and apply an AHe closure temperature of 55°C and a geothermal gradient of 25°C/km, the average exhumation rates from the AHe data for the Balsas and Sihuas regions are 0.24 ± 0.05 mm/yr and 0.30 ± 0.09 mm/yr, respectively. However, it is shown that a significant increase in erosion rate affects the thermal structure, by causing isotherms to migrate, therefore affecting calculations of exhumation rates. We use M. Brandon's code RESPTIME (Ehlers et al., 2005) to model an erosional perturbation to the system by increasing the erosion rate from the background rate of 0.05 mm/yr, which is the regional average we estimated from the ZHe ages, to an estimated 0.25 mm/yr. Due to the sensitivity of the AHe system, by ~3 Ma after the modeled instantaneous increase in erosion rate, the AHe closure isotherm has adjusted to within 0.5°C of the new steady state condition. We use this new thermal condition to recalculate the exhumation rates from Balsas and Sihuas, which are 0.19 ± 0.03 mm/yr and 0.25 ± 0.05 mm/yr, respectively (Fig. 4.6). They are slightly slower than originally predicted because faster advection of rock and compression of isotherms occurs due to the modeled increased erosion signal. Given the 200 km distance spanned between these two sites, we interpret this as a regional signal of enhanced exhumation driven by an increase in regional erosion rates, which in turn is possibly a coupled response to increased rock uplift rates.

Contrary to scattered Mesozoic-aged zircon cooling ages in the Sihuas and Balsas sections, the ZHe ages of the Rio Pampas transect show a Miocene cooling history. The three highest samples span ~20-13 Ma during the mid-to-late Miocene and cover an elevation difference of 350 m, yields an exhumation rate of 0.024 ± 0.013 mm/yr, using the approach of Braun (2002a), which does not require any assumptions about thermal structure or cooling rate, but does assume that the thermal field did not change significantly during exhumation. However, the lowest sample yields a late Pliocene-Pleistocene cooling age of 2.7 ± 0.2 Ma and the youngest apatite age measured in this study, 2.0 ± 0.2 Ma. Taken together, the zircon and apatite ages from this transect indicate exhumation rates increased dramatically during the late Miocene or Pliocene. These very young ages are consistent with other thermochronologic data from the Cordillera Blanca region (Giovanni, 2007), and are most likely related to cooling after batholithic emplacement and rapid tectonic exhumation accommodated along the Cordillera Blanca Detachment Fault System (McNulty and Farber, 2002; Rousse et al., 2003; Giovanni et al., 2010). Regional magmatism in the Cordillera Blanca and Huayhuash Range to the south occurred in the Late Miocene, which Garver et al. (2005) suggest elevated geothermal gradients to ca. 40°-50°C/km regionally, and from ZHe and ZFT data, determine a cooling rate of 12-30°C/my. Applying these values, we calculate a range of possible exhumation rates from 0.60 – 0.88 mm/yr for our AHe data, and 1.26 – 1.84 mm/yr for our ZHe data (Fig. 4.6). These data, from the Rio Pampas, located at north of the Cordillera

Blanca Batholith, exhibit some of the fastest exhumation rates documented in Peru, which we believe are recording rapid exhumation accommodated by the Cordillera Blanca Detachment System.

4.7 Discussion

These new data document recent accelerations in exhumation in the central Peruvian Andes, specifically, i) in the Balsas and Sihuas transects, an increase in exhumation initiated prior to the late Miocene, and ii) in the Rio Pampas transect rapid exhumation initiated in the latest Miocene-Pliocene. A signal of accelerated exhumation can be accomplished by increased denudation, often coupled with increased rock uplift, or, a major thermal perturbation with associated cooling and denudation. We treat the data in the Rio Pampas section, which is in close proximity to the late Miocene-aged Cordillera Blanca Batholith, by applying an elevated geothermal gradient and fast cooling rates. However, there is little evidence to suggest the Rio Marañon corridor experienced any major thermal perturbations since the Miocene. Thus, we attribute the accelerated exhumation signal in the Sihuas and Balsas sites to enhanced erosional exhumation, coupled with rock uplift. We explore the following possible mechanisms that could be responsible for the accelerated rock exhumation we document: i) surface uplift driven by delamination of the lower crust, ii) rock uplift by increasing magmatism, iii) rock/surface uplift by lower crustal flow,

iv) tectonic exhumation associated with extensional tectonics and v) erosional exhumation associated with a regional climate change.

Lithospheric delamination typically produces surface uplift only, not necessarily requiring exhumation, therefore thermochronometers are unlikely to record the signal. However, as delamination is proposed to explain recent, rapid uplift of the Altiplano plateau (Garzione et al., 2008), it is an important mechanism to consider in the broader context of models for Andean orogenesis. In the central Peruvian Andes, delamination of the lower crust since the late Miocene seems unlikely, as this region has been characterized by flat-slab subduction, a lack of an active volcanic arc, and very low heat flow, suggesting an absence of hot asthenosphere at shallow levels (Henry and Pollack, 1988). Recently, Pelletier et al. (2010) show that the processes of eclogitic root production, delamination of the root, and climatically controlled surface erosion maintain a mass balance for crustal thickness. Given the tectonic and climatic variation between the northern Andes and the Central Andes, Pelletier et al. (2010) suggest that while delamination events are plausible in the Central Andes, high rates of erosion in the Northern Andes (i.e. central Peru) have lead to higher rates of mass removal thereby preventing eclogitic production and inhibiting delamination. Other models for Andean uplift, such as increased magmatism and lower crustal flow also appear unlikely. The absence of a volcanic arc since the late Miocene rules out magmatism as an important recent process. Lower crustal flow, typically modeled as a low-viscosity material flowing

laterally away from the keel of the orogen in response to a topographic load (Bird, 1991) does not fit the morphology of the north-central Peruvian Andes, where unlike the Tibetan Plateau (Clark and Royden, 2000) and the Altiplano (Husson and Sempere, 2003), is characterized by a narrow zone of high topography. Thus, magmatism, delamination and lower crustal flow all appear to be unlikely mechanisms for recent rock uplift in the Peruvian Andes.

It has been noted that localized basins in the Western Cordillera of the Peruvian Andes exhibited active extensional tectonics in the Miocene, (i.e. the Cajamarca, San Marcos and Namora basins) (Bonnot et al., 1988; Bellier et al., 1989), as well as the Cordillera Blanca mountain range (McNulty and Farber, 2002). Certainly, extensional tectonics like those observed along the Cordillera Detachment Fault System could produce an exhumation signal like we document in this study. The Rio Pampas site, just north of the Cordillera Blanca proper, we believe is recording the tectonic exhumation associated with Mio-Pliocene slip along the Cordillera Detachment Fault System. However, at present, there is no evidence for active or recently active extensional features east of the Western Cordillera, specifically, within the Rio Marañon corridor and we do not attribute the late Miocene accelerated exhumation signal in the Rio Marañon corridor to extensional features.

Increased precipitation to the northeastern Andean slope brought about by a regional climate change may provide a more plausible explanation for the accelerated exhumation signal we observe in the Rio Marañon sample sites. A shift to higher

erosion rates in the Eastern Andes in the mid-late Miocene is consistent with documented increases in sedimentation rates in the Amazon basin (Fig.uerido et al., 2009; Uba et al., 2009), changes in stable isotopes in the Sub-Andean foreland deposits of the Chaco Basin, Bolivia (Mulch et al., 2010) and regional climate modeling that indicates the late Miocene was characterized by initiation and intensification of convective rainfall (Poulsen et al., 2010). These studies support the notion that regional climate change c.a. 8-10 Ma was characterized by 1) more intense convective precipitation along the eastern margin of the Andes, 2) increased orogenic erosion rates, and 3) higher sedimentation rates into the Amazon basin, which may explain the Miocene increase in exhumation rates we document in the Rio Marañon corridor of the Eastern Cordillera.

4.8 Conclusions

We show a regional acceleration in exhumation rates during the Miocene and Pliocene-Pleistocene in the north-central Peruvian Andes. This late Miocene pulse of rock exhumation is not accompanied by any of the thermal signatures expected from magmatism or lithospheric delamination and is more consistent with the timing of regional climate perturbations that brought increased precipitation to the region. While the active tectonic extension presently occurring along the Cordillera Detachment Fault System likely explains the exhumation signal we document in the

Rio Pampas site, we do not believe active extension is the driver of the exhumation signal we show in the two sites within the Rio Marañon corridor. We suggest a regional climate shift characterized by increased amounts and intensity of precipitation enhanced orogenic erosion and exhumation of the north-central Peruvian Andes. This scenario is consistent with both the acceleration in exhumation rates we show here, and the lack of a development of an over-thickened eclogitic root (Pelletier et al., 2010). Thus, in contrast to the Central Andes, where there is a similar, late Miocene timing of uplift and exhumation, the morphologic and tectonic history of the Northern Andes does not reflect any of the geodynamical mechanisms that have been proposed for the Altiplano, such as a delamination event, increased magmatism, or lower crustal flow, rather, the Northern Andes likely reflects orogenesis and along-strike relief growth through a strong coupling of tectonic and climatic forces.

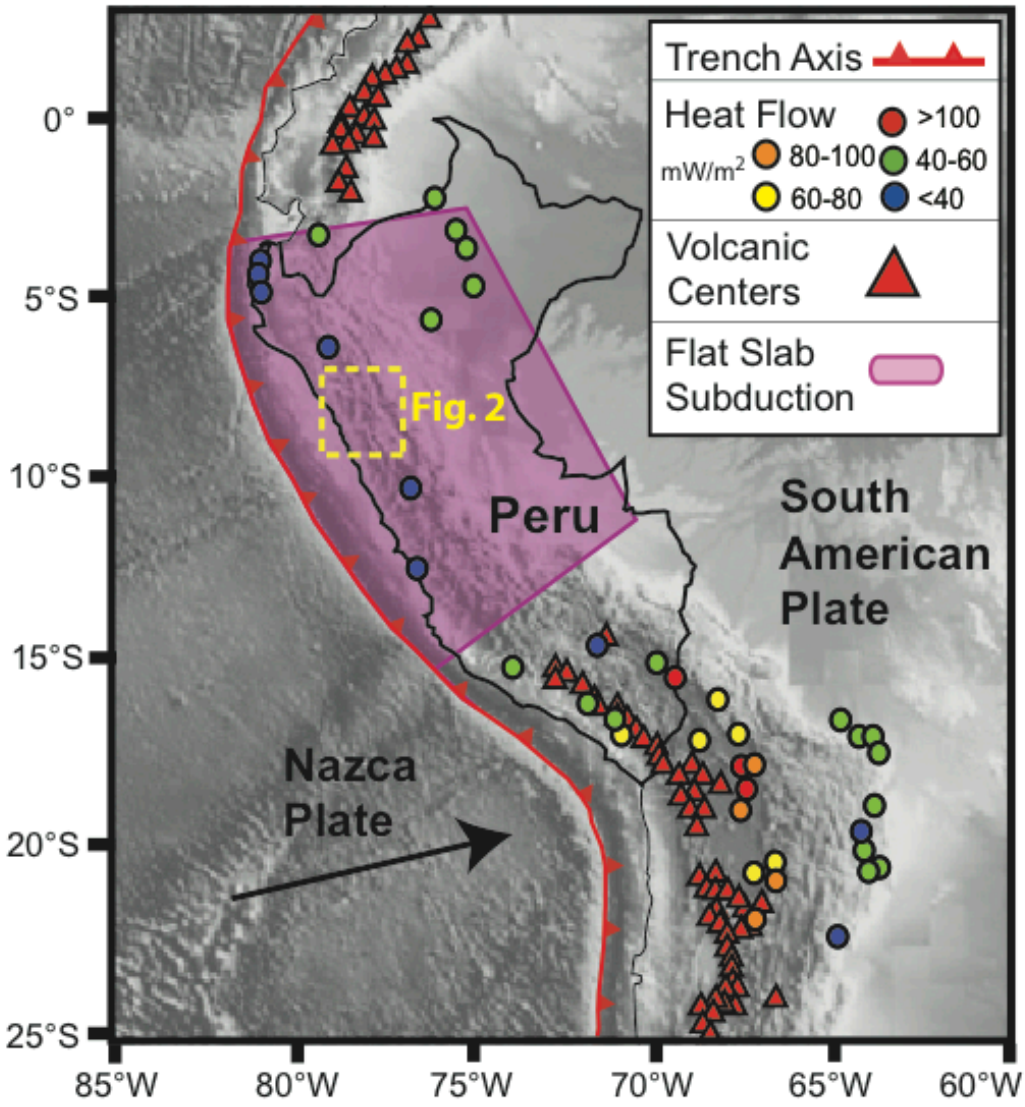

Figure 4.1: The Andean margin showing the trench axis, active volcanism and heat flow values (modified from Barazangi and Isacks, 1976; Henry and Pollack, 1988). The study area is denoted by the yellow dashed box (Fig 4.2).

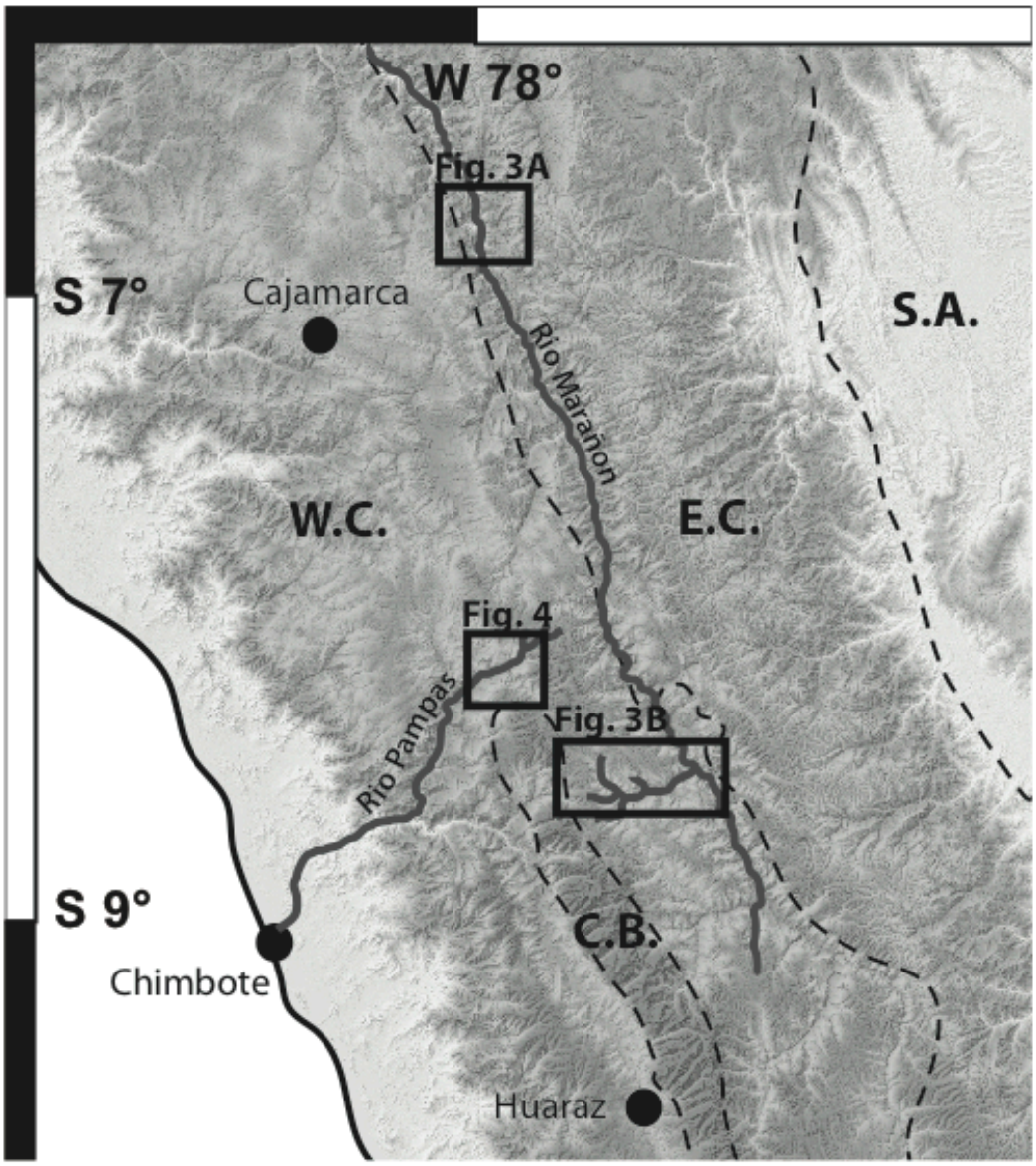

Figure 4.2: A DEM of the regional study area, highlighting the three study areas where apatite and zircon were sampled for (U-Th)/He thermochronology. The dashed line separate the following tectonomorphic provinces, the Western Cordillera (W.C.), the Eastern Cordillera (E.C.), and the Sub-Andean zone (S.A.). The Cordillera Blanca Batholith (C.B.) region is outlined in solid black.

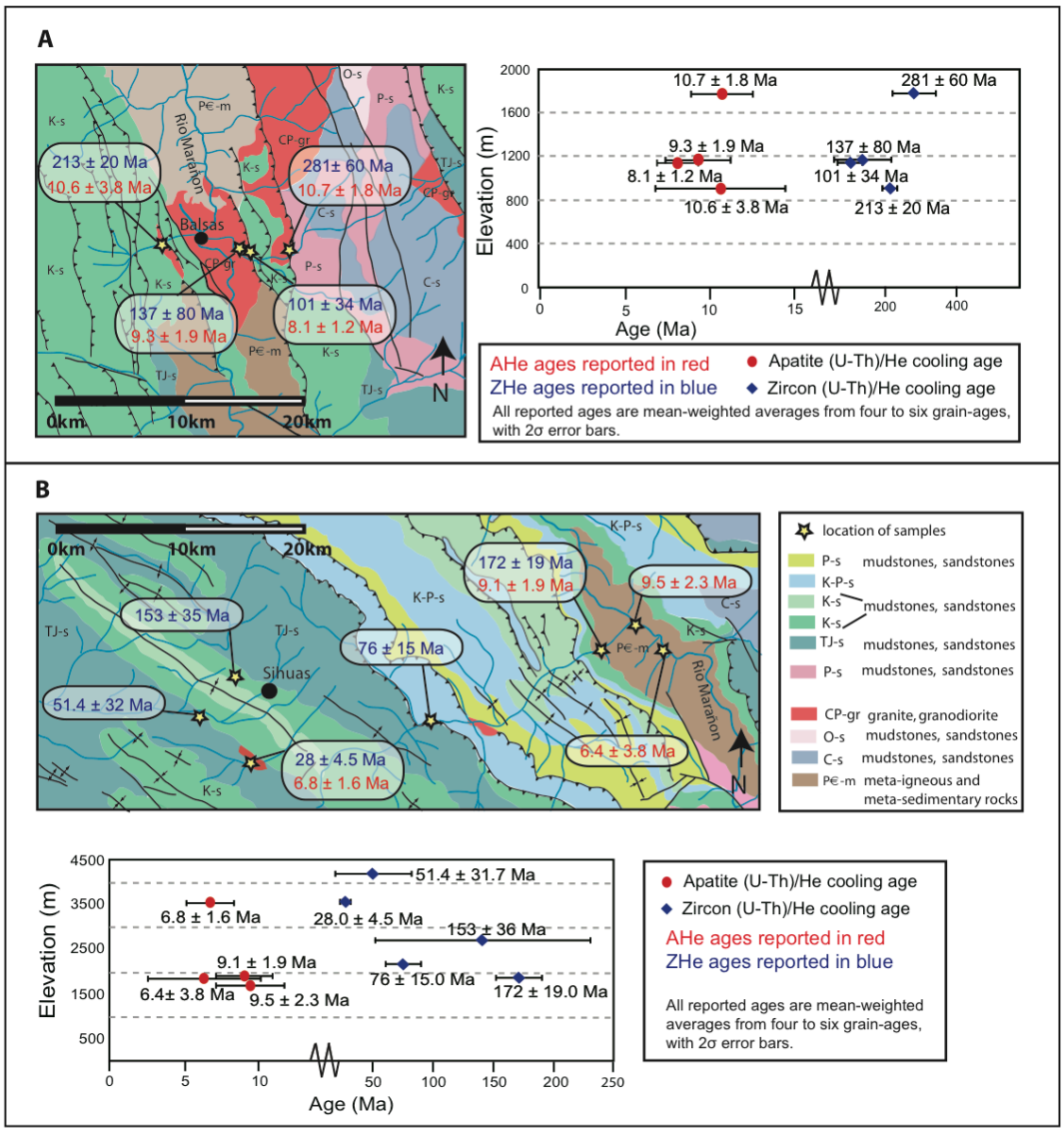

Figure 4.3A: Regional geology and zircon and apatite (U-Th)/He thermochronology results from the Balsas section of the Rio Marañon, shown as cooling age vs. elevation plots. **4.3B**: Regional geology and zircon and apatite (U-Th)/He thermochronology results from the Sihuas section of the Rio Marañon, shown as cooling age vs. elevation plots. The mean ages and error bars represent the mean weighted average of the measured single grains. Geologic map adapted from INGEMMET, 1998, Lima, Peru.

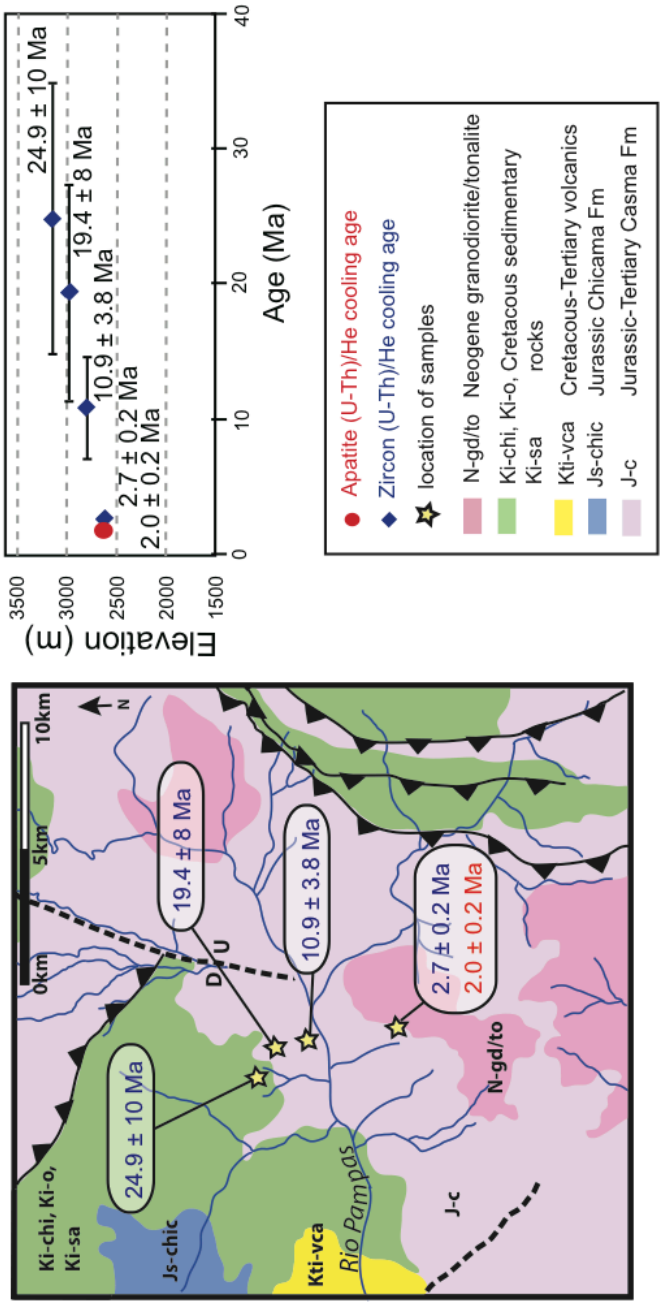

Figure 4.4: Regional geology and zircon and apatite (U-Th)/He thermochronology results from the Rio Pampas section, shown as cooling age vs. elevation plots. The mean ages and error bars represent the mean weighted average of the measured single grains. Geologic map adapted from INGEMMET, 1998, Lima, Peru.

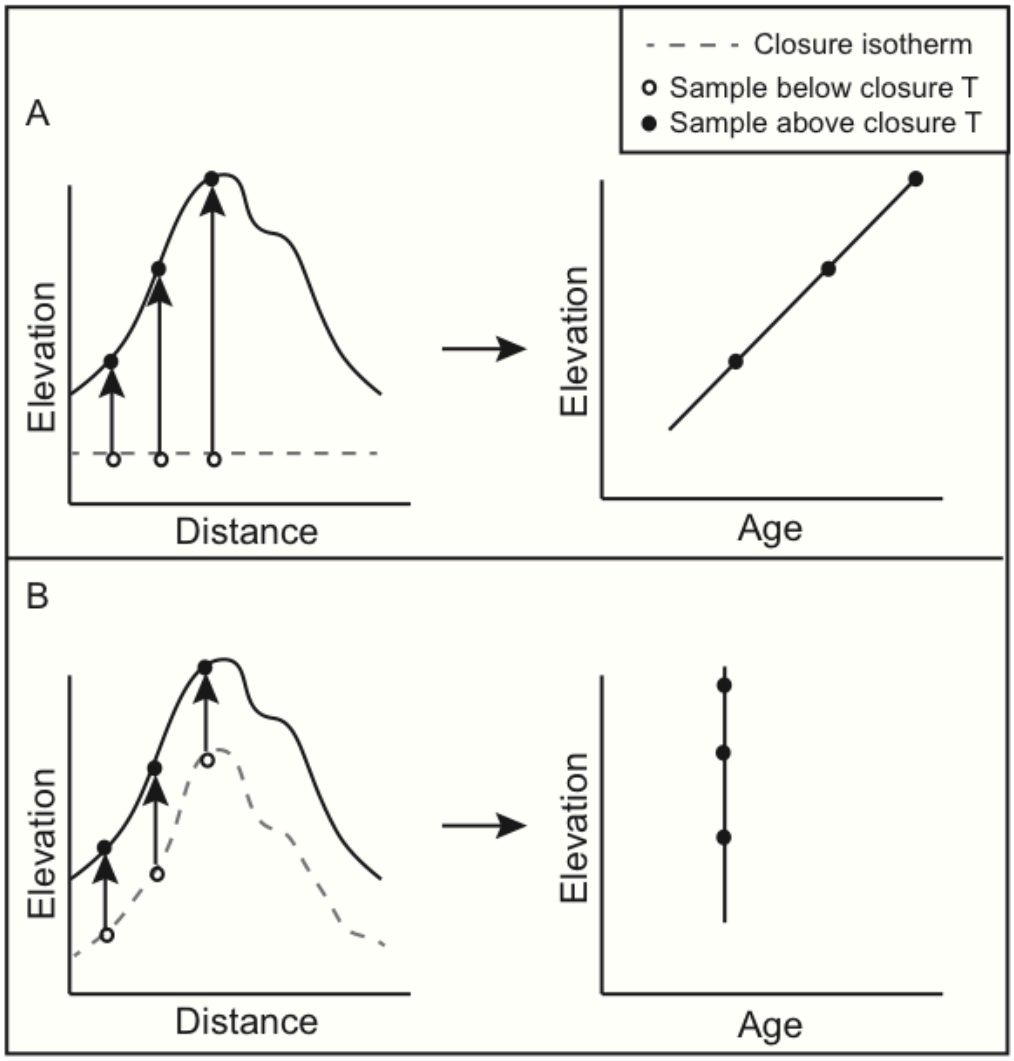

Figure 4.5: Two end-member cases demonstrating position and shape of the closure isotherm with respect to topography and their respective schematic age vs. elevation relationships, AERs (adapted from Braun 2002b). 5A shows the case of a flat closure isotherm, which yields an AER with a slope that is the exhumation rate, and 5B shows the case of a closure isotherm that mimics topography perfectly, resulting in a vertical AER.

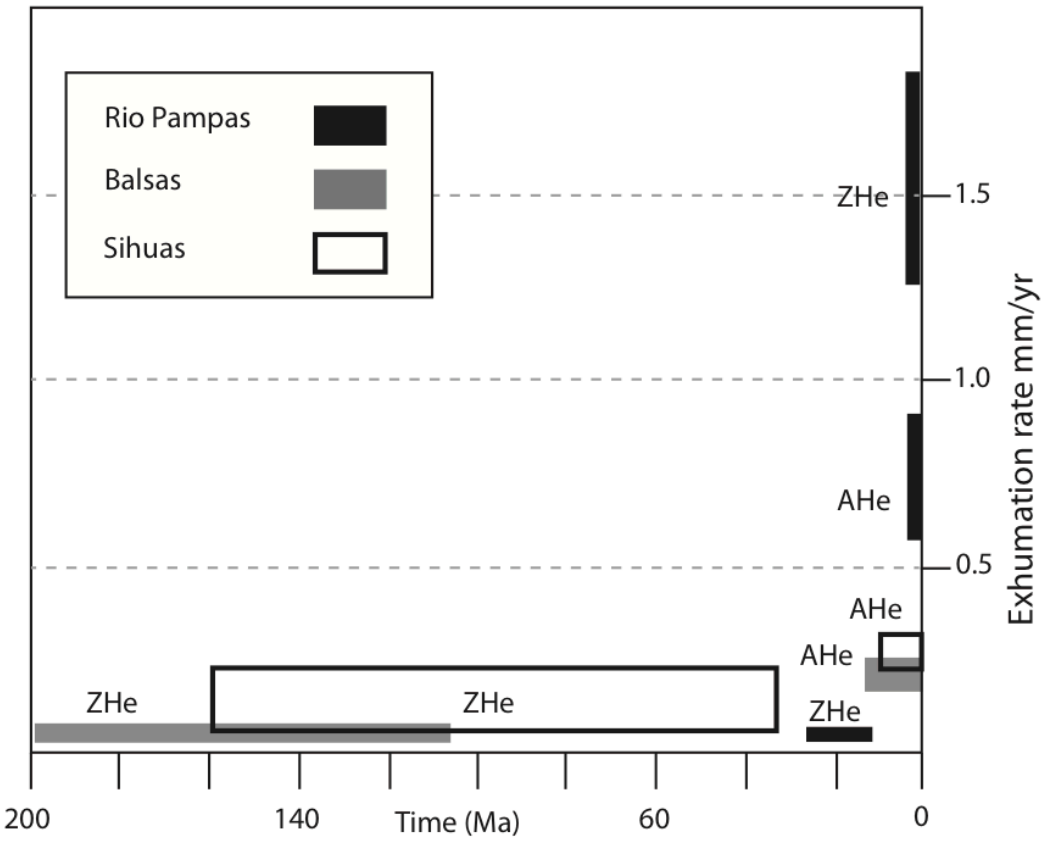

Figure 4.6: Calculated exhumation rates (in mm/yr) versus time (Ma) for all the sampled geologic sections. For the Rio Pampas ZHe section, the Braun (2002a) approach is applied, for all other sections, average regional age is used, with 2σ errors and time-averaged.

Appendix 4.1 (U-Th)/He Apatite and Zircon Thermochronology Data Table

Sample	Mineral	He, mol	U, ppm	Th, ppm	Grain mass, g	Ft*	Age, Ma	±(error)†	Mean-weighted avg. age w/ assigned 9% 2-sigma reproducibility error§	Rock type	Elevation, m
Sihuas Site											
RM07-P3	Zircon	8.255E-13	227.8	103.0	4.0819E-06	0.744	195.24	5.60	**172 ± 19**	granite	1864
RM07-P3	Zircon	3.989E-13	435.8	72.2	1.5836E-06	0.658	153.73	4.99		granite	1864
RM07-P3	Zircon	4.074E-13	360.0	81.8	1.7006E-06	0.683	167.93	3.16		granite	1864
RM07-P3	Zircon	5.180E-13	272.4	127.8	2.6676E-06	0.681	171.02	3.47		granite	1864
RM07-P3	Zircon	3.122E-13	291.8	66.1	1.5205E-06	0.660	183.45	5.50		granite	1864
RM07-P5	Zircon	3.136E-13	506.2	186.4	1.8723E-06	0.677	82.27	1.58	**76 ± 15**	sandstone	2195
RM07-P5	Zircon	1.469E-13	398.6	91.5	1.2319E-06	0.622	83.40	2.11		sandstone	2195
RM07-P5	Zircon	2.196E-13	319.3	52.1	2.2158E-06	0.686	79.77	1.65		sandstone	2195
RM07-P5	Zircon	1.429E-13	244.5	88.1	2.1700E-06	0.699	65.05	0.96		sandstone	2195
RM07-P6	Zircon	2.003E-13	113.1	102.5	2.1914E-06	0.664	182.10	4.74	**141 ±90**	sandstone	2706
RM07-P6	Zircon	1.699E-13	182.0	108.0	1.9805E-06	0.665	113.53	3.20		sandstone	2706
RM07-P6	Zircon	1.783E-13	111.8	51.3	2.3409E-06	0.684	163.44	4.25		sandstone	2706
RM07-P10	Zircon	2.348E-13	108.5	30.1	1.3284E-05	0.811	34.65	0.66	**28 ± 4.5**	granitoid	3553
RM07-P10	Zircon	6.837E-14	127.1	55.2	4.2641E-06	0.747	28.17	0.65		granitoid	3553
RM07-P10	Zircon	8.423E-14	74.6	23.9	9.7847E-06	0.811	24.34	0.52		granitoid	3553
RM07-P10	Zircon	6.651E-14	175.0	76.5	2.9570E-06	0.715	29.95	0.52		granitoid	3553
RM07-P10	Zircon	8.824E-14	161.0	67.8	4.6190E-06	0.742	26.76	0.51		granitoid	3553
RM07-P13	Zircon	2.193E-13	142.8	40.5	4.2748E-06	0.750	82.17	1.97	**51.4 ± 31.7**	quartzite	4196
RM07-P13	Zircon	1.117E-13	100.2	28.1	3.0010E-06	0.744	85.70	2.26		quartzite	4196
RM07-P13	Zircon	1.591E-13	100.8	35.2	7.2152E-06	0.794	46.75	0.93		quartzite	4196
RM07-P13	Zircon	1.048E-13	129.7	46.8	6.4148E-06	0.814	26.22	0.78		quartzite	4196
RM07-P13	Zircon	6.568E-14	197.8	105.4	4.3345E-06	0.768	16.32	0.33		quartzite	4196
RM07-P1	Apatite	3.448E-16	2.2	3.3	5.7990E-06	0.885	4.12	0.28	**6.4 ± 3.8**	gneiss	1856
RM07-P1	Apatite	4.496E-16	1.1	1.3	6.8380E-06	0.891	9.68	0.63		gneiss	1856
RM07-P1	Apatite	4.051E-16	1.6	2.0	4.9340E-06	0.878	8.40	0.49		gneiss	1856
RM07-P1	Apatite	1.224E-15	2.1	3.4	9.8170E-06	0.903	8.79	0.56		gneiss	1856
RM07-P1	Apatite	1.245E-15	1.2	1.7	1.2880E-05	0.916	12.41	0.63		gneiss	1856

*Ft=alpha-ejection correction factor based on mineral shape and volume (Hourigan et al., 2005); †error= analytical error; §mean-weighted average age is calcuated using Isoplot 3.00 (Ludwig, 2003)

Appendix 4.1 (U-Th)/He Apatite and Zircon Thermochronology Data Table

Sample	Mineral	He, mol	U, ppm	Th, ppm	Grain mass, g	Ft*	Age, Ma	±(error)†	Mean-weighted avg. age w/ assigned 9% 2-sigma reproducibility error§	Rock type	Elevation, m
Sihuas Site con't.											
RM07-P2	Apatite	2.688E-15	6.5	2.3	8.5590E-06	0.873	9.46	0.90	**9.5 ± 2.3**	gneiss	1709
RM07-P2	Apatite	8.103E-17	0.1	0.4	7.0100E-06	0.864	14.02	2.71		gneiss	1709
RM07-P2	Apatite	4.949E-15	9.3	1.7	1.2130E-05	0.912	8.51	0.71		gneiss	1709
RM07-P2	Apatite	2.680E-15	8.8	2.6	5.7250E-06	0.875	10.44	0.60		gneiss	1709
RM07-P2	Apatite	1.644E-15	7.4	20.9	3.4280E-06	0.856	8.37	0.40		gneiss	1709
RM07-P3	Apatite	1.372E-15	37.3	41.8	1.0383E-06	0.687	7.51	0.83	**9.1 ± 1.9**	granite	1864
RM07-P3	Apatite	7.224E-16	1.7	8.9	3.8437E-06	0.780	11.66	2.48		granite	1864
RM07-P3	Apatite	2.008E-15	12.4	5.2	3.9739E-06	0.796	8.57	0.70		granite	1864
RM07-P3	Apatite	1.426E-14	27.6	7.6	9.7982E-06	0.865	10.53	0.24		granite	1864
RM07-P3	Apatite	2.108E-15	16.1	30.7	2.3369E-06	0.775	9.20	0.69		granite	1864
RM07-P10	Apatite	7.087E-16	2.5	4.3	4.6263E-06	0.795	10.06	2.20	**6.8 ± 1.6**	granitoid	3553
RM07-P10	Apatite	1.785E-15	2.0	2.8	1.3022E-05	0.859	10.84	1.24		granitoid	3553
RM07-P10	Apatite	7.448E-16	2.1	2.7	1.0958E-05	0.852	5.42	1.10		granitoid	3553
RM07-P10	Apatite	7.774E-16	2.1	2.7	9.3199E-06	0.847	6.69	1.48		granitoid	3553
RM07-P10	Apatite	1.204E-15	1.6	2.9	1.5834E-05	0.869	7.14	1.06		granitoid	3553
RM07-P10	Apatite	4.336E-16	1.7	3.4	6.9540E-06	0.816	5.64	1.94		granitoid	3553
RM07-P10	Apatite	1.040E-15	1.5	4.2	1.2652E-05	0.853	7.15	1.08		granitoid	3553

*Ft=alpha-ejection correction factor based on mineral shape and volume (Hourigan et al., 2005); †error= analytical error; §mean-weighted average age is calcuated using Isoplot 3.00 (Ludwig, 2003)

Appendix 4.1 (U-Th)/He Apatite and Zircon Thermochronology Data Table

Sample	Mineral	He, mol	U, ppm	Th, ppm	Grain mass, g	Ft*	Age, Ma	±(error)†	Mean-weighted avg. age w/ assigned 9% 2-sigma reproducibility error§	Rock type	Elevation, m
Balsas site											
RM07-1	Zircon	1.076E-12	351.8	182.1	3.3620E-06	0.729	201.45	4.25	**213 ± 20**	granitoid	900
RM07-1	Zircon	1.036E-12	227.3	111.0	4.3090E-06	0.741	231.14	11.14		granitoid	900
RM07-1	Zircon	1.581E-12	241.8	121.8	6.2820E-06	0.780	215.83	4.67		granitoid	900
RM07-1	Zircon	1.316E-12	295.0	145.9	4.6760E-06	0.750	206.39	9.25		granitoid	900
RM07-2	Zircon	6.045E-12	847.8	178.2	2.6400E-05	0.860	54.83	1.35	**101 ± 34**	granitoid	1135
RM07-2	Zircon	7.196E-12	483.4	217.9	1.8400E-05	0.839	158.37	5.19		granitoid	1135
RM07-2	Zircon	3.894E-13	213.1	59.3	4.3710E-06	0.750	95.55	3.16		granitoid	1135
RM07-2	Zircon	2.504E-13	410.9	170.7	1.5620E-06	0.675	96.11	2.88		granitoid	1135
RM07-2	Zircon	1.289E-13	244.3	105.5	1.3130E-06	0.651	102.27	2.90		granitoid	1135
RM07-3	Zircon	1.384E-12	524.3	183.4	3.5360E-06	0.738	169.76	3.68	**137 ± 80**	true granite	1162
RM07-3	Zircon	8.894E-13	287.5	127.5	4.2490E-06	0.756	158.51	2.50		true granite	1162
RM07-3	Zircon	9.246E-13	604.2	212.9	3.1290E-06	0.740	111.40	1.88	**281 ± 60**	true granite	1162
RM07-6	Zircon	4.397E-12	296.4	158.7	9.4820E-06	0.799	311.88	7.47		granodiorite	1768
RM07-6	Zircon	3.998E-12	304.8	167.7	9.5070E-06	0.800	274.92	4.87		granodiorite	1768
RM07-6	Zircon	9.568E-13	201.8	114.2	3.9050E-06	0.732	263.71	11.64		granodiorite	1768
RM07-1	Apatite	1.090E-15	4.5	10.4	3.9140E-06	0.875	8.45	0.76	**10.6 ± 3.8**	granitoid	900
RM07-1	Apatite	1.221E-15	4.3	9.4	4.8270E-06	0.881	8.07	0.73		granitoid	900
RM07-1	Apatite	1.654E-15	6.7	18.1	2.0750E-06	0.840	15.86	1.43		granitoid	900
RM07-1	Apatite	7.591E-15	2.4	6.3	3.7630E-05	0.941	10.19	0.92		granitoid	900
RM07-2	Apatite	2.633E-15	4.6	10.9	7.7590E-06	0.903	9.65	0.87	**8.1 ± 1.2**	granitoid	1135
RM07-2	Apatite	1.550E-15	1.6	3.8	1.5030E-05	0.920	8.34	0.75		granitoid	1135
RM07-2	Apatite	8.609E-15	5.9	7.8	3.2690E-05	0.930	6.75	0.61		granitoid	1135
RM07-2	Apatite	3.364E-15	3.3	7.1	1.9660E-05	0.926	6.90	0.62		granitoid	1135
RM07-2	Apatite	6.121E-15	6.7	13.4	1.3620E-05	0.910	9.26	0.83		granitoid	1135

*Ft=alpha-ejection correction factor based on mineral shape and volume (Hourigan et al., 2005); †error= analytical error; §mean-weighted average age is calcuated using Isoplot 3.00 (Ludwig, 2003)

Appendix 4.1 (U-Th)/He Apatite and Zircon Thermochronology Data Table

Sample	Mineral	He, mol	U, ppm	Th, ppm	Grain mass, g	Ft*	Age, Ma	±(error)†	Mean-weighted avg. age w/ assigned 9% 2-sigma reproducibility error§	Rock type	Elevation, m
Balsas site con't.											
RM07-3	Apatite	4.705E-14	26.0	113.6	1.7280E-05	0.907	10.47	0.94	**9.3 ± 1.9**	true granite	1162
RM07-3	Apatite	3.575E-14	33.4	175.1	1.0100E-05	0.896	9.76	0.88		true granite	1162
RM07-3	Apatite	2.952E-13	2.8	14.9	1.0000E-03	0.969	11.80	1.06		true granite	1162
RM07-3	Apatite	1.530E-14	23.4	112.6	7.8470E-06	0.877	8.20	0.74		true granite	1162
RM07-3	Apatite	9.320E-15	21.2	72.2	7.8290E-06	0.887	6.46	0.58		true granite	1162
RM07-6	Apatite	7.975E-15	7.1	19.3	8.5580E-06	0.839	17.57	1.58	**10.7 ± 1.8**	granodiorite	1768
RM07-6	Apatite	5.869E-15	8.8	23.4	7.5560E-06	0.817	12.22	1.10		granodiorite	1768
RM07-6	Apatite	7.110E-16	7.0	17.2	1.4230E-06	0.737	11.35	1.02		granodiorite	1768
RM07-6	Apatite	1.258E-14	3.4	7.6	1.6250E-05	0.874	31.43	2.83		granodiorite	1768
RM07-6	Apatite	3.882E-15	9.3	26.1	5.0110E-06	0.841	10.94	0.98		granodiorite	1768
RM07-6	Apatite	1.090E-15	4.5	10.4	3.9140E-06	0.875	8.45	0.76		granodiorite	1768

*Ft=alpha-ejection correction factor based on mineral shape and volume (Hourigan et al., 2005); †error= analytical error; §mean-weighted average age is calcuated using Isoplot 3.00 (Ludwig, 2003)

Appendix 4.1 (U-Th)/He Apatite and Zircon Thermochronology Data Table

Sample	Mineral	He, mol	U, ppm	Th, ppm	Grain mass, g	Ft*	Age, Ma	±(error)†	Mean-weighted avg. age w/ assigned 9% 2-sigma reproducibility error§	Rock type	Elevation, m
Rio Pampas site											
RP07-1	Zircon	3.633E-14	711.9	117.9	7.0510E-07	0.578	22.18	0.34	**24.9 ± 10**	quartzite	3129
RP07-1	Zircon	4.807E-14	454.0	93.8	1.4450E-06	0.685	18.75	0.60		quartzite	3129
RP07-1	Zircon	5.917E-14	345.4	166.3	1.0970E-06	0.660	39.02	2.45		quartzite	3129
RP07-1	Zircon	2.050E-14	751.7	90.8	9.7370E-07	0.668	7.51	0.90		quartzite	3129
RP07-1	Zircon	8.319E-15	136.0	83.4	8.4130E-07	0.597	19.58	0.38		quartzite	3129
RP07-2	Zircon	6.105E-14	340.9	146.3	1.2560E-06	0.681	34.94	0.52	**19.4 ± 8**	quartzite	2968
RP07-2	Zircon	3.895E-15	117.7	49.9	9.6660E-07	0.627	9.15	0.31		quartzite	2968
RP07-2	Zircon	5.376E-14	155.5	100.2	3.6920E-06	0.776	19.28	0.33		quartzite	2968
RP07-2	Zircon	2.217E-14	163.5	88.2	1.7860E-06	0.713	17.39	0.27		quartzite	2968
RP07-2	Zircon	2.920E-14	427.5	79.5	6.6250E-07	0.565	32.12	0.47		quartzite	2968
RP07-3	Zircon	1.642E-14	281.0	150.0	1.0970E-06	0.607	14.35	0.29	**10.9 ± 3.8**	quartzite	2788
RP07-3	Zircon	2.648E-14	202.6	79.2	2.4470E-06	0.724	12.43	0.17		quartzite	2788
RP07-3	Zircon	3.447E-15	55.3	41.4	2.2280E-06	0.733	5.97	0.36		quartzite	2788
RP07-3	Zircon	2.706E-14	471.9	448.2	1.2190E-06	0.641	11.05	0.24		quartzite	2788
RP07-6	Zircon	1.437E-14	298.1	190.2	4.2470E-06	0.758	2.40	0.04	**2.7 ± 0.2**	granite	2626
RP07-6	Zircon	1.627E-14	319.3	206.1	3.8680E-06	0.743	2.84	0.05		granite	2626
RP07-6	Zircon	1.044E-14	184.6	148.0	4.2830E-06	0.764	2.68	0.05		granite	2626
RP07-6	Zircon	1.135E-14	146.8	96.5	5.4320E-06	0.776	2.93	0.05		granite	2626
RP07-6	Apatite	1.425E-15	2.5	7.3	3.3770E-05	0.932	1.97	0.09	**2.0 ± 0.2**	granite	2626
RP07-6	Apatite	1.007E-15	2.1	5.7	2.2790E-05	0.929	2.56	0.13		granite	2626
RP07-6	Apatite	6.684E-16	2.4	7.7	1.5530E-05	0.909	2.07	0.11		granite	2626
RP07-6	Apatite	1.322E-15	1.9	6.2	4.2250E-05	0.935	1.82	0.09		granite	2626
RP07-6	Apatite	7.715E-16	3.6	11.5	1.2870E-05	0.877	2.00	0.11		granite	2626
RP07-6	Apatite	3.623E-16	1.9	6.2	1.1350E-05	0.904	1.93	0.12		granite	2626

REFERENCES CITED:

*Ft=alpha-ejection correction factor based on mineral shape and volume (Hourigan et al., 2005); †error= analytical error; §mean-weighted average age is calcuated using Isoplot 3.00 (Ludwig, 2003)

4.9 References

Allmendinger, R.W., Jordan, T.E., Kay, S.M. and Isacks, B.L., 1997. The evolution of the Altiplano-Puna plateau of the Central Andes. Annual Review Of Earth And Planetary Sciences, 25: 139-174.

Atherton, M. P. & Petford, N., 1993. Generation of sodium-rich magmas from newly underplated basaltic crust Nature 362, 144-146.

Barazangi, M., and Isacks, B.L., 1976, Spatial-Distribution of Earthquakes and Subduction of Nazca Plate beneath South-America: Geology, v. 4, p. 686-692.

Barnes, J.B., Ehlers, T.A., McQuarrie, N., O'Sullivan, P.B., Tawackoli, S., 2008. Thermochronometer record of central Andean plateau growth, Bolivia (19.5 degrees S), Tectonics, 27:TC3003.

Barnes, J.B., and Ehlers, T.A., 2009, End member models for Andean Plateau uplift: Earth- Science Reviews, v. 97, p. 105-132.

Beck, S.L. and Zandt, G., 2002. The nature of orogenic crust in the central Andes. Journal Of Geophysical Research-Solid Earth, 107(B10).

Bellier, O., M. Se´brier, F. Gasse, E. Fourtanier, and I. Robles, 1989. Evolution ge ´odynamique mio plioce`ne et quaternaire des bassins de la cordille`re occidentale du Nord-Pe´rou: Les bassins de Cajabamba, San Marcos et Namora (de´partement de Cajamarca), Geodynamique, 4, 93 – 118.

Benjamin, M. T.; Johnson, N. M.; and Naeser, C.W. 1987. Recent rapid uplift in the Bolivian Andes: evidence from fission-track dating. Geology 15:680–683.

Bershaw, J., Garzione, C.N., Higgins, P., MacFadden, B.J., Anaya, F., and Alvarenga, H., 2010, Spatial-temporal changes in Andean plateau climate and elevation from stable isotopes of mammal teeth: Earth and Planetary Science Letters, v. 289, p. 530-538.

Bonnot, D., M. Sebrier, and J. Mercier, Evolution ge´odynamique plio-quaternaire du bassin intracordillerain du Callejo´n de Huaylas et de la Cordille`re Blanche, Pe´rou, Geodynamique, 3, 57 – 83, 1988.

Bookhagen, B., and Strecker, M.R., 2008. Orographic barriers, high-resolution TRMM rainfall, and relief variations along the eastern Andes, Geophysical Research Letters, 35.

Bowman, I. 1906. The Andes of southern Peru´ , Geological reconnaissance along the 73 meridian. Am. Geogr. Soc. Spec. Publ. 1, 336 p.

Braun, J., 2002a, Estimating exhumation rate and relief evolution by spectral analysis of age- elevation datasets: Terra Nova, v. 14, p. 210-214.

Braun, J., 2002b, Quantifying the effect of recent relief changes on age-elevation relationships: Earth and Planetary Science Letters, v. 200, p. 331-343

Capitanio, F.A., Faccenna, C., Zlotnik, S. and Stegman, D.R., 2011. Subduction dynamics and the origin of Andean orogeny and Bolivian Orocline, Nature, 480, 83-86, doi: 10.1038/nature10596

Carrapa, B., Adelman, D., Hilley, G.E., Mortimer, E., Sobel, E.R., and Strecker, M.R., 2005, Oligocene uplift and development of plateau morphology in the southern central Andes: Tectonics, v. 24, p. 1–19, doi: 10.1029/2004TC001762.

Clark, M. K. & Royden, L. H., 2000. Topographic ooze: Building the eastern margin of Tibet by lower crustal flow. Geology 28, 703-706.

Cobbing, E.J., and Pitcher, W.S., 1972. Plate tectonics and the Peruvian Andes: Nature, v. 246, p. 51-53.

Cobbing, E. J.; Pitcher, W. S.; Wilson, J. J.; Baldock, W. P.; McCourt, W.; and Snelling, N. J. 1981. The geology of the western Cordillera of northern Peru. Overseas Mem. Inst. Geol. Sci. Lond. Mem. 5, 143 p.

Cobbing, E. J.; Sauchez, A. F.; Martinez, V.W.; and Zarate, O. H. 1997. Geologica de los Cuadrangulos de Huaraz, Recuay, La Union, Chiquian y Yanahuanca; hojas 20- h, 20-I, 21-I, 21-j. Bol. Inst. Geol. Minero Metalurgico Peru´ , Ser. A, Carta Geologica Nacional Rep. 76, 286 p.

Coutand, I., Carrapa, B., Deeken, A., Schmitt, A.K., Sobel, E.R., Strecker, M.R., 2006. Orogenic plateau formation and lateral growth of compressional basins and ranges: insights from sandstone petrography and detrital apatite

fission-track thermochronology in the Angastaco Basin, NW Argentina. Basin Res. 18, 1–26.

Dodson, M.H., 1973, Closure Temperature in Cooling Geochronological and Petrological Systems: Contributions to Mineralogy and Petrology, v. 40, p. 259-274.

Dewey, J. F., and J. M. Bird, 1970. Mountain belts and the new global tectonics, J . Geophys Res., 75, 2625-2647.

Ege, H., Sobel, E.R., Scheuber, E., Jacobshagen, V., 2007. Exhumation history of the southern Altiplano plateau (southern Bolivia) constrained by apatite fission-track thermochronology. Tectonics 26, TC1004.

Ehlers, T.A., and Poulsen, C.J., 2009, Influence of Andean uplift on climate and paleoaltimetry estimates: Earth and Planetary Science Letters, v. 281, p. 238-248.

Ehlers, T.A. and Farley, K.A., 2003. Apatite (U-Th)/He thermochronometry: methods and applications to problems in tectonic and surface processes. Earth And Planetary Science Letters, 206(1-2): 1-14.

Ehlers, T.A., Chaudhri, T., Kumar, S., Fuller, C.W., Willett, S.D., Ketcham, R.A., Brandon, M.T., Belton, D.X., Kohn, B.P., Gleadow, A.J.W., Dunai, T.J., and Fu, F.Q., 2005, Computational tools for low-temperature thermochronometer interpretation: Reviews in Mineralogy and Geochemistry, v. 58, p. 589–622, doi: 10.2138/rmg.2005.58.22.

Farley, K.A., 2000. Helium diffusion from apatite: General behavior as illustrated by Durango fluorapatite. Journal Of Geophysical Research-Solid Earth, 105(B2): 2903-2914.

Farley, K.A., 2002, (U-Th)/He dating: techniques, calibrations and applications: Reviews in Mineralogy & Geochemistry, v. 47, p. 819-844.

Fig.ueiredo, J., Hoorn, C., van der Ven, P., and Soares, E., 2009, Late Miocene onset of the Amazon River and the Amazon deep-sea fan: Evidence from the Foz do Amazonas Basin: Geology, v. 37, p. 619-622.

Garver, J.I., Reiners, P.W., Walker, L.J., Ramage, J.M., and Perry, S.E., 2005, Implications for timing of Andean uplift from thermal resetting of radiation damaged zircon in the Cordillera Huayhuash, northern Peru: Journal of Geology, v. 113, p. 117-138.

Garzione, C.N., Molnar, P., Libarkin, J.C. and MacFadden, B.J., 2006. Rapid late Miocene rise of the Bolivian Altiplano: Evidence for removal of mantle lithosphere. Earth And Planetary Science Letters, 241(3-4): 543-556.

Garzione, C.N., Hoke, G.D., Libarkin, J.C., Withers, S., MacFadden, B., Eiler, J., Ghosh, P., and Mulch, A., 2008. Rise of the Andes: Science, v. 320, p. 1304-1307.

Ghosh, P., Garzione, C.N., and Eiler, J.M., 2006, Rapid uplift of the Altiplano revealed through C-13-O-18 bonds in paleosol carbonates: Science, v. 311, p. 511-515.

Gillis, R. J., B. K. Horton, and M. Grove (2006), Thermochronology, geochronology, and upper crustal structure of the Cordillera Real: Implications for Cenozoic exhumation of the central Andean plateau, Tectonics, 25, TC6007, doi: 10.1029/2005TC001887.

Giovanni, 2007. Tectonic and thermal evolution of the Cordillera Blanca detachment system, Peruvian Andes: Implications for normal faulting in a contractional orogen, Ph.D. dissertation, 238 pp, Univ. of California, Los Angeles, Calif.

Giovanni, M.K., Horton, B.K., Garzione, C.N., McNulty, B., and Grove, M., 2010, Extensional basin evolution in the Cordillera Blanca, Peru: Stratigraphic and isotopic records of detachment faulting and orogenic collapse in the Andean hinterland: Tectonics, v. 29.

Gregory-Wodzicki, K.M., 2000. Uplift history of the Central and Northern Andes: A review. Geological Society Of America Bulletin, 112(7): 1091-1105.

Gunnell, Y., Thouret, J., Brichau, S., Carter, A., and Gallagher, K., 2010. Low-temperature thermochronology in the Peruvian Central Andes: implications for long-term continental denudation, timing of plateau uplift, canyon incision and lithosphere dynamics. Journal of the Geological Society, London, Vol. 167, pp. 803-815. Doi: 10.1144/0016-76492009-166

Henry, S.G. and Pollack, H.N., 1988. Terrestrial heat-flow above the Andean subduction zone in Bolivia and Peru. Journal of Geophysical Research-Solid Earth and Planets, 93(B12): 15153-15162.

Hermoza, W., Brusseta, S., Baby, P., Gil, W., Roddaza, M., Guerrerob, N. and Bolanos, M., 2005. The Huallaga foreland basin evolution: Thrust propagation in a deltaic environment, northern Peruvian Andes. Journal of South American Earth Sciences, 19 : 21–34.

Hoke, G.D., Isacks, B.L., Jordan, T.E., Blanco, N., Tomlinson, A.J., Ramezani, J., 2007. Geomorphic evidence for post-10 Ma uplift of the western flank of the central Andes 18°30′–22°S. Tectonics 26, TC5021. doi: 10.1029/2006TC002082.

Hoke, G.D., and Garzione, C.N., 2008, Paleosurfaces, paleoelevation, and the mechanisms for the late Miocene topographic development of the Altiplano plateau: Earth and Planetary Science Letters, v. 271, p. 192-201.

Horton, B. K., and DeCelles, P. G., 1997, The modern foreland basin system adjacent to the central Andes: Geology, v. 25, p. 895–898.

Hourigan, J.K., Reiners, P.W., and Brandon, M.T., 2005, U-Th zonation-dependent alpha- ejection in (U-Th)/He chronometry: Geochimica Et Cosmochimica Acta, v. 69, p. 3349-3365.

Husson, L. and Sempere, T., 2003. Thickening the Altiplano crust by gravity-driven crustal channel flow. Geophysical Research Letters, 30(5).

INGEMMET, 1995a. Insitituto Geologico Minero y Metalurgico, Mapa Geologico del cuadrangulo de las Pallasca. Scale 1:100,000.

INGEMMET, 1995b. Insitituto Geologico Minero y Metalurgico, Mapa Geologico del cuadrangulo del Corongo. Scale 1:100,000.

INGEMMET, 1998. Insitituto Geologico Minero y Metalurgico, Mapa Geologico del cuadrangulo de las Balsas. Scale 1:100,000.

Isacks, B.L., 1988. Uplift of the central Andean plateau and bending of the Bolivian orocline. Journal Of Geophysical Research-Solid Earth And Planets, 93(B4): 3211-3231.

James, D.E., 1971. Plate-tectonic model for the evolution of the central Andes, Geological Society of America Bulletin (82): 3325-3346.

Kay, R.W. and Kay, S.M., 1993. Delamination and Delamination Magmatism, Tectonphysics, 219:177-189.

Lamb, S., and Hoke, L., 1997. Origin of the high plateau in the Central Andes, Bolivia, South America, Tectonics, 16(4), p. 623-649.

Lamb, S., 2011. Did shortening in thick crust cause rapid Late Cenozoic uplift in the northern Bolivian Andes? J. Geol. Soc. 168, 1079–1092.

Laubacher, G., and Naeser, C.W., 1994, Fission-Track Dating of Granitic-Rocks from the Eastern Cordillera of Peru - Evidence for Late Jurassic and Cenozoic Cooling: Journal of the Geological Society, v. 151, p. 473-483.

Masek, J.G., Isacks, B.L., Gubbels, T.L., and Fielding, E.J., 1994, Erosion and Tectonics at the Margins of Continental Plateaus: Journal of Geophysical Research-Solid Earth, v. 99, p. 13941-13956.

McLaughlin, D.H.,1984. Geology and physiography and the Peruvian Cordillera, departments of Junin and Lima, Geol. Soc. Am. Bull., 355, 591-632.

Mckee, E.H., and Noble, D.C., 1982, Miocene Volcanism and Deformation in the Western Cordillera and High Plateaus of South-Central Peru: Geological Society of America Bulletin, v. 93, p. 657-662.

McNulty, B. A.; Farber, D. L.; Wallace, G. S.; Lopez, R., and Palacios, O, 1998. Role of plate kinematics and plate-slip-vector partitioning in continental magmatic arcs: evidence from the Cordillera Blanca, Peru. Geology 26:827–830.

McNulty, B., and Farber, D., 2002, Active detachment faulting above the Peruvian flat slab: Geology, v. 30, p. 567-570.

McQuarrie, N., Horton, B.K, Zandt, G., Beck, S., and DeCelles, P.G., 2005. Lithospheric evolution of the Andean fold-thrust belt, Bolivia, and the origin of the central Andean plateau, Tectonophysics, 399: 15-37.

McQuarrie, N., Ehlers, T.A., Barnes, J.B., and Meade, B., 2008, Temporal variation in climate and tectonic coupling in the central Andes: Geology, v. 36, p. 999-1002.

Megard, F., 1978. Etude geoloqique des Andes de Perou central, O.R.S.T.O.M. Mem. 86, 310 pp.

Megard, F., 1984. The Andean orogenic period and its major structure in central and northern Peru. Geological Society of London, 141, p. 893-900.

Mišković, A., Spikings, R.A., Chew, D.M., Kosler, J., Ulianov, A., and Schaltegger, U., 2009. Tectonomagnetic evolution of Western Amazonia: Geochemical characterization of zircon U-Pb geochronologic constraints from the Peruvian Eastern Cordillera granitoids, GSA Bulletin; v. 121; no. 9/10; p. 1298-1324; doi: 10.1130/B26488.1

Montgomery, D.R., Balco, G., and Willett, S.D., 2001, Climate, tectonics, and the morphology of the Andes: Geology, v. 29, p. 579-582.

Mulch, A., Uba, C.E., Strecker, M.R., Schoenberg, R., and Chamberlain, C.P., 2010, Late Miocene climate variability and surface elevation in the central Andes: Earth and Planetary Science Letters, v. 290, p. 173-182.

Myers, J. S. 1980. Geologia de los Cuadrangulos de Huarmey y Huayllapampa (hojas: 21-j y 21-h). Lima, Inst. Geol. Minero Metalurgico Bol. 33, 154 p.

Noble, D.C., McKee, E.H., Mourier, T.; Megard, F., 1990. Cenozoic stratigraphy, magmatic activity, compressive deformation, and uplift in Northern Peru, Geological Society of American Bulletin, 102: 1105-1113.

Pelletier, J.D., DeCelles, P.G., and Zandt, G., 2010, Relationships among climate, erosion, topography, and delamination in the Andes: A numerical modeling investigation: Geology, v. 38, p. 259-262.

Poulsen, C.J., Ehlers, T.A., and Insel, N., 2010, Onset of Convective Rainfall During Gradual Late Miocene Rise of the Central Andes: Science, v. 328, p. 490-493.

Reiners, P.W. and Brandon, M.T., 2006. Using thermochronology to understand orogenic erosion. Annual Review Of Earth And Planetary Sciences, 34: 419-466.

Reiners, P.W., Spell, T.L., Nicolescu, S. and Zanetti, K.A., 2004. Zircon (U-Th)/He thermochronometry: He diffusion and comparisons with Ar-40/Ar-39 dating. Geochimica Et Cosmochimica Acta, 68(8): 1857-1887, 2004.

Reiners, P.W., 2005, Zircon (U-Th)/He Thermochronometry: Reviews in Mineralogy & Geochemistry, v. 58, p. 151-179.

Rousse, S., Gilder, S., Farber, D., McNulty, B., Patriat, P., Torres, V., and Sempere, T., 2003, Paleomagnetic tracking of mountain building in the Peruvian Andes since 10 Ma: Tectonics, v. 22.

Safran, E. B., A. E. Blythe, and T. Dunne (2006), Spatially variable exhumation rates in orogenic belts: An Andean example, J. Geol., 114, 665 – 681, doi: 10.1086/507613.

Schildgen, T.F., Hodges, K.V., Whipple, K.X, Reiners, P.W., and Pringle, M.S., 2007, Uplift of the western margin of the Andean plateau revealed from canyon incision history, southern Peru: Geology, v. 35, p. 523–526.

Schildgen, T.F., Hodges, K.V., Whipple, K.X., Pringle, M.S., van Soest, M., Cornell, K.M., 2009. Late Cenozoic structural and tectonic development of the western margin of the Central Andean Plateau in southwest Peru. Tectonics 28, TC4007.

Sebrier, M., Lavenu, A., Fornari, M., and Soulas, J.P. 1988. Tectonics and uplift in Central Andes (Peru, Bolivia, and Northern Chile) from Eocene to present. Géodynamique. 3(1- 2), 85-106.

Sempere, T., Hérail, G., Oller, J. and Bonhomme, M.G., 1990. Late Oligocene Early Miocene major tectonic crisis and related basins in Bolivia. Geology, 18(10): 946-949.

Sobel, E., and M. R. Strecker (2003), Uplift, exhumation and precipitation: tectonic and climatic control of late Cenozoic landscape evolution in the northern Sierras Pampeanas, Argentina, Basin Res., 15, 431 – 451.

Stockli, D.F., Farley, K.A., and Dumitru, T.A., 2000, Calibration of the apatite (U-Th)/He thermochronometer on an exhumed fault block, White Mountains, California: Geology, v. 28, p. 983-986.

Strecker, M.R., Alonso, R.N., Bookhagen, B., Carrapa, B., Hilley, G.E., Sobel, E.R., and Trauth, M.H., 2007, Tectonics and climate of the southern central Andes: Annual Review of Earth and Planetary Sciences, v. 35, p. 747-787.

Tosdal, R.M.; Clark, A. H.; and Farrar, E. 1984. Cenozoic polyphase landscape and tectonic evolution of the Cordillera Occidental, southernmost Peru´ . Geol. Soc. Am. Bull. 95:1318–1332.

Uba, C. E., J. Kley, M. R. Strecker, and A. K. Schmitt, 2009. Unsteady evolution of the Bolivian Subandean thrust belt: The role of enhanced erosion and clastic wedge progradation, Earth and Planetary Science Letters, 281:134-146.

Whipple K. X., 2009. The influence of climate on the tectonic evolution of mountain belts: Nature Geoscience, v. 2, p. 97-104.

Wilson, J., and Reyes, L., 1964, Geología del Cuadrángulo de Pataz: Lima, Instituto Geológico Minero y Metalúrgico, Carta Geológica Nacional, Boletín Serie A, v. 9, 91 p., scale 1:100,000.

Wipf, M. 2006. Evolution of the Western Cordillera and coastal margin of Peru: evidence from low-temperature thermochronology and geomorphology. PhD thesis, ETH Zurich.

Chapter 5.

Cenozoic exhumation of the Western Cordillera of the Peruvian Andes (5-12ºS)

5.1 Introduction

The South American Andes form a large segment of the Circum-Pacific mountain system, spanning 60° of latitude from the equator to near the Antarctic peninsula. Characterized by some of the worlds highest topography, a large plateau, and drastic precipitation gradients, the Andes provide an excellent natural laboratory for studying orogenesis and the interactions of processes responsible for the growth and decay of mountainous topography.

The Andes, considered the archetypal orogen of oceanic-continental plate convergence, have been produced by subduction of the Nazca plate under the South America plate, which initiated in the Jurassic (e.g. James, 1971). The high topography is organized along-strike into two major chains, the Western and Eastern Cordilleras; they diverge between 15 and 27ºS, flanking the Altiplano-Puna plateau, Earth's second largest continental plateau (Fig. 5.1). Despite a subduction setting since the Jurassic, the topography of the Western and Eastern Cordilleras and the Altiplano-Puna plateau has uplifted since the Eocene (Isacks, 1988, Allmendinger et al., 1997; Isacks, 1988; Sempere, 1990, Barnes and Ehlers, 2009). Active deformation is presently focused east of the Cordilleras along the Subandean zone which is

characterized by an active fold-and-thrust belt (Horton and DeCelles, 1997; Hermoza et al., 2005). While the general tectonic setting of the Andes is known, significant questions remain with respect to i) the timing and magnitude of the uplift of the Andes, ii) the mechanism(s) responsible for uplift, and iii) how the tectonically segmented nature of the orogen affects the nature, timing and magnitude of uplift and deformation.

Most recent work in the Andes has focused on Altiplano-Puna Plateau, and there remains disagreement as to the nature and timing of plateau uplift. Some studies support a period of very rapid uplift of the between 10 and 4 Ma (Garzione et al., 2008; Ghosh et al., 2006; Gregory-Wodzicki, 2000; Hoke et al., 2007; Lamb, 2011) whereas other suggests more steady uplift since Eocene time (Barnes and Ehlers, 2009; McQuarrie et al., 2005). The timing of the uplift has direct bearing on the geodynamic models proposed to explain the development of the Altiplano. Presently a number of models have been suggested, including crustal shortening and thinning (Isacks et al., 1988); lithospheric delamination (Garzione et al., 2006; Kay and Kay, 1993); lower-crustal ductile flow (Beck and Zandt, 2002; Husson and Sempere, 2003); mass addition through sedimentation and magmatism (Lamb and Hoke, 1997) and the dynamic effects of the subducting oceanic lithosphere (Capitanio et al., 2011). However, it is unclear if the mechanisms important to driving uplift in one region will be equally as important in other regions of the range. Given the tectonic segmentation, morphological changes and structural deflections along-strike, it is

important to address regions outside the Altiplano region, in order to characterize Andean orogenesis holistically. In this paper, we quantify rates of crustal exhumation using low temperature thermochronology in the Western Cordillera of the Peruvian Andes between 5 and 12°S, and show that the timing and magnitude of exhumation in this region of the Andes is very similar to timings seen in the Central Andes, indicating an along-strike signal of Miocene rock exhumation that is not just restricted to the central Andean Altiplano region.

5.2 General Geologic Setting

5.2.1 The Andean Orogen of Peru

In the Peruvian segment of the Andes, morphotectonic features occur in remarkably consistent parallel structural zones. From west to east these are i) the Coastal Batholith associated with Mesozoic arc magmatism which has intruded into Precambrian metamorphic rocks and is overlain by Cenozoic continental sediments and volcanics, ii) folded and faulted Precambrian-Paleozoic low-grade metamorphic basement and minor intrusive rocks and iii) folded and faulted Mesozoic-Cenozoic marine and continental sedimentary deposits of the Sub-Andean fold-and-thrust belt (James, 1971; Cobbing and Pitcher, 1972; Megard, 1984; Sebrier et al., 1988; Lamb and Hoke, 1997) (Fig. 2).

In the Peruvian Andes between ~5°S-15°S, the tectonic chronology has been described in terms of five or more short, compressive pulses of activity separated by

longer periods of quiescence or extensional stress (Megard et al., 1984; Noble et al., 1990; McKee and Noble, 1982). The first major phase of deformation recognized within the Peruvian Andes, the 'Peruvian phase' began ~85-70Ma, affecting the Paleozoic rocks of the eastern side of the Western Cordillera and was coincident with intense volcanism along the entire Andean arc (Megard, 1978). The deformation front propagated eastward in the Paleocene-Eocene 'Incaic phases' (I and II) which affected the Eastern Cordillera and produced the Marañon fold and thrust Belt, followed by the Miocene-Pliocene 'Quechua phases' (I, II, and III) that primarily affected the Eastern Cordillera and Sub-Andean zones (Megard, 1984; Noble et al., 1990; Sebrier et al., 1988). At present the major crustal deformation is focused along the Sub-Andean Fold-and-Thrust Belt (Hermoza et al., 2005; Horton and DeCelles, 1997).

5.2.2 Orogen Morphology

Morphologically, the Peruvian Andes are host to two major orogenic deflections, which are abrupt changes in the direction of major structures, the Huancabamba Deflection (~6°S) and the Abancay Deflection (~13.5°S) (Fig. 5.1; Thornburg and Kulm, 1981; Cobbing et al., 1981). Changes in subduction slab angle are also observed along the Andean margin, where shallower angles of subduction are associated with lack of active volcanism (Barazangi and Isacks, 1976; Hasegawa and Sacks, 1981; Pilger, 1981). Between 5°N and 2°S the subducting slab dips at 35° and

represents a sector of "normal" subduction with active volcanism. At latitudes 5°S -14°S, in the Peruvian segment, the location of the Wadati-Benioff zone indicates that the Nazca Plate initially descends to a depth of 100 km at an angle of 30° before extending horizontally to the east for several hundred kilometers. Between 14°S and 16°S, the angle of subduction abruptly increases to 30° and active volcanism is present. The location of this change in subduction angle and coincides with the map position of the Abancay deflection, but how the two are linked is unknown.

Several explanations have been suggested to explain the Peruvian flat slab region, including intraplate hydrostatic suction (Jischke, 1975), subduction of young and buoyant lithosphere (Wortel and Vlaar, 1976; Cloos, 1993; Abbott et al., 1994), the curvature of the Andean margin (Cahill and Isacks, 1992; Gephart, 1994), and the presence of a buoyant oceanic plateau that has subducted along with the Nazca Ridge (Gutscher, 1999). While these hypotheses may explain some of the observations in the Peruvian segment, they are not necessarily applicable of other to flat subduction zones around the globe. Thus, it remains enigmatic not only how flat slab subduction lithosphere evolves, but how it may affect crustal thickening, the development of geologic structures, and orogenic uplift.

Slab geometry is known to change through time, in the Central Andean segment, which currently is characterized by 30°, "normal" angle subduction, experienced a flattening ca. 30-35Ma, and after 10m.y. of flat-slab style subduction, asthenospheric corner flow presumably resumed at ca. 21-25Ma (Haschke et al.,

2006; Hoke and Lamb, 2007). Based on the presence of an active volcanic arc until about 7-10 Ma, is thought that flat slab subduction in the Peruvian segment initiated in the Late Miocene (Coira et al., 1982; Jordan et al., 1983).

5.2.3 The Coastal Batholith of the Peruvian Segment

The Western Cordillera of Peru is flanked by the ~1600 km long Coastal Batholith, which represents the major phase of Mesozoic magmatism (Fig. 5.2; Cobbing and Pitcher 1972, Myers 1976, Pitcher and Bussell 1977). Over 1000 plutons have been mapped, consisting mainly of tonalite, with diorite, granodiorite and granite. The ages of intrusion range from 100-37Ma (Cobbing and Pitcher, 1972; Mukasa, 1986; Atherton and Petford, 1996). Unlike other major batholiths in other orogens, (e.g. the Sierra Nevada Batholith of the Western U.S.) the Coastal Batholith of Peru is not thought to be the unroofed plutonic root of a volcanic arc. Instead, as the Coastal Batholith lies along a major trench-parallel crustal-scale lineament, and crops out almost entirely within the mid-Cretaceous marginal basin. The basin is thought to have been formed by rifting of continental crust and filling with ~10km of basaltic rocks (Atherton et al., 1985). Shallow melting of these basaltic rocks at the bottom of the basin resulted in the formation of the magmas of the Coastal Batholith (Atherton, 1990, Haederle and Atherton, 2002). Melting was induced by major basaltic dyke swarms that produced anomalously high heat flow (Atherton 1990). As large amounts of magma were rapidly produced, they quickly intruded up fractures parallel to the plutonic crustal-scale lineament, then horizontally to form a thin

tabular geometry, within the marginal basin basaltic rocks, suggested by gravity modeling (Haederle and Atherton, 2002). Haederle and Atherton (2002) also show that the present lower bound of the batholith does not extend deeper than 3km. While this mid-Cretaceous marginal basin extends nearly 10,000km from Columbia to south Chile (Aguirre et al., 1989), and Cretaceous plutons intrude in many places, the Coastal Batholith of the Peruvian segment is among the best studied and thoroughly described (Cobbing and Pitcher, 1972; Pitcher and Bussell, 1977; Atherton, 1985; 1990).

Early workers described a major period of uplift from the Late Cretaceous through early Tertiary in the forearc, including the Coastal Batholith, (Atherton and Petford, 1996). In Southern Peru, it is noted that the presence of cobbles of batholithic rocks in the lower Moquegua formation provides evidence that at least some unroofing of the batholith, occurred by the Oligocene, requiring a phase of exhumation and uplift by this time (Huaman, 1985; Roperch et al., 2006). More recent work in Southern Peru calls for up to 3km of uplift of the forearc since ~10Ma, from quantification of canyon incision (Schildgen et al., 2007; 2009a,b; Gunnell et al., 2010).

5.2.4 Western Cordillera of Peru: Previous low-T Thermochronology

Low-temperature thermochronology is a helpful tool to deconstruct uplift and exhumation histories, canyon incision rates and magnitudes, as well as explore the

thermal history in an orogenic belt. In the Western Cordillera of Peru, it has been applied to investigate along-strike exhumation histories in an attempt to image the effect of the subducting Nazca ridge along the margin of Peru (Wipf, 2006), to quantify canyon incision rates to infer magnitudes of Altiplano surface uplift in Southern Peru (Schildgen et al., 2007; 2009a,b; Gunnell et al., 2010) and to provide insights on past thermal gradients in this region (Gunnell et al., 2010). Wipf (2006) use zircon and apatite fission track (ZFT and AFT) and apatite (U-Th)/He (AHe) from lower elevations (<600m) in the forearc to investigate rates of exhumation along-strike from 5°S to 15°S. They show that ZFT ages range between 130 and 45Ma with a cluster between 80 and 60Ma, and AFT ages lie between 124 and 24Ma. There is little variation in along-strike age spectra, thus, Wipf (2006) concludes the AFT and ZFT systems are not sensitive enough to detect changes in exhumation rate due to the subduction of the Nazca ridge. However, few AHe ages show a weak correlation with location of the ridge, and thermal modeling shows a small increase in exhumation after 10Ma in the vicinity of the Nazca ridge (Wipf, 2006).

A suite of thermochonometers (AFT, ZFT, AHe and ZHe) as well as thermal modeling and other geologic and geochronologic evidence have been used to explore the tectonic and incision histories of the Cotahuasi-Ocona and Colca-Majes canyons of the forearc in Southern Peru (~16°S) (Thouret et al., 2007; Schildgen et a., 2007; 2009a,b; Gunnell et al., 2010). While regional uplift was occurring by 24Ma (Gunnell et al., 2010), the modern-day deep canyons experienced a large magnitude of canyon

incision (2.4-3km) from ~14 - 2.2Ma (Schildgen et al., 2009a). Thus, it is thought that the rapid canyon incision is a response to dramatic uplift of the Altiplano-Puna plateau at this time (Thouret et al., 2007; Schildgen et a., 2007; 2009a,b; Gunnell et al., 2010).

Here, we quantify crustal exhumation recorded by apatite and zircon (U-Th)/He thermochronology along three E-W transects along three river canyons in the Western Cordillera of Peru at 5, 8 and 12°S, all within the 'flat slab' portion of the north-central Peruvian Andes. We show that fast exhumational signals characterize the higher relief sections of the river canyons, a similar pattern that is observed elsewhere, in the Southern Peruvian Andes (Schildgen et al., 2007). Finally, we explore the implications of these results in the context of models of Andean uplift.

5.3 Methods

5.3.1. Apatite and Zircon (U-Th)/He thermochronology

Low-temperature thermochronometer systems measure cooling due to exhumation. In this study, we use both apatite and zircon (U-Th)/He thermochronology, closure temperatures of 60ºC, (Farley, 2002) and 180ºC (Reiners at al., 2005), respectively. Apatite and zircon (U-Th)/He thermochronometers (AHe and ZHe, respectively) are sensitive to changes in erosion rates, thermal perturbations, and changes in topography, and thus are ideal for the study of growth and decay of orogens (e.g. Stockli et al., 2000; Ehlers and Farley, 2003; Reiners and

Brandon, 2006). In these isotopic systems, radiogenic helium produced by alpha decay diffuses out of the mineral at high temperatures, but below it's closure temperature (Dodson, 1973), ^{4}He is retained. The time since the sample cooled through the closure isotherm is referred to as a cooling age. Cooling ages are calculated from the measured ratios of $^{4}He/^{3}He$, and parent isotopes of U, Th and Sm (Farley, 2000; Reiners et al., 2004), and we apply an alpha ejection correction based on mineral volume and shape (Hourigan et al., 2005).

In this study, we measure both AHe and ZHe cooling ages for every hand sample, provided there are quality grains of each, and sample along an along-valley transect. This approach is especially powerful, because it gives us the ability to detect both spatial and temporal changes in exhumation.

5.3.2 Crustal thermal assumptions

The common approach to analyzing sampled transects of thermochronometers is an age vs. elevation profile, however, the long-wavelength monocline topography that characterizes the forearc is more consistent with isotherms have fully adjusted to the topography and there is thus little information to be extracted from the age vs. elevation approach (Braun, 2002). In this study, the large spatial distance over which we sample in two of the three canyons requires some consideration of laterally changing thermal fields, due to the likely changes in geothermal gradient moving away from the oceanic trench, toward the internal part of the range. This effect is

greater in regions of the orogen where there is an active volcanic arc and normal angle subduction, which permits asthenospheric corner flow (Gutscher et al., 2000). Due to the complicated history of changing slab angle along the Andean margin throughout the Miocene, it is critical to consider the thermochronologic cooling ages in the thermal field that most likely represents the region during the time of cooling that the thermochronometers capture. The leading hypothesis for flattening of the slab in the Peruvian segment involves the subduction of the aseismic Nazca ridge, the timing of which is also coincident with the cessation of magmatism in Peru, which occurred at the latest by 5Ma (Leeman, 1983; Gutscher et al., 2002). Because the time span over which the thermochonometers we sampled represents Oligocene through Late Miocene cooling, the thermal conditions that existed during this time most likely resembled the conditions that presently characterize the central Andean segment.

We apply the boundary conditions of the thermal field of Springer (1999) who fit a cross-sectional thermal model of the the Andean subduction margin at 21ºS to measured modern heat flow data. Springer's model used fixed thermal boundary conditions and typical values of lithospheric density, thermal conductivity, diffusivity, specific heat, radiogenic heat production, lithospheric thickness and plate velocities to vary subduction angle and plate shear stress in order to fit the heat flow data at 21ºS. Schildgen et al., (2009b) also applied Springer's (1999) 2-D thermal model in southern Peru where they used a range of basal crustal boundary conditions of 110-400ºC at 60km depth at the coast, and a lateral temperature gradient of

10.5-15ºC/km inland along the 60km depth, to a maximum of 1400ºC in the orogen interior. Here we test a similar range of values to predict a range of geothermal gradients used to calculate the depths to closure of the apatite and zircon (U-Th)/He thermochonologic systems.

5.3.3 LA-ICP-MS U-Pb zircon geochronology

While extensive studies of the geochronology of the Coastal Batholith have been conducted (e.g. Cobbing and Pitcher, 1972; Pitcher and Bussell, 1977; Atherton, 1985; 1990), not every individual pluton has been dated. We dated the crystallization U-Pb ages on several of the samples used for thermochronologic analysis, in order to better inform our assignment of a thermal field. Magmatism elevates the thermal field, and it important to our thermochronologic interpretation to understand the past thermal structure of this area, on a local and regional level. *In situ* laser ablation-inductively coupled plasma-mass spectrometry (LA-ICP-MS) was conducted on seven rock samples, where 14-17 individual zircon grains were analyzed at the UCSC LA-ICP-MS laboratory, which couples a Thermo Element XR single-collector ICP-MS to a Photon Machines Analyte 193H ArF excimer laser ablation system. Analyses included 26um spot-sizes, 30 seconds of baseline data collection followed by 30 seconds of on-peak data collection. The ablated zircon material is carried from the ablation cell by helium gas, mixed with argon sample gas and injected into an inductively coupled plasma stream where it is measured using the XR single-collector

ICP-MS. Data reduction was conducted using Iolite, a free software available on the Igor Pro platform (Paton et al., 2011) where downhole fractionation and common-Pb corrections were made.

5.4 Results

We sampled three E-W along-valley transects: 1) at 5ºS, which we call the Morropan transect; 2) at 8ºS, the Rio Moche transect; and 3) 12ºS, the Rio Rimac transect (Fig. 5.3; Appendix 5.1). All samples were bedrock and taken from the Coastal Batholith lithologies, to ensure high quality zircon and apatite separates. The river valleys sampled increase in maximum relief from the north to the south. The elevations of the sample localities ranged from 217 to 2234 m.a.s.l., and the distances from the coast ranged from 20 to 125 km inland. We have derived the mean (U-Th)/He cooling ages from the analysis of 4-6 individual grains of zircon and apatite (ZHe and AHe, respectively), as well as the range of predicted cooling rates given our thermal assumptions (Fig. 5.4).

5.4.1 Morropan

At Morropan, the morphology of the coast differs from the two southern transects; the topographic front lies 100km inland from a wide coastal plain. The Morropan transect extends for only 5km and comprises four samples which were collected along a small river valley, from 326-791m.a.s.l. The canyon walls ascend to 2000 m.a.s.l. proximal to the samples while the highest elevations in the catchment

area top out around 3000 m.a.s.l. The small areal extent of this transect was limited by the available outcrops of the plutonic lithologies of the batholith. Four samples yielded quality zircons, but unfortunately no quality apatite grains. Zircon ages lie within a small range, 36.6 ± 6.1Ma, 33.6 ± 4.1Ma, 37.4 ± 5.1Ma, 33.5 ± 5.6Ma (from low to high elevation, Fig. 5.3A). The U-Pb zircon ages for three of the four samples are 45.3 ± 0.8Ma, 50.0 ± 1.7Ma, and 50.5 ± 0.8Ma (Fig. 5.3D).

5.4.2 Rio Moche

The Rio Moche is an E-W oriented river that drains to the Pacific ocean just south of the city of Trujillo. Here, we collected seven along-valley samples over a range of 20-50km inland from the coast, at elevations of 217 - 2191m.a.s.l. The average elevation of the canyon rim in the catchment headwaters is 3.5km. All seven of the bedrock samples were taken from batholithic rocks, yielded quality zircons and in three samples we were able to recover high quality apatites. The ZHe ages exhibited no distinguishable pattern with either elevation or distance from the coast. The range of ZHe ages is 20.9 ± 2.4Ma at the youngest, and 29.2 ± 2.6Ma at the oldest. The apatite separates also did not produce a convincing age spectral pattern with either elevation or distance from the coast, as the three mean ages, from west to east are 8.4 ± 0.8Ma, 14.8 ± 1.6Ma and 13.6 ± 3.7Ma (Fig. 5.3B). In addition, four samples were dated for U-Pb analyses, and the ages are similar; from west to east they are, 30.6 ± 1.6, 30.0 ± 0.6, 31.1 ± 0.8, 31.5 ± 0.7 (Fig. 5.3E)

5.4.3 Rio Rimac

The Rio Rimac is also an orogen perpendicular river draining to the Pacific ocean, through the city of Lima, Peru. In this drainage, the along-valley sampled transect extends from 35km inland from the coast at 635m.a.s.l to 80km inland from the coast at 2234m.a.s.l. The surrounding canyon rim is perched at 4.5km with a maximum canyon relief of 2.8km. In this river canyon, we collected six bedrock samples, five of which yielded quality zircons and four of which produced quality apatites. Unlike the other two transects, both the ZHe and AHe cooling ages show a clear spectral pattern of younging-inland. The ZHe ages, from west to east are 48.7 ± 3.3Ma, 26.1 ± 7.6Ma, 14.4 ± 0.7Ma, 9.3 ± 3.5Ma and 9.3 ± 0.9Ma. The AHe ages, also reported up river, are 10.5 ± 1.9Ma, 8.1 ± 1.1Ma, 6.8 ± 3.9Ma and 4.4 ± 2.5 Ma (Fig. 5.3C). In addition, three samples were dated for U-Pb analyses, and the ages from west to east are, 84.4 ± 3.7, 85.8 ± 1.6, and 23.1 ± 3.2 (Fig. 5.3F).

5.5 Discussion

5.5.1. Along-valley sampled bedrock transects

We discuss each of the three along-valley bedrock transects, from north to south, the modeled exhumation rates, and then discuss implications for regional uplift models.

5.1.1. Morropan transect

Due to the proximity of sample locations, as all four samples only span five kilometers of distance and less than 500m in elevation difference, it is not surprising that the data yield the same cooling ages, within error. Thus, we treat this area as a small crustal block that has experienced the same exhumation history. The range in geothermal gradients predicted by the thermal field applied are 26.8-27.9ºC/km, corresponding to closure depths of 6.4-6.9km (Fig. 5.4), predicting exhumation rates for these samples range from 0.13-0.22mm/yr, which are a time-averaged rate since passage through the zircon closure temperature c.a. 35Ma, and we are unable to determine accelerations of decelerations of exhumation rate over this time period.

However, Pleisotocene-Holocene denudation rates from basin-averaged sand samples using cosmogenic radionuclides in the nearby Rio Piura are of a similar scale, from 0.09-0.3mm/yr (Abbuhl et al., 2010). Thus, while our data do not permit us to explore temporal changes in exhumation rate, the modern denudation rates match the time-averaged exhumation rates very well, indicating that on short and long timescales, it's possible the landscape has been somewhat close to steady state, with roughly 7km of erosion in the past ~35Ma.

5.1.2 Rio Moche transect

In the Rio Moche transect, located at 8ºS, we analyze seven ZHe ages and three AHe ages, and unlike the Morropan transect, are able to spatially and temporally resolve changes in exhumation rates. Using the range of thermal boundary conditions

explained above, geothermal gradients are estimated at 20-26ºC/km, and closure depths for the ZHe cooling ages range from 9.8 to 6.7km, and 2.3-2.4km for AHe (Fig. 5.4). These values correspond to exhumation rates ranging from 0.16-0.34mm/yr, and record a deceleration in cooling rates recorded by the AHe ages in the mid-to-late Miocene. We explore two possibilities, that the decrease in cooling is due to a changing thermal gradient, or a deceleration in exhumation, which could be due to slowing erosion rates.

As the cessation of magmatic intrusions in the Coastal Batholith occurred by 30Ma, it is reasonable to assume that thermal conditions changed at this time, perhaps cooling to the thermal field similar to what we see in the modern. We use a range of geothermal gradients from 12-15ºC/km as a first order test to interpret the three AHe ages in this transect. The three sampled ages span 7km of along-valley distance and over 700m in elevation. From coast to inland, the ages are 8.4 ± 0.8Ma, 14.8 ± 1.6Ma and 13.6 ± 3.7Ma, resulting in exhumation rates of 0.29 - 0.55mm/yr, where the fastest rate is derived from the youngest age. Ignoring for a moment this young sample, we see similar exhumation rates for both the AHe and the ZHe exhumation data from this proposed changing thermal condition. If this is a realistic thermal adjustment to make, we image relatively constant exhumation of ~0.3mm/yr since ~25Ma to the present, on the order of a total of ~7.5km of erosion since the late Oligocene-early Miocene.

One way rapid exhumation or uplift in the early Miocene might be induced is by changes in the subducting slab angle, and the subduction of the buoyant Nazca ridge. However, It is thought that the angle of subducting lithosphere in the Peruvian segment was occurring at a normal, 30º angle prior to 7-10Ma. Thus, the timings of these tectonic events does not correlate with the enhanced exhumation rates we see at 25-14Ma., The Nazca ridge is calculated to have impacted the coast at 8ºS at 8Ma (McNulty and Farber, 2000), well after the supposed deceleration in exhumation. Finally, it is worth examining the extent to which changes in the climate of the forearc could produce the signal we find. Modern climate produces extremely low background denudation and weathering rates, however, it is possible that during the early Miocene, the orogen experienced an accelerated exhumation signal due to enhanced, focused precipitation. It is difficult to evaluate this scenario, as regional paleoclimate in the Western Cordillera of the central Peruvian Andes is not well constructed prior to the Late Miocene. The onset of hyperaridity for northern Chile is estimated to have existed since 25 Ma from cosmogenic radionuclide exposure ages (Dunai et al. 2005). However, others estimate hyperaridity onset at 19-13 Ma (Rech et al. 2006), between 14.7 and 8.7 Ma (Alpers and Brimhall 1988) and as recent as ~4 Ma (Hartley, 2003). In Late Miocene time, it is proposed that convective rainfall increases on the eastern flank of the Andean orogen (Mulch et al., 2010; Poulsen et al., 2010). Without direct evidence for a climate change in the Western Peruvian Andes between 25 and 14Ma, climate change is not a convincing explanation for the

window of possible accelerated exhumation. As there are few convincing geological or geophysical explanations to explain a scenario of rapid exhumation from 25-14Ma, and slowing by a factor of 2-4 from 14-0Ma, we favor the explanation that the thermal field has not been constant since the Oligocene, due to an elevated thermal field resulting from Oligocene-aged intrusives, and that exhumation of the orogen at this locality has been more or less constant since ~25Ma.

5.1.3 Rio Rimac transect

The Rio Rimac transect lies east of the major city of Lima, Peru, at about 12ºS in latitude, our most southern field location. Here, analyzing both ZHe and AHe cooling ages enhance our interpretation. The sampled distance of 45km of the along-valley transect is the longest transect of our three, affording the ability to quantify exhumation spatially. Here we see a strong trend in both the ZHe and AHe age spectra. Ages young inland, from 48.7 ± 3.3Ma to 9.3 ± 0.9Ma from the ZHe data and 10.5 ± 1.9Ma to 4.4 ± 2.4Ma from the AHe cooling ages (Fig. 5.3). Using the initial thermal boundary conditions explained above, geothermal gradients are predicted to range from 15-24ºC along this 50km along-valley transect. The corresponding closure depths, range from 10.5-7.5km (coast to inland) for the ZHe ages and 2.9-2.1km (coast to inland) for the AHe ages (Fig. 5.4C). These spatially variable exhumation rates are, by definition, temporally variable as well, as the wide spread in cooling

ages limits the information available; i.e. a 9.3Ma ZHe cooling age cannot constrain the exhumation rate prior to this time period at this location.

However, the pattern of inland-younging ZHe and AHe ages is significant and seen as well in the Colca-Majes and Cotahausi-Ocona canyons in Southern Peru, where it was interpreted as a signal of late Miocene upstream propagating canyon incision (Schildgen et al., 2007). This incision in southern Peru is believed to be a direct response to uplift of the margin and the Altiplano (Schildgen et al., 2007; 2009b; Gunnell et al., 2010).

While the general trends of ages in the Rio Rimac, at 12º and the Cotahausi-Ocono canyon at 16ºS are similar, a major difference between the two datasets is the average cooling ages. Schildgen et al. (2007) report ZHe ages of 43-158 Ma and AHe ages of 5.3-72.5 Ma, over similar elevations and similar distances from the coast as our data from the Rio Rimac. The much younger ZHe ages in the Rio Rimac transect imply that while Southern Peru experienced slow exhumation during the Mesozoic and early Cenozoic, until the late Miocene when canyon incision accelerated crustal cooling, the Rio Rimac transect at 12ºS is characterized by at least 0.15 mm/yr of exhumation starting in the Eocene.

We calculate a significant increase in the exhumation rate since the mid-to-late Miocene from 0.23mm/yr (40km from coast) to 0.74mm/yr (80km from coast) in the ZHe cooling ages, and 0.3mm/yr (50km from coast) - 0.52mm/yr (80km from coast) in the AHe cooling ages. Taking the three most-inland samples and their ZHe-AHe

pairs together, this implies a short period of rapid exhumation followed by a slowing signal for the three sample pairs (Fig. 5.4). Additionally, the signal of faster exhumation propagates up valley, occurring from 14.4 - 8.1Ma (RMC10-3), 9.3 - 6.8Ma (RMC10-2) and 9.3 - 4.4Ma (RMC10-1).

These exhumation rates are extremely rapid for this part of the Andes, and represent ~7.5km of exhumation in the upper reaches of the Rio Rimac, since 14Ma. Due to the absence of geologic indicators such as easily dated, undeformed volcanic units that provide bounds on timing of canyon incision, we are cautions to relate the magnitude of crustal exhumation we show solely to canyon incision, and surface uplift. In fact, the maximum relief of the Rio Rimac canyon in the sampled area is 3.8km. Even given the end member case where topography was flat in the early Miocene and surface uplift and associated canyon incision was entirely responsible for the exhumation documented here, this would only account for 3.8km of exhumation, of the 7.5km we show.

We explore two possible scenarios to explain the extremely young cooling ages we find in the upper reaches of the Rio Rimac valley. One, we suggest that perhaps background exhumation rates were much higher, due to a more actively eroding margin. Two, we test the idea that the exhumation signal shown here is largely due to a falling geothermal gradient. Schildgen et al. (2009b) use background exhumation rates of 0.03 - 0.07mm/yr to their data in Southern Peru, as the Atacama desert of Southern Peru is not only currently one of the driest places in the world but

appears to have experienced negligible erosion and weathering for at least the last 7Ma. This is in part due to the orographic effect of the Central Andes and Altiplano-Puna Plateau, which were at least 2km high in the mid-Miocene according to the most conservative models (Garzione et al., 2008), and possibly higher (Barnes and Ehlers, 2009). However, the paleotopography of the Eastern Cordillera of Peru between 5 and 12ºS is poorly understood. It is possible that lower elevations permitted more moisture to the forearc in the north-central Peruvian Andes, resulting in higher background erosion and denudation rates. If we apply a background erosion rate of 0.20mm/yr, this accounts for ~3km of exhumation since the mid-Miocene (14Ma), requiring that ~4km of additional exhumation was accomplished by incision of the Rio Rimac, which is reasonable given the calculated exhumation rates.

Alternatively, we assume that topography has roughly been in steady state since ~14Ma and attribute the exhumation signal fully to a falling geothermal gradient. Garver et al. (2005) interprets Miocene-aged ZFT and ZHe data from the Cordillera Huayash as recording a falling geothermal gradient from 40-50ºC/km in the late Miocene, due to intrusion of the Cordillera Blanca to the south. For example, a geothermal gradient of 40ºC/km that falls to 15ºC/km, would record 7.5km of exhumation in the ZHe system, but require some erosion to exhume the thermally perturbed rocks to the surface. However, given that the major pulse of magmatism in this area occurred by 80Ma (Mukasa, 1986), and only isolated plutons exist in this

region to be much younger, a geothermal gradient decrease of that magnitude is surprising and unlikely, especially since last 14Ma.

5.6 Conclusions

The Andes are a long-lived subduction margin, but interestingly, their uplift is a more recent phenomenon. The mechanism(s) that caused the uplift as well as the timing of uplift are a subject of current debate. Further, models for Andean uplift have largely focused on data from the central Andean Altiplano region, and it is unclear how and if the northern and southern Andes fit in with these models for uplift of the plateau. In quantifying exhumation rates from the Coastal Batholith of the Western Cordillera, aided by thermal constraints from intrusion ages and a modeled thermal field, we show that the forearc of Peru has exhumed relatively consistently along-strike and in time, at rates of 0.2-0.3mm/yr. The interesting exception is in the upper part of the Rio Rimac, which has experienced fast cooling since the mid-Miocene. We suggest a combination of background exhumation rates of ~0.15mm/yr and focused river incision to account for this exhumation. The rates of cooling and age spectra in the Rio Rimac show a similar pattern as those presented in the Cotahuasi-Ocona and Colca-Majes canyons (Schildgen et al., 2007; Schildgen et al., 2009a,b; Gunnell et al. 2010). This is an intriguing result, as those authors explain the rapid cooling signal by fast canyon incision due to uplift of the Altiplano Plateau. Our data at 12º show a similar signal, yet this region along the Andean margin is characterized by a distinct

lack of the broad-plateau topography that is observed to the south. Perhaps the uplift signal seen in Southern Peru along the flanks of the Altiplano is not recording isolated uplift of the Altiplano only. Taking these studies together, we suggest that a regional, along-strike signal of significant uplift along the Peruvian margin characterized the Western Cordillera of the Andean margin since the early-to-mid Miocene.

Further, the region of study in this paper lies entirely within the Peruvian flat-slab zone. The tectonic segmentation of the Andes has inspired models for its formation (Isacks, 1988; Husson and Sempere, 2003; Lamb and Davis, 2003; Capitanio et al., 2011). We show here, similar timings of crustal exhumation in the flat-slab north-central Peruvian Andes margin, compared to the Southern Peruvian margin within the region of normal angle subduction and active arc. While we cannot rule out the importance of late Miocene lower crustal flow and lower lithospheric removal in the Central Andes, it is unlikely these mechanism operated in the flat-slab setting of the Peruvian Andes, which is inferred to have existed since the late Miocene. Very low values of crustal heat flow do not support the thermal signals typically seen in areas that permit lower lithospheric delamination (Henry and Pollack, 1988), and while the crust is relatively thick in the north-central Peruvian chain (~50-60km thick), a narrow (<200km) band of high topography does not fit the morphology of crustal models that predict lateral flow in the mid-to-low crust (e.g. Bird, 1991; Clark and Royden, 2000). Thus, if there is a unifying mechanism that is

facilitating uplift of the Andes since the mid-Miocene, it is must be a mechanism that operates similarly across the tectonic and morphological segmentation of the Andes.

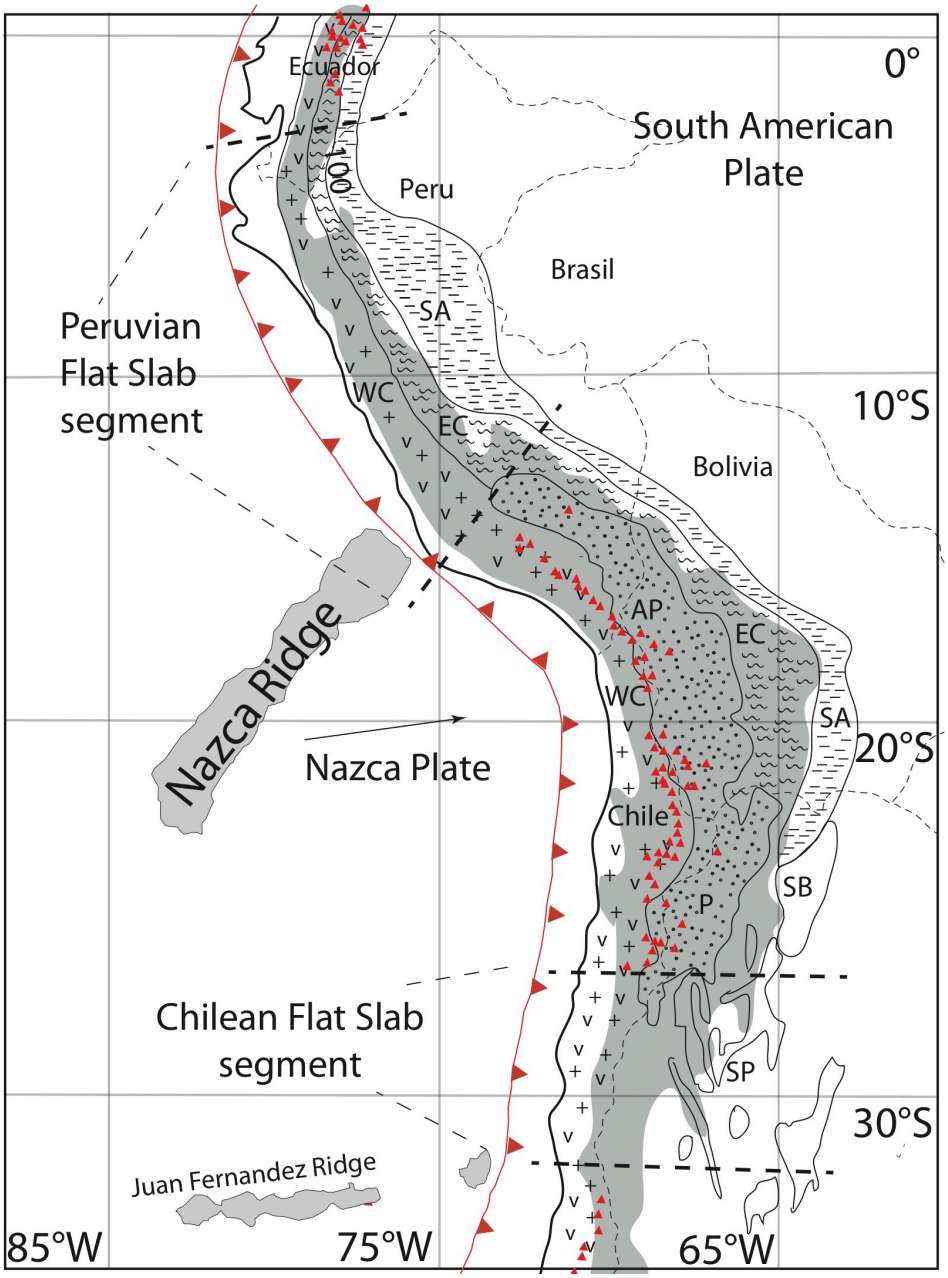

Figure 5.1. Shows the morphotectonic zones of the northern and central South American Andes. Elevation above 1500km is shown in gray, red triangles represent active volcanic centers; WC=Western Cordillera; EC=Eastern Cordillera; AP=Altiplano; P=Puna; SA=Sub Andean Fold and thrust belt; SB=Santa Barbara fold and thrust belt; SP=Sierra Pampenas fold and thrust belt. Flat slab zones are marked in between the dashed lines.

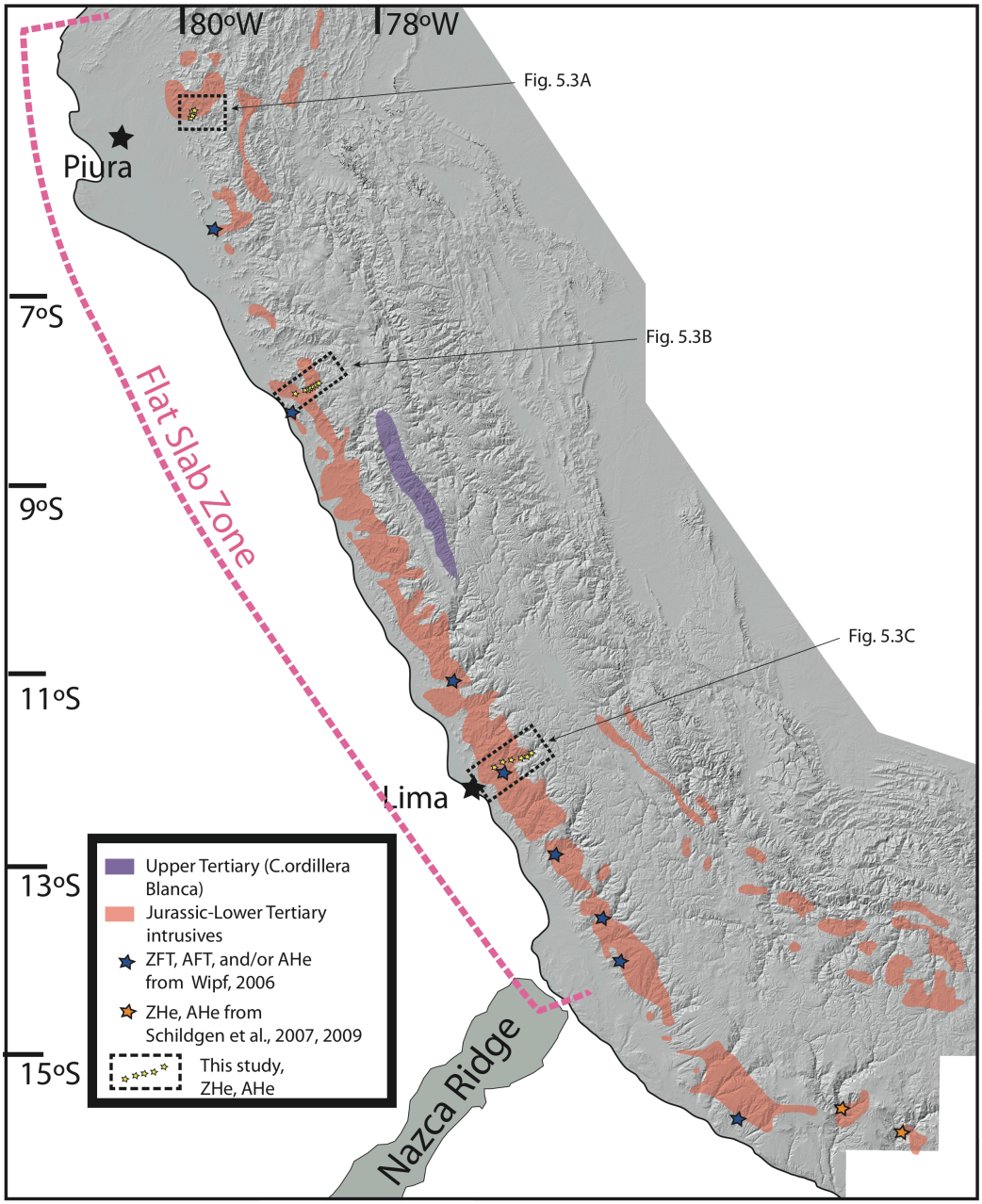

Figure 5.2. All Cenozoic batholithic rocks shown on a DEM of the Peruvian Andes. Black boxes show field areas. Modified from Cobbing et al., 1977.

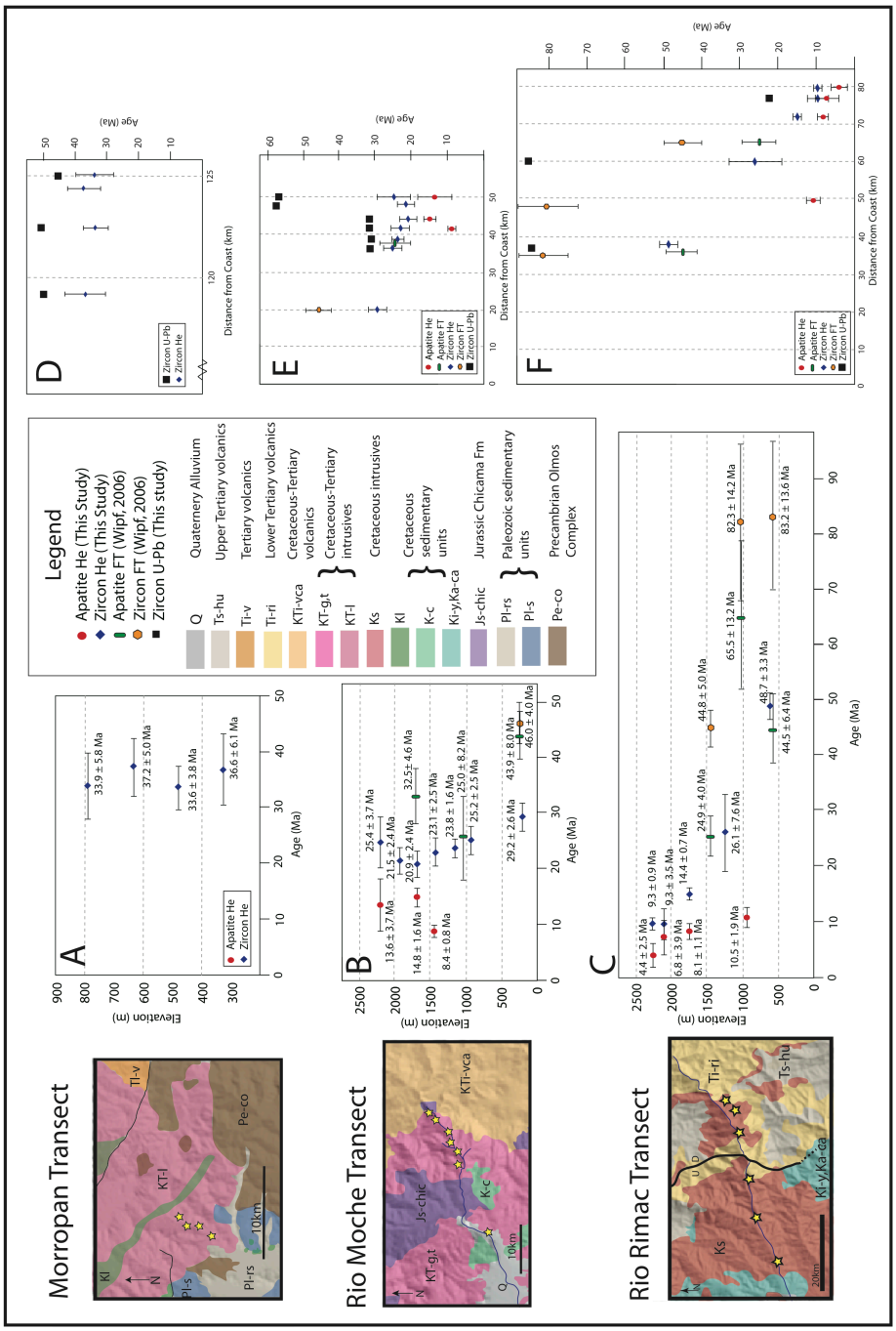

Figure 5.3. Apatite and zircon (U-Th)/He and zircon U-Pb results for all three sampled locations. In A, B and C, the cooling ages are plotted with respect to elevation. In D, E and F, the cooling ages are shown as distance from coast along the valley bottom.

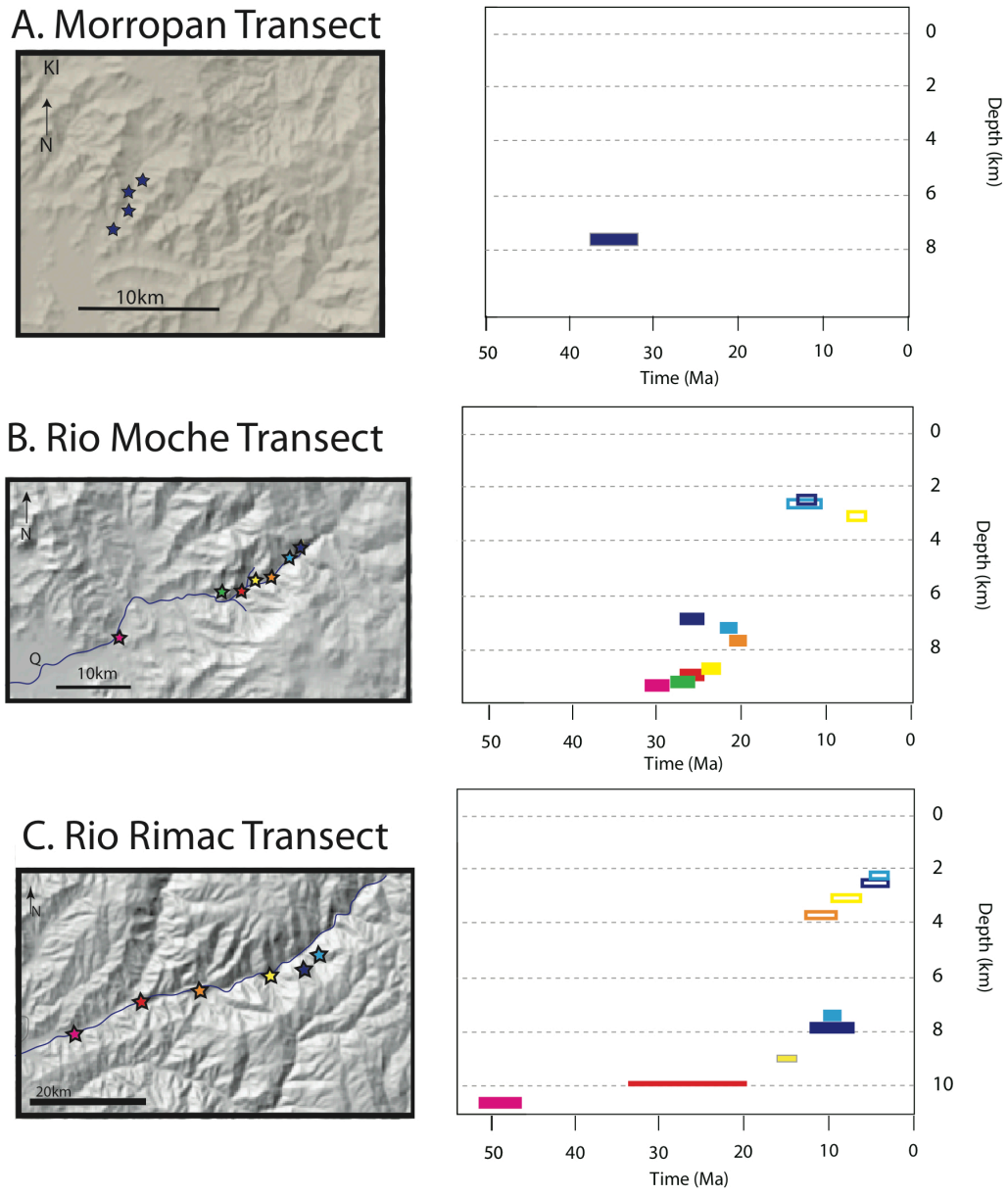

Fig. 5.4. DEMs of each sampled transect showing location of samples. Colors represent corresponding location of sample in the closure depth-time- space. Solid colored boxes show depth-time data from ZHe cooling ages, where hollow boxes show depth-time data from AHe cooling ages.

Appendix 5.1 Zircon and apatite (U-Th)/He results

Sample	Mineral	He, mol	U, ppm	Th, ppm	Grain mass, g	Ft*	Age, Ma	±(error)†	Mean-weighted avg. age (Ma)	Elevation, m
Morropan Site										
RLG10-1-2	zircon	1.18E-13	489.3	128.4	1.99E-06	0.671	31.21	0.87	**33.5 ± 5.6**	791
RLG10-1-3	zircon	8.43E-13	686.6	174.8	8.50E-06	0.8	31.3	0.52		791
RLG10-1-4	zircon	7.81E-13	603.9	135.2	7.66E-06	0.788	37.38	0.85		791
RLG10-1-5	zircon	2.99E-13	364.6	86	4.95E-06	0.758	38.03	0.87		791
RLG10-2-1	zircon	4.82E-13	821.6	219.8	4.02E-06	0.738	34.15	0.82	**37.4 ± 5.1**	634
RLG10-2-2	zircon	1.68E-13	133.4	40.3	7.69E-06	0.787	35.66	0.79		634
RLG10-2-3	zircon	4.52E-13	555.5	153.3	5.37E-06	0.756	34.58	0.68		634
RLG10-2-4	zircon	3.20E-13	493.6	166.1	3.57E-06	0.729	42.33	0.8		634
RLG10-2-5	zircon	1.50E-13	443.5	151.5	1.96E-06	0.688	42.71	0.94		634
RLG10-3-1	zircon	5.33E-13	892.1	194.5	4.26E-06	0.743	33.02	0.82	**33.6 ± 4.1**	480
RLG10-3-2	zircon	9.31E-14	635.5	390.6	1.08E-06	0.612	35.51	0.59		480
RLG10-3-3	zircon	4.29E-13	1001	218.1	3.42E-06	0.743	29.5	0.49		480
RLG10-3-4	zircon	6.09E-13	1335.6	226.1	2.98E-06	0.728	37.08	0.63		480
RLG10-3-5	zircon	1.15E-13	435	162.8	1.86E-06	0.683	34.98	0.67		480
RLG4-1	zircon	6.87E-13	766.1	213.3	5.58E-06	0.749	36.96	0.73	**36.6 ± 6.1**	326
RLG4-3	zircon	5.12E-13	349.9	92.2	9.25E-06	0.794	34.51	0.69		326
RLG4-4	zircon	2.77E-13	173.5	49.4	1.04E-05	0.8	32.92	0.69		326
RLG4-5	zircon	1.86E-13	411.4	129.8	3.04E-06	0.699	36.36	0.63		326

*Ft=alpha-ejection correction factor based on mineral shape and volume (Hourigan et al., 2005); †error= analytical error; §mean-weighted average age is calcuated using Isoplot 3.00 (Ludwig, 2003)

Appendix 5.1 Zircon and apatite (U-Th)/He results

Sample	Mineral	He, mol	U, ppm	Th, ppm	Grain mass, g	Ft*	Age, Ma	±(error)†	Mean-weighted avg. age (Ma)	Elevation, m
Rio Moche Site										
RMC10-1-1	zircon	1.05E-12	1861.6	1873.2	4.88E-06	0.752	22.86	0.39	**25.4 ± 3.7**	2191
RMC10-1-2	zircon	9.21E-13	617.8	387.1	1.15E-05	0.822	25.23	0.47		2191
RMC10-1-3	zircon	1.01E-12	840.5	644.5	5.92E-06	0.741	42.6	0.91		2191
RMC10-1-5	zircon	1.24E-12	503.5	403.5	1.77E-05	0.826	26.09	0.57		2191
RMC10-2-1	zircon	9.52E-13	693.1	605	1.12E-05	0.781	23.87	0.54	**21.4 ± 2.4**	1928
RMC10-2-2	zircon	5.12E-13	1046.7	1132.2	5.06E-06	0.742	19.09	0.35		1928
RMC10-2-3	zircon	5.94E-13	556.4	437.1	9.75E-06	0.8	21.24	0.41		1928
RMC10-2-4	zircon	4.86E-13	967.9	788.5	4.44E-06	0.747	23.34	0.42		1928
RMC10-2-5	zircon	7.44E-13	990.7	788.7	7.25E-06	0.747	21.48	0.41		1928
RMC10-3-1	zircon	6.98E-13	580.3	357.3	1.21E-05	0.799	19.97	0.33	**20.9 ± 2.4**	1685
RMC10-3-2	zircon	3.32E-13	306.9	171.6	9.76E-06	0.806	22.35	0.57		1685
RMC10-3-4	zircon	6.01E-13	342.4	209.6	1.48E-05	0.827	23.07	0.44		1685
RMC10-3-5	zircon	3.08E-12	670.3	407.6	4.12E-05	0.883	20.3	0.44		1685
RMC10-3-5	zircon	3.08E-12	663.5	406.6	4.12E-05	0.883	20.49	0.45		1685
RMC10-4-2	zircon	2.02E-13	331.5	207.5	5.35E-06	0.73	24.98	0.6	**23.2 ± 2.2**	1432
RMC10-4-3	zircon	5.07E-13	280.2	136	1.50E-05	0.83	23.97	0.59		1432
RMC10-4-4	zircon	4.92E-13	409.1	223.2	1.09E-05	0.791	22.78	0.41		1432
RMC10-4-5	zircon	2.07E-13	432.8	229.4	4.88E-06	0.751	21.34	0.67		1432
RMC10-5-1	zircon	4.48E-13	675.8	162.3	6.23E-06	0.775	23.93	0.47	**24.1 ± 1.4**	1149
RMC10-5-2	zircon	3.43E-13	830.6	142.3	4.57E-06	0.731	21.83	0.64		1149
RMC10-5-3	zircon	7.59E-13	825.2	88.8	8.52E-06	0.799	24.22	0.66		1149
RMC10-5-4	zircon	1.95E-13	932.8	166.6	2.12E-06	0.695	25.05	0.58		1149
RMC10-5-5	zircon	1.02E-12	870.2	94	1.06E-05	0.806	24.71	0.49		1149

*Ft=alpha-ejection correction factor based on mineral shape and volume (Hourigan et al., 2005); †error= analytical error; §mean-weighted average age is calcuated using Isoplot 3.00 (Ludwig, 2003)

Appendix 5.1 Zircon and apatite (U-Th)/He results

Sample	Mineral	He, mol	U, ppm	Th, ppm	Grain mass, g	Ft*	Age, Ma	±(error)†	Mean-weighted avg. age (Ma)	Elevation, m
Rio Moche Site, con't										
RMC10-6-1	zircon	4.30E-13	1018.2	605.7	3.29E-06	0.723	28.62	0.54	**25.6 ± 2.4**	932
RMC10-6-2	zircon	1.79E-12	899.5	187.8	1.67E-05	0.832	25.16	0.54		932
RMC10-6-3	zircon	1.24E-13	528	389.3	2.17E-06	0.666	25.52	0.48		932
RMC10-6-4	zircon	5.70E-13	774.7	187.6	7.12E-06	0.788	22.82	0.63		932
RMC10-6-5	zircon	5.70E-13	920	262.6	5.54E-06	0.759	25.37	0.5		932
RMC10-1	zircon	1.99E-13	310.8	152.9	4.80E-06	0.745	29.50	0.56	**29.2 ± 2.6**	217
RMC10-2	zircon	3.96E-13	470.5	197.3	6.40E-06	0.772	28.51	0.52		217
RMC10-3	zircon	3.82E-13	612.2	204.3	4.93E-06	0.744	28.96	0.62		217
RMC10-4	zircon	1.02E-12	467.5	120.7	1.34E-05	0.815	34.70	0.83		217
RMC10-5	zircon	3.96E-13	481.1	214.8	6.35E-06	0.771	27.90	0.50		217
RMC1-Ap3	apatite	3.94E-15	7.5	26.1	4.70E-06	0.731	15.44	0.39	**13.6 ± 3.7**	2191
RMC1-Ap4	apatite	5.56E-15	19.3	31.4	4.23E-06	0.737	12.28	0.26		2191
RMC1-Ap5	apatite	1.31E-14	8.1	29.4	1.39E-05	0.816	14.12	0.28		2191
RMC3-Ap1	apatite	1.14E-14	35.3	33.9	4.82E-06	0.704	14.24	0.33	**14.8 ± 1.6**	1685
RMC3-Ap2	apatite	1.39E-14	68.2	42.3	3.49E-06	0.713	13.15	0.35		1685
RMC3-Ap3	apatite	1.81E-14	145.3	121.9	1.82E-06	0.652	16.18	0.39		1685
RMC3-Ap4	apatite	1.25E-14	116.9	91.9	1.62E-06	0.633	16.15	0.42		1685
RMC3-Ap5	apatite	4.50E-15	47.7	39.2	1.53E-06	0.631	15.12	0.39		1685
RMC4-Ap1	apatite	3.53E-15	18.5	33.9	3.99E-06	0.724	8.46	0.19	**8.4 ± 0.8**	1432
RMC4-Ap3	apatite	5.16E-15	16.7	27.9	6.31E-06	0.764	8.46	0.18		1432

*Ft=alpha-ejection correction factor based on mineral shape and volume (Hourigan et al., 2005); †error= analytical error; §mean-weighted average age is calcuated using Isoplot 3.00 (Ludwig, 2003)

Appendix 5.1 Zircon and apatite (U-Th)/He results

Sample	Mineral	He, mol	U, ppm	Th, ppm	Grain mass, g	Ft*	Age, Ma	±(error)†	Mean-weighted avg. age (Ma)	Elevation, m
Rio Rimac Site										
RR1-1	zircon	4.21E-14	718.1	291.4	1.83E-06	0.637	8.47	0.13	**9.3 ± 0.9**	2234
RR1-2	zircon	2.48E-14	339.4	195	1.86E-06	0.662	9.63	0.14		2234
RR1-3	zircon	2.41E-14	556	214.6	1.25E-06	0.61	9.60	0.25		2234
RR1-4	zircon	1.26E-14	291.4	175.4	1.29E-06	0.628	8.61	0.19		2234
RR1-5	zircon	8.82E-15	739.3	344.7	4.19E-07	0.465	10.16	0.17		2234
RR1-6	zircon	1.87E-14	258.2	153.2	1.70E-06	0.643	10.70	0.28		2234
RR2-1	zircon	7.74E-14	866.5	547	2.10E-06	0.672	10.16	0.19	**9.3 ± 3.5**	2108
RR2-2	zircon	1.20E-13	857.9	540.4	3.60E-06	0.723	8.60	0.15		2108
RR2-3	zircon	1.85E-13	1740	1416.9	1.54E-06	0.641	16.65	0.32		2108
RR2-4	zircon	5.05E-14	947	1506.3	1.47E-06	0.633	7.68	0.13		2108
RR2- 5	zircon	1.52E-14	595.9	612.2	5.35E-07	0.499	14.12	0.35		2108
RR3-1	zircon	6.76E-14	235.8	114.2	4.37E-06	0.734	14.74	0.31	**14.4 ± 0.7**	1743
RR3-2	zircon	6.59E-14	348.4	212.3	2.91E-06	0.696	15.05	0.26		1743
RR3-3	zircon	5.26E-14	324.9	178.2	2.61E-06	0.695	14.53	0.35		1743
RR3-4	zircon	1.62E-13	335.4	132.6	7.70E-06	0.769	13.72	0.23		1743
RR3-5	zircon	4.63E-14	268.2	165.6	2.79E-06	0.699	14.20	0.27		1743
RR4-2	zircon	3.24E-13	235.8	99.8	9.39E-06	0.787	31.05	0.67	**26.1 ± 7.6**	1262
RR4-3	zircon	2.14E-13	224	113.3	7.66E-06	0.779	26.28	0.50		1262
RR4-4	zircon	3.47E-13	419.9	85.7	1.00E-05	0.798	18.16	0.64		1262
RR4-5	zircon	2.89E-13	247.9	89.6	8.95E-06	0.791	27.94	0.48		1262
RR6-1	zircon	3.43E-12	646	113.3	2.33E-05	0.848	47.29	0.91	**48.7 ± 3.3**	635
RR6-2	zircon	2.77E-13	379.8	192.8	3.53E-06	0.717	47.19	0.71		635
RR6-3	zircon	2.26E-12	531.3	180.8	1.58E-05	0.821	55.72	1.17		635
RR6-4	zircon	1.64E-12	470.1	177.6	1.48E-05	0.804	49.28	0.70		635
RR6-5	zircon	2.99E-13	346.6	148	4.17E-06	0.724	47.75	0.75		635

*Ft=alpha-ejection correction factor based on mineral shape and volume (Hourigan et al., 2005); †error= analytical error; §mean-weighted average age is calcuated using Isoplot 3.00 (Ludwig, 2003)

Appendix 5.1 Zircon and apatite (U-Th)/He results

Sample	Mineral	He, mol	U, ppm	Th, ppm	Grain mass, g	Ft*	Age, Ma	±(error)†	Mean-weighted avg. age (Ma)	Elevation, m
Rio Rimac Site con't										
RR1-Ap1	apatite	4.37E-15	11.6	24.9	1.54E-05	0.813	3.67	0.07	**4.4 ± 2.5**	2234
RR1-Ap3	apatite	1.36E-15	17.2	21.9	2.76E-06	0.689	5.89	0.23		2234
RR1-Ap4	apatite	5.24E-16	5.8	15.1	2.43E-06	0.684	6.22	0.47		2234
RR1-Ap5	apatite	1.43E-15	21.8	54.4	1.56E-06	0.626	7.80	0.28		2234
RR2-Ap1	apatite	4.75E-16	61.1	47.9	4.21E-07	0.48	5.97	0.36	**6.8 ± 3.9**	2108
RR2-Ap3	apatite	7.68E-16	60.5	54.6	5.79E-07	0.507	6.58	0.32		2108
RR2-Ap4	apatite	1.15E-15	48	49.2	4.58E-07	0.481	16.14	0.72		2108
RR2-Ap5	apatite	1.52E-15	90.4	102.6	7.11E-07	0.54	6.36	0.22		2108
RR3-Ap1	apatite	1.15E-14	12.1	21.6	2.00E-05	0.836	7.39	0.15	**8.1 ± 1.1**	1743
RR3-Ap2	apatite	5.16E-15	16.7	27.9	6.31E-06	0.764	8.46	0.18		1743
RR3-Ap3	apatite	2.38E-15	12.2	22.9	3.63E-06	0.707	9.69	0.30		1743
RR3-Ap4	apatite	6.86E-15	10.5	32	9.88E-06	0.784	9.06	0.18		1743
RR3-Ap5	apatite	1.16E-14	39.1	41.7	7.52E-06	0.781	7.45	0.14		1743
RR5-Ap1	apatite	4.26E-14	31.7	47.1	2.24E-05	0.822	9.96	0.18	**10.5 ± 1.9**	941
RR5-Ap2	apatite	1.02E-14	28.1	44.8	6.70E-06	0.763	9.52	0.17		941
RR5-Ap4	apatite	4.34E-14	49.5	56.1	1.61E-05	0.812	9.76	0.18		941
RR5-Ap5	apatite	1.91E-14	36	39.2	9.07E-06	0.796	10.75	0.20		941

*Ft=alpha-ejection correction factor based on mineral shape and volume (Hourigan et al., 2005); †error= analytical error; §mean-weighted average age is calcuated using Isoplot 3.00 (Ludwig, 2003)

5.7 References

Abbott, D., Drury, R., and Smith, W.H., 1994, Flat to Steep Transition in Subduction Style: Geology, v. 22, p. 937-940.

Abbuhl, L.M., Norton, K.P., Jansen, J.D., Schlunegger, F., Aldahan, A., Possnert, G., 2010. Erosion rates and mechanisms of knickzone retreat inferred from 10Be measured across strong climate gradients on the northern and central Andes Western Escarpment. Earth Surface Processes and Landforms, v.36, p1464-1473.

Aguirre, I., Levi, B., and Nystrom, J. O. 1989. The link btetween mctamorphism, volcanism and geotectonic setting during the evolution of the Andes. In: Daly. J. S.. Cliff. R. A,. and Yardley. B. W. D. (Eds). Evolution of Metamorphic Belts. Geological Society Special Publication, 43. 223-232

Alpers, C.N., Brimhall, G.H., 1988. Middle Miocene climatic change in the Atacama Desert, northern Chile: evidence from supergene mineralization at La Escondida. Geological Society of America Bulletin 100, 1640–1656.

Allmendinger, R.W., Jordan, T.E., Kay, S.M. and Isacks, B.L., 1997. The evolution of the Altiplano-Puna plateau of the Central Andes. Annual Review Of Earth And Planetary Sciences, 25: 139-174.

Atherton, M.P., Warden, V., and Sanderson, L.M., 1985, The Mesozoic marginal basin of Central Peru: A geochemical study of within-plate-edge volcanism, in Pitcher, W.S., Cobbing, E.J., and Beckinsale, R.D., eds., Magmatism at a Plate Edge: The Peruvian Andes: London, Blackie Halsted Press, p. 47-58.

Atherton, M.P. 1990. The Coastal Batholith of Peru: the product of rapid recycling of new crust formed within rifted continental margin. Geological Journal 25, 331-349.

Atherton, M. P. & Petford, N., 1993. Generation of sodium-rich magmas from newly underplated basaltic crust Nature 362, 144-146.

Atherton, M.P. & Petford, N., 1996. Plutonism and the growth of Andean Crust at 9S from 100 to 3 Ma. Journal of South American Earth Sciences, v. 9, pp.1-9.

Barazangi, M., and Isacks, B.L., 1976, Spatial-Distribution of Earthquakes and Subduction of Nazca Plate beneath South-America: Geology, v. 4, p. 686-692.

Barnes, J.B., and Ehlers, T.A., 2009, End member models for Andean Plateau uplift: Earth- Science Reviews, v. 97, p. 105-132.

Beck, S.L. and Zandt, G., 2002. The nature of orogenic crust in the central Andes. Journal Of Geophysical Research-Solid Earth, 107(B10).

Bird, P., 1991, Lateral extrusion of lower crust from under high topography, in the isostatic limit: Journal of Geophysical Research, v. 96, p. 10,275–10,286.

Braun, J., 2002, Estimating exhumation rate and relief evolution by spectral analysis of age-elevation datasets: Terra Nova, v. 14, p. 210-214.

Cahill, T., and Isacks, B.L., 1992, Seismicity and Shape of the Subducted Nazca Plate: Journal of Geophysical Research-Solid Earth, v. 97, p. 17503-17529.

Capitanio, F.A., Faccenna, C., Zlotnik, S. and Stegman, D.R., 2011. Subduction dynamics and the origin of Andean orogeny and Bolivian Orocline, Nature, 480, 83-86, doi: 10.1038/nature10596

Clark, M. K. & Royden, L. H., 2000. Topographic ooze: Building the eastern margin of Tibet by lower crustal flow. Geology 28, 703-706.

Cloos, M., 1993, Lithospheric Buoyancy and Collisional Orogenesis - Subduction of Oceanic Plateaus, Continental Margins, Island Arcs, Spreading Ridges, and Seamounts: Geological Society of America Bulletin, v. 105, p. 715-737.

Cobbing, E.J., and Pitcher, W.S., 1972. Plate tectonics and the Peruvian Andes: Nature, v. 246, p. 51-53.

Cobbing, E. J.; Pitcher, W. S.; Wilson, J. J.; Baldock, W. P.; McCourt, W.; and Snelling, N. J. 1981. The geology of the western Cordillera of northern Peru. Overseas Mem. Inst. Geol. Sci. Lond. Mem. 5, 143 p.

Coira, B., Davidson, J., Mpodozis, C., Ramos, V., 1982. Tectonic and magmatic evolution of the Andes of northern Argentina and Chile. Earth Sci. Rev. 18, 303–332.

Dodson, M.H., 1973, Closure Temperature in Cooling Geochronological and Petrological Systems: Contributions to Mineralogy and Petrology, v. 40, p. 259-274.

Dunai, T.J., Gonzalez Lopez, G.A., and Juez Larre, J., 2005, Oligocene-Miocene age of aridity in the Atacama Desert revealed by exposure dating of erosion-s ensitive landforms, Geological Society of America (GSA). Boulder CO United States. 2005., 321-324 p.

Ehlers, T.A., and Poulsen, C.J., 2009, Influence of Andean uplift on climate and paleoaltimetry estimates: Earth and Planetary Science Letters, v. 281, p. 238-248.

Ehlers, T.A. and Farley, K.A., 2003. Apatite (U-Th)/He thermochronometry: methods and applications to problems in tectonic and surface processes. Earth And Planetary Science Letters, 206(1-2): 1-14.

Farley, K.A., 2000. Helium diffusion from apatite: General behavior as illustrated by Durango fluorapatite. Journal Of Geophysical Research-Solid Earth, 105(B2): 2903-2914.

Farley, K.A., 2002, (U-Th)/He dating: techniques, calibrations and applications: Reviews in Mineralogy & Geochemistry, v. 47, p. 819-844.

Garver, J.I., Reiners, P.W., Walker, L.J., Ramage, J.M., and Perry, S.E., 2005, Implications for timing of Andean uplift from thermal resetting of radiation damaged zircon in the Cordillera Huayhuash, northern Peru: Journal of Geology, v. 113, p. 117-138.

Garzione, C.N., Molnar, P., Libarkin, J.C. and MacFadden, B.J., 2006. Rapid late Miocene rise of the Bolivian Altiplano: Evidence for removal of mantle lithosphere. Earth And Planetary Science Letters, 241(3-4): 543-556.

Garzione, C.N., Hoke, G.D., Libarkin, J.C., Withers, S., MacFadden, B., Eiler, J., Ghosh, P., and Mulch, A., 2008. Rise of the Andes: Science, v. 320, p. 1304-1307.

Gephart, J.W., 1994, Topography and subduction subduction geometry in the central Andes: Clues to the mechanics of a non-collisional orogen: Journal of Geophysical Research, v. 99, p. 12,279–12,288, doi: 10.1029/94JB00129.

Ghosh, P., Garzione, C.N., and Eiler, J.M., 2006, Rapid uplift of the Altiplano revealed through C-13-O-18 bonds in paleosol carbonates: Science, v. 311, p.511-515.

Gregory-Wodzicki, K.M., 2000. Uplift history of the Central and Northern Andes: A review. Geological Society Of America Bulletin, 112(7): 1091-1105.

Gunnell, Y., Thouret, J., Brichau, S., Carter, A., and Gallagher, K., 2010. Low-temperature thermochronology in the Peruvian Central Andes: implications for long-term continental denudation, timing of plateau uplift, canyon incision and lithosphere dynamics. Journal of the Geological Society 2010; v. 167; p. 803-815. doi:10.1144/0016-76492009-166

Gutscher, M.A., Olivet, J.L., Aslanian, D., Eissen, J.P., and Maury, R., 1999, The "lost Inca Plateau": cause of flat subduction beneath Peru?: Earth and Planetary Science Letters, v. 171, p. 335-341.

Gutscher, M.A., Spakman, W., Bijwaard, H., Engdahl, R.E., 2000. Geodynamics of flat slab subduction: Seismicity and tomographic constraints from the Andean margin. Tectonics; v. 19, no.5, p. 814-833.

Haederle, M., and Atherton, M.P., 2002, Shape and intrusion style of the Coastal Batholith, Peru: Tectonophysics, v. 345, p. 17-28.

Hartley, A.J., 2005, What caused Andean uplift, 6th International Symposium on Andean Geodynamics (ISAG 2005): Barcelona, p. 824-827.

Haschke, M., Günther, A., Melnick, D., Echtler, H., Reutter, K.-J., Scheuber, E., Oncken, O., 2006. Central and southern Andean tectonic evolution inferred from arc magmatism. In: Oncken, O., Chong, G., Franz, G., Giese, P., Götze, H.-J., Ramos, V.A., Strecker, M.R., Wigger, P. (Eds.), The Andes Active Subduction Orogeny, vol. 1.Springer, Berlin Heidelberg New York, pp. 337–353. chap. 16.

Hasegawa, A., and Sacks, I.S., 1981, Subduction of the Nazca Plate beneath Peru as Determined from Seismic Observations: Journal of Geophysical Research, v. 86, p. 4971-4980.

Henry, S.G. and Pollack, H.N., 1988. Terrestrial heat-flow above the Andean subduction zone in Bolivia and Peru. Journal of Geophysical Research-Solid Earth and Planets, 93(B12): 15153-15162.

Hermoza, W., Brusseta, S., Baby, P., Gil, W., Roddaza, M., Guerrerob, N. and Bolanos, M., 2005. The Huallaga foreland basin evolution: Thrust propagation in a deltaic environment, northern Peruvian Andes. Journal of South American Earth Sciences, 19 : 21–34.

Hoke, G.D., Isacks, B.L., Jordan, T.E., Blanco, N., Tomlinson, A.J., Ramezani, J., 2007. Geomorphic evidence for post-10 Ma uplift of the western flank of the central Andes 18°30′–22°S. Tectonics 26, TC5021. doi: 10.1029/2006TC002082.

Horton, B. K., and DeCelles, P. G., 1997, The modern foreland basin system adjacent to the central Andes: Geology, v. 25, p. 895–898.

Hourigan, J.K., Reiners, P.W., and Brandon, M.T., 2005, U-Th zonation-dependent alpha- ejection in (U-Th)/He chronometry: Geochimica Et Cosmochimica Acta, v. 69, p. 3349-3365.

Huaman, D., 1985, Évolution tectonique cénozoique et néotectonique du piémont pacifique dans la région d'Arequipa (Andes du Sud du Pérou): Orsay, Paris.

Husson, L. and Sempere, T., 2003. Thickening the Altiplano crust by gravity-driven crustal channel flow. Geophysical Research Letters, 30(5).

Isacks, B.L., 1988. Uplift of the central Andean plateau and bending of the Bolivian orocline. Journal Of Geophysical Research-Solid Earth And Planets, 93(B4): 3211-3231.

James, D.E., 1971. Plate-tectonic model for the evolution of the central Andes, Geological Society of America Bulletin (82): 3325-3346.

Jischke, M.C., 1975, Dynamics of Descending Lithospheric Plates and Slip Zones: Journal of Geophysical Research, v. 80, p. 4809-4813.

Jordan, T.E., Isacks, B.L., Ramos, V.A., and Allmendinger, R.W., 1983, Mountain Building in the Central Andes: Episodes, p. 20-26.

Kay, R.W. and Kay, S.M., 1993. Delamination and Delamination Magmatism, Tectonphysics, 219:177-189.

Lamb, S., and Davis, P., 2003. Cenozoic climate change as a possible cause for the rise of the Andes, Nature, 425(23).

Lamb, S., and Hoke, L., 1997. Origin of the high plateau in the Central Andes, Bolivia, South America, Tectonics, 16(4), p. 623-649.

Lamb, S., 2011. Did shortening in thick crust cause rapid Late Cenozoic uplift in the northern Bolivian Andes? J. Geol. Soc. 168, 1079–1092.

McLaughlin, D.H.,1984. Geology and physiography and the Peruvian Cordillera, departments of Junin and Lima, Geol. Soc. Am. Bull., 355, 591-632.

Megard, F., 1978. Etude geoloqique des Andes de Perou central, O.R.S.T.O.M. Mem. 86, 310 pp.

Megard, F., 1984. The Andean orogenic period and its major structure in central and northern Peru. Geological Society of London, 141, p. 893-900.

Mckee, E.H., and Noble, D.C., 1982, Miocene Volcanism and Deformation in the Western Cordillera and High Plateaus of South-Central Peru: Geological Society of America Bulletin, v. 93, p. 657-662.

McNulty, B., and Farber, D., 2002, Active detachment faulting above the Peruvian flat slab: Geology, v. 30, p. 567-570.

McQuarrie, N., Horton, B.K, Zandt, G., Beck, S., and DeCelles, P.G., 2005. Lithospheric evolution of the Andean fold-thrust belt, Bolivia, and the origin of the central Andean plateau, Tectonophysics, 399: 15-37.

Mulch, A., Uba, C.E., Strecker, M.R., Schoenberg, R., and Chamberlain, C.P., 2010, Late Miocene climate variability and surface elevation in the central Andes: Earth and Planetary Science Letters, v. 290, p. 173-182.

Mukasa, S.B., 1986, Zircon U-Pb Ages of Super-Units in the Coastal Batholith, Peru - Implications for Magmatic and Tectonic Processes: Geological Society of America Bulletin, v. 97, p. 241-254.

Myers, J.S., 1976, Erosion surfaces and ignimbrite eruption, measures of Andean uplift in northern Peru: Journal of Geology, v. 11, p. 29-44.

Noble, D.C., McKee, E.H., Mourier, T.; Megard, F., 1990. Cenozoic stratigraphy, magmatic activity, compressive deformation, and uplift in Northern Peru, Geological Society of American Bulletin, 102: 1105-1113.

Paton, C., Hellstrom, J., Paul, B., Woodhead, J., and Hergt, J., 2011. Iolite:Freeware for the visualization and processing of mass spectrometric data. J. Anal. At. Spectrom, DOI: 10.1039/c1ja10172b

Pilger, R.H., 1981, Plate Reconstructions, Aseismic Ridges, and Low-Angle Subduction beneath the Andes: Geological Society of America Bulletin, v. 92, p. 448-456.

Pitcher, W. S,, and Bussell, M. A., 1977, Structural control of batholithic emplacement in Peru: A review: Geological Society of Lond an Journal, v. 133, p. 249-255.

Poulsen, C.J., Ehlers, T.A., and Insel, N., 2010, Onset of Convective Rainfall During Gradual Late Miocene Rise of the Central Andes: Science, v. 328, p. 490-493.

Rech, J., Currie, B., Michalski, G., Cowan, A., 2006. Neogene climate change and uplift in the Atacama Desert, Chile. Geology 34, 761–764.

Reiners, P.W. and Brandon, M.T., 2006. Using thermochronology to understand orogenic erosion. Annual Review Of Earth And Planetary Sciences, 34: 419-466.

Reiners, P.W., Spell, T.L., Nicolescu, S. and Zanetti, K.A., 2004. Zircon (U-Th)/He thermochronometry: He diffusion and comparisons with Ar-40/Ar-39 dating. Geochimica Et Cosmochimica Acta, 68(8): 1857-1887, 2004.

Reiners, P.W., 2005, Zircon (U-Th)/He Thermochronometry: Reviews in Mineralogy & Geochemistry, v. 58, p. 151-179.

Roperch, P., Sempere, T., Macedo, O., Arriagada, C., Fornari, M., Tapia, C., Garcia, M., Laj, C., 2006. Counterclockwise rotation of late Eocene–Oligocene

fore-arc deposits in southern Peru and its significance for oroclinal bending in the central Andes. Tectonics 25, TC3010. doi:10.1029/2005TC001882.

Rousse, S., Gilder, S., Farber, D., McNulty, B., Patriat, P., Torres, V., and Sempere, T., 2003, Paleomagnetic tracking of mountain building in the Peruvian Andes since 0 Ma: Tectonics, v. 22.

Safran, E. B., A. E. Blythe, and T. Dunne (2006), Spatially variable exhumation rates in orogenic belts: An Andean example, J. Geol., 114, 665 – 681, doi: 10.1086/507613.

Schildgen, T.F., Hodges, K.V., Whipple, K.X, Reiners, P.W., and Pringle, M.S., 2007, Uplift of the western margin of the Andean plateau revealed from canyon incision history, southern Peru: Geology, v. 35, p. 523–526.

Schildgen, T.F., Hodges, K.V., Whipple, K.X., Pringle, M.S., van Soest, M., Cornell, K.M., 2009a. Late Cenozoic structural and tectonic development of the western margin of the Central Andean Plateau in southwest Peru. Tectonics 28, TC4007.

Schildgen, T.F., Ehlers, T.A., Whipp, D.M., van Soest, M.C., Whipple K.X., Hodges, K.V., 2009b. Quantifying canyon incision and Andean Plateau surface uplift, southwest Peru: A thermochronometer and numerical modeling approach. Journal of Geophysical Research, v.114, F04014, doi:10.1029/2009JF001305

Sebrier, M., Lavenu, A., Fornari, M., and Soulas, J.P. 1988. Tectonics and uplift in Central Andes (Peru, Bolivia, and Northern Chile) from Eocene to present. Géodynamique. 3(1- 2), 85-106.

Sempere, T., Hérail, G., Oller, J. and Bonhomme, M.G., 1990. Late Oligocene Early Miocene major tectonic crisis and related basins in Bolivia. Geology, 18(10): 946-949.

Springer, M. (1999), Interpretation of heat-flow density in the central Andes, Tectonophysics, 306, 377–395, doi:10.1016/S0040-1951(99)00067-0.

Stockli, D.F., Farley, K.A., and Dumitru, T.A., 2000, Calibration of the apatite (U-Th)/He thermochronometer on an exhumed fault block, White Mountains, California: Geology, v. 28, p. 983-986.

Thornburg, T.; Kulm, L.O. 1981. Sedimentary basins of the Peru continental margin; structure, stratigraphy, and Cenozoic tectonics from 60S to 16°5 latitude: in Nazca Plate; crustal formation and Andean (Kulm, L.O.; editor et al.). Geological Society of America, Memoir, No. 154, p. 393-422.

Thouret, J.-C., G. Wo¨rner, Y. Gunnell, B. Singer, X. Zhang, and T. Souriot, 2007. Geochronologic and stratigraphic constraints on canyon incision and Miocene uplift of the central Andes in Peru, Earth Planet. Sci. Lett., 263, 151– 166, doi:10.1016/j.epsl.2007.07.023.

Wipf, M. 2006. Evolution of the Western Cordillera and coastal margin of Peru: evidence from low-temperature thermochronology and geomorphology. PhD thesis, ETH Zurich.

Wortel, M.J.R., and Vlaar, N.J., 1976, Age-Dependent Subduction of Oceanic Lithosphere beneath Central and South-America: Transactions-American Geophysical Union, v. 57, p. 676-676.

Chapter 6.
Conclusion

6.1 Goals

The main goals of this thesis are:

1) To test models of Andean orogensis by quantifying rock exhumation, using low-temperature thermochronology, and develop a model of regional uplift in the north-central Peruvian Andes (Chapters 4 and 5).

2) To investigate early Andean topography and tectonics, by using detrital U-Pb zircon geochronology in the Cretaceous back-arc basin of the Andes, which now occupies the Eastern Cordilleran spine of the Andean Orogen. (Chapter 3).

6.2 Summary of Findings

Prior to this work, thermochonologic studies in the Peruvian Andes were few and spatially confined. From six sites in the Peruvian Andes between 5 and 12°S, we use both apatite and zircon (U-Th)/He thermochronology to determine rates and timings of crustal cooling due to exhumation. These sites lie within different tectonomorphic and geologic regions of Peru, from the Mesozoic Coastal Batholith of the Western Cordillera, to the Cordillera Blanca Batholith region to the Marañon corridor of the Eastern Cordillera. In this work, we find:

i) Slow cooling throughout the Mesozoic, and plausible partial retention of He from zircon (U-Th)/He thermochronometers in the Rio Marañon corridor from two sample sites that span several kilometers of elevation. Apatite (U-Th)/He ages from the same samples in these sites records late Miocene cooling. Taking these two systems together, we image a regional acceleration in rock exhumation increasing by roughly and order of magnitude, from ~0.04mm/yr to 0.25mm/yr by late Miocene time.

ii) A shift from Paleozoic basement to Amazon cratonic sources from detrital U-Pb zircons within the Cretaceous sandstones of the Marañon fold-and-thrust belt. The source shift most likely results from subsidence and burial of the Marañon High, which changes fluvial and eolian sources from the Marañon High to the cratons of the Amazon shelf. This provenance change is show in two sample sites, at 6.5 and 8.5°S, indicating that if local basins were isolated, they were fed by the same sources.

iii) a Miocene rock cooling signal using both zircon and apatite (U-Th)/He thermochronologic systems in the Coastal Batholith of the Western Cordillera in Peru, from three sites at 5, 8 and 12°S, while U-Pb zircon geochonologic ages on the same samples vary from late-Cretaceous to Oligocene. In the site at 12°S, along the Rio Rimac, the age spectra displays younging orogen-ward, indicating a spatial gradient

in exhumation, where faster rock exhumation occurs in the internal part of the orogen, compared to the coast.

The thermochronologic findings of this dissertation provide the first regionally extensive study in north-central Peru using multiple low temperature chronometer systems. We image a previously undocumented acceleration in regional rock exhumation rates in the Marañon Corridor of the Eastern Cordillera. In spite of structural and stratigraphical studies that assign the major deformation pulse of the Eastern Cordillera to Eocene time, from this data, we show that rock exhumation rates were actually slow during the Eocene. U-Pb detrital zircon provenance from the Cretaceous aged-sandstones and quartzite samples from the Marañon sample sites confirms that the ZHe cooling ages are not reflecting unreset ages, rather, partial retention of He near the closure depth of Zr. Thus, in piecing together the time-temperature history of the Marañon fold-and-thrust belt from the Cretaceous to the present, we document cratonic sources sources for the Marañon (West Peruvian Trough) basin, accompanied by subsidence of the Paleozoic-aged Marañon High. Despite active subduction and an active magmatic arc to the west, the back-arc basin remained near sea level until the Tertiary. During the Eocene, structural relationships record intense deformation and folding and faulting, but our thermochronologic data do not record significant exhumation until the late Miocene. The AHe data record increasing rock exhumation rates in the late Miocene, which we attribute to a regional change in enhanced erosion, driven by a regional shift in climate.

In the Western Cordillera, Miocene rock cooling signal is also observed, despite an entirely different geologic setting compared to the Eastern Cordillera. Here, in the Coastal Batholithic rocks of the Western Cordillera, which were emplaced largely in the late Cretaceous through Oligocene, exhumation recorded by both zircon and apatite thermochronometers are Miocene. In general, at two sites at 8 and 12°S, cooling ages are observed to be younger farther toward the orogen, away from the coast, even after applying the lateral thermal gradients we would expect in an arc-type setting. A younging-inland pattern of cooling ages is also observed in Southern Peru, where deep canyons incise the flanks of the Altiplano Plateau (Schildgen et al., 2009). The similar pattern of ages and age spectra we document in the Peruvian Andes lie within regions of the Andes that lack the high plateau. Thus, despite differing tectonic settings, and range morphology, the timings and patterns of rock exhumation are similar. This result is intriguing, because it may suggest a more unifying, along-strike mechanism driving Miocene rock exhumation along the chain of the Andes, and that Miocene rock exhumation and uplift is not just restricted to the central Andes, which contain the Altiplano-Puna Plateau.

6.3 Concluding Remarks

Pioneering geologists of the early 20th century working Peru noted the presence of planar surfaces, stranded several kilometers above sea level (Bowman, 1916; McLaughlin, 1924; Steinmann, 1929). They surmised that uplift of these

surfaces had occurred since the mid-to-late Miocene, or perhaps even more recently. In 1916, Bowman wrote, "proof of the rapid and great uplift of certain now lofty mountain ranges in late geologic time is one of the largest contributions of physiography to geologic history." Such a simple, but astute observation was made decades before reliable geochronologic techniques were developed, and before the theory of global plate tectonics was presented. Since then, seismic imagery, GPS data, geochronological, techniques, refined geologic mapping, and numerical modeling have developed upon the platform of what these original geologists posed; the topography of the modern Andean Orogen has formed largely in the latter half of the Cenozoic, despite its tectonic record of oceanic-continental convergence since the early Mesozoic.

Of great interest to scientists working in the Andes over the past few decades has been explaining the morphological differences along-strike; the Andes, despite long-lived subduction with little exotic terrane accretion, display major bends in strike, as well as a large plateau that only exists in the central portion of the Andes. The regional area of focus of this work, within the north-central Peruvian Andes, which display narrow topography and "flat slab" subduction, is quite different than the relatively well-studied central Andean segment that contains the Altiplano-Puna Plateau. In comparing these two regions, we seek to characterize the differences and similarities in order to investigate models of Andean formation. At present, controversy remains as to the precise timing, mechanisms and magnitude of uplift of

the central Andes (Barnes and Ehlers, 2009). However, we find here that the general timings (Miocene to present) of rock exhumation in the north-central Peruvian Andes are similar to the timings of uplift and generation of modern topography documented in the Central Andean segment, despite such tectonomorphic differences between the two regions. Perhaps the tectonic and morphological segmentation of the Andes is not as strong of a control on the timings and mechanisms of Andean formation as we initially thought. A unifying mechanism that has previously been proposed to account for regional and global uplift is global climate change. Late Cenozoic climate change and orogenesis on a global scale have been suggested to be profoundly linked (Molnar and England, 1990; Raymo and Ruddiman, 1992). While quantifying the details of the specific feedbacks between climate and tectonics remain challenging, the notion of Late Cenozoic climate change influencing along-strike relief growth of the Andes, despite along-strike tectonomorphic heterogeneities is a provocative, yet, simple explanation for the results presented in this dissertation.

6.4 References

Bowman, I., 1916. The Andes of Southern Peru, American Geographical Society, NY, 336p.

McLaughlin, D.H., 1924. Geology and physiography of the Peruvian cordillera, Departments of Junin and Lima. Geological Society of American Bulletin, 35: 591-632.

Molnar, P., and P. England,L ate Cenozoicu plift of mountain ranges and global climatic change: Chicken or egg?, Nature, 346, 29-34, 1990.

Raymo, M.E., and Ruddiman, W.F., 1992, Tectonic forcing of late Cenozoic climate: Nature, v. 359, p. 117–122, doi: 10.1038/359117a0.

Schildgen, T.F., Hodges, K.V., Whipple, K.X., Pringle, M.S., van Soest, M., Cornell, K.M., 2009. Late Cenozoic structural and tectonic development of the western margin of the Central Andean Plateau in southwest Peru. Tectonics 28, TC4007.

Steinmann, G., 1929. Geologie von Peru, Carl Winters Universitatsbuchhandlung, 448p.